D. Wolfe

December 1980
Boulder, Colorado

U.S. DEPARTMENT OF COMMERCE
NOAA/ERL Wave Propagation Laboratory

TURBULENCE STATISTICS FOR DESIGN OF WIND TURBINE GENERATORS

Preprint of Report to DOE

TURBULENCE STATISTICS FOR DESIGN OF WIND TURBINE GENERATORS

Preprint of Report to DOE

J.C. Kaimal
J.E. Gaynor
D.E. Wolfe

Report Number Three
December 1980

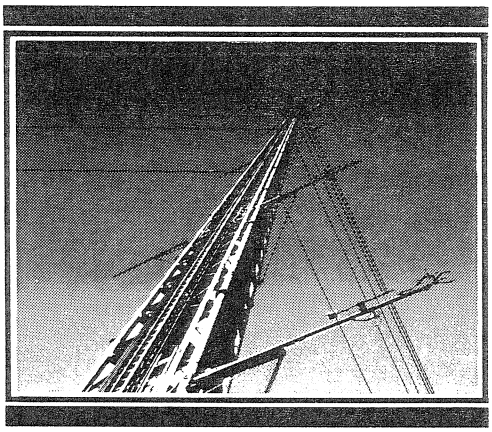

NOAA
Boulder Atmospheric Observatory

U.S. Department of Commerce
National Oceanic and Atmospheric Administration
Environmental Research Laboratories

A NOAA publication available from NOAA/ERL, Boulder, CO 80303.

NOTICE

Prepared by the Wave Propagation Laboratory, NOAA/ERL, Boulder, Colorado 80303 for the United States Department of Energy under Interagency Agreement No. DE-A106-79ET23115

CONTENTS

NOMENCLATURE

S	Wind speed
D	Wind direction
u,v,w	Longitudinal, lateral, and vertical wind components
z	Height above ground
n	Cyclic frequency (Hz)
$S(n)$	Spectral estimate
λ	Wavelength ($\approx \bar{u}/n$)
λ_i	Lower limit of inertial subrange
λ_M	Wavelength at spectral peak
τ_ℓ	Lowpass filter time
τ_h	Highpass filter time
Δt	Differencing interval
ΔX	Differenced variable X where X = S or D
L	Integral length scale
$[\quad]_F$	Filtered time series
$\sigma(X)$	Standard deviation of X
$\sigma_{rms}(X)$	Root-mean-square of X
$+A_0$, $-A_0$	GUST 0 amplitudes
$+T_0$, $-T_0$	GUST 0 times
$+A_1$, $-A_1$	GUST 1 amplitudes
$+T_1$, $-T_1$	GUST 1 times.

TURBULENCE STATISTICS FOR DESIGN OF WIND TURBINE GENERATORS

J. C. Kaimal, J. E. Gaynor and D. E. Wolfe

ABSTRACT

Characteristics of moments and probability distributions for two high-wind episodes observed at the Boulder Atmospheric Observatory are examined in depth. The two episodes represent entirely different stability conditions. Statistics for the GUST 0 and GUST 1 models for different heights and bandpass filters are the main focus.

1.0 INTRODUCTION

A great deal of attention has been directed in recent years to the development of energy technologies that depend on sources not as easily depleted as the fossil fuels in use today. The main focus of such attention has been on such sources as the wind, the sun, and vegetation. As a source of energy, the wind offers a clean, virtually inexhaustible, though not always predictable, supply that can be harnessed; with each increase in price of fossil fuel, its conversion to electrical power becomes more cost-effective.

Wind Energy Conversion Systems (WECS) under development cover a range of sizes and output capacities, from small systems suitable for farm and rural use to large megawatt systems designed for use in existing utility grids. Not surprisingly, the costs of fabrication and maintenance rise sharply with size, so operating efficiency and fatigue life become matters of primary concern in the design of the larger WECS systems. Of fundamental importance is an understanding of a system's response to spatial and temporal fluctuations in the wind.

A WECS is typically a wind turbine generator with rotor blades mounted either vertically or horizontally. Larger systems tend to be conventional propeller types with horizontal axes. They operate in a region of the atmosphere's boundary layer where wind shears and turbulence intensities can be very large. Spatial and temporal fluctuations in the velocity field cause bending moments and vibrations that affect machine performance and reliability. Furthermore, as the blades rotate through air moving at different speeds and directions they are subjected to varying loads. All of these factors have to be considered in any description of the wind field to which the wind turbine is exposed (See, e.g., Connell, 1979; a detailed discussion of all the factors can be found in the same proceedings volume.)

Development of gust models to characterize the wind field has proceeded along two distinct lines. One approach uses statistics that can be derived from accepted turbulence definitions. The frequency of an event such as exceedance of the velocity fluctuation or velocity change with time (Cliff and Fichtl, 1978; Huang and Fichtl, 1979) beyond a prescribed limit is estimated indirectly from turbulence spectra and length scales. The other approach uses the statistics of discrete events defined on the basis of arbitrary criteria such as the time interval between zero crossings or successive positive and negative peaks (Ramsdell, 1975; Powell, 1979). The most promising of these models, GUST 0 and GUST 1, proposed by Powell (1979) involve a velocity amplitude and a corresponding time scale. A detailed comparison of various gust models is given by Powell and Connell (1980).

The Boulder Atmospheric Observatory (BAO) with its ability to collect and process turbulence data over a depth of 300 m for long observation periods has been useful for verifying the statistics used in some of the proposed gust models. In this report we examine in depth the characteristics of moments and probability distributions for two highwind episodes observed at the BAO.

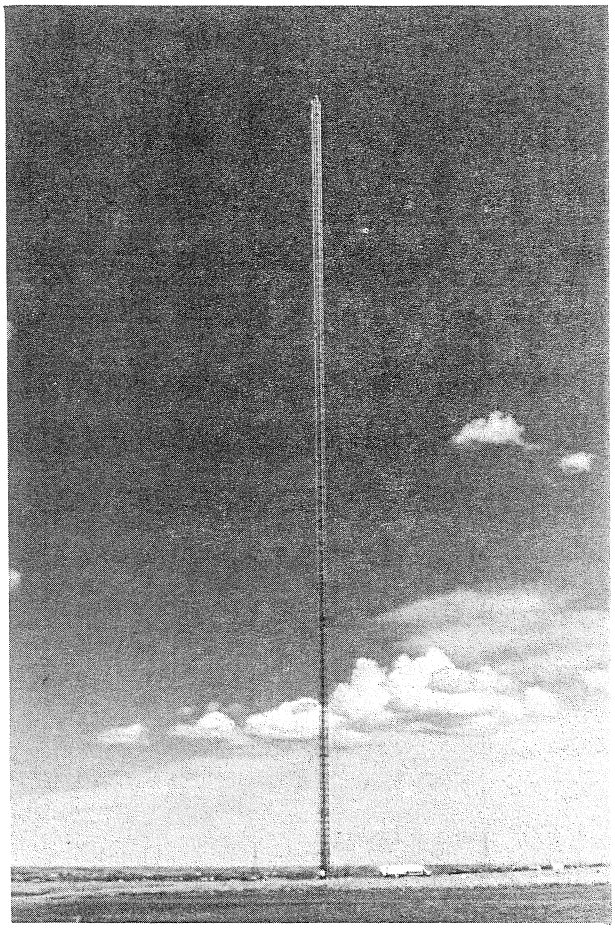

Figure 2.1--Instrumented 300-m tower at the Boulder Atmospheric Observatory.

2.0 THE BOULDER ATMOSPHERIC OBSERVATORY

The BAO is located on gently rolling terrain 25 km east of the foothills of the Colorado Rocky Mountains. This research facility operated by the Wave Propagation Laboratory of NOAA is designed to provide high-quality measurements of atmospheric turbulence for boundary layer studies and for calibration and comparison of atmospheric sensors. Installations at the site include a 300-m instrumented tower (Fig. 2.1), a variety of remote sensors, and a computer system that controls the acquisition and processing of data. The contour map of the immediate surroundings (Fig. 2.2) reveals small-scale undulations superimposed on a mean slope downward from south to north. The rolling nature of the terrain is highlighted by the exaggerated vertical scale in the three-dimensional terrain profile of Fig. 2.3.

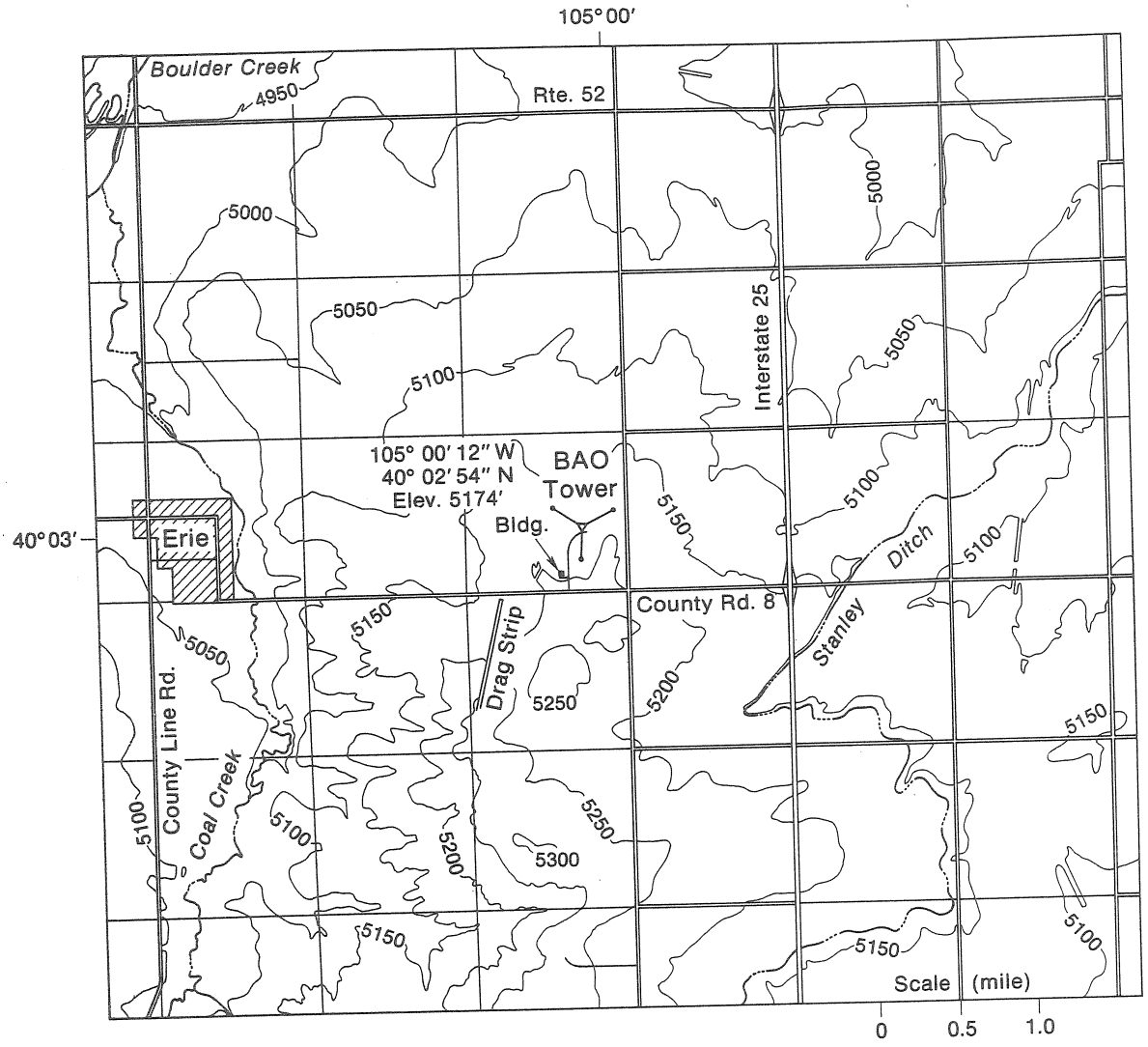

Figure 2.2--Topographical map of the area around the Boulder Atmospheric Observatory. Height contours are in feet.

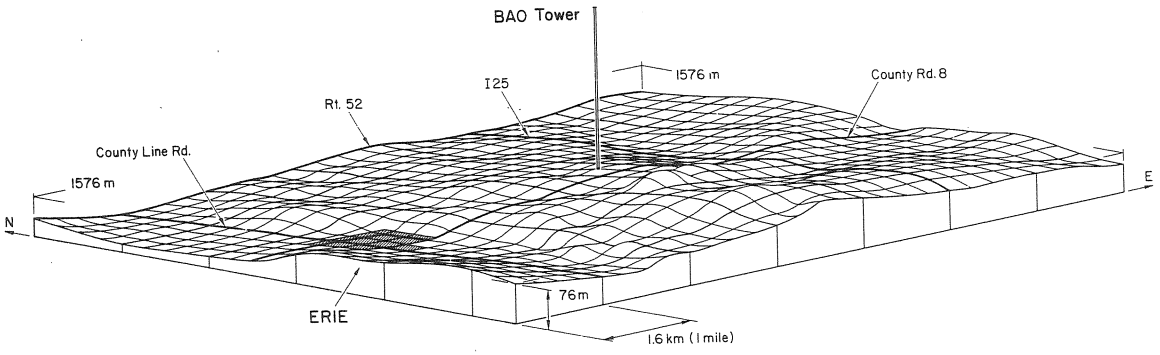

Figure 2.3--Three-dimensional terrain profile of area shown in Fig. 2.2.

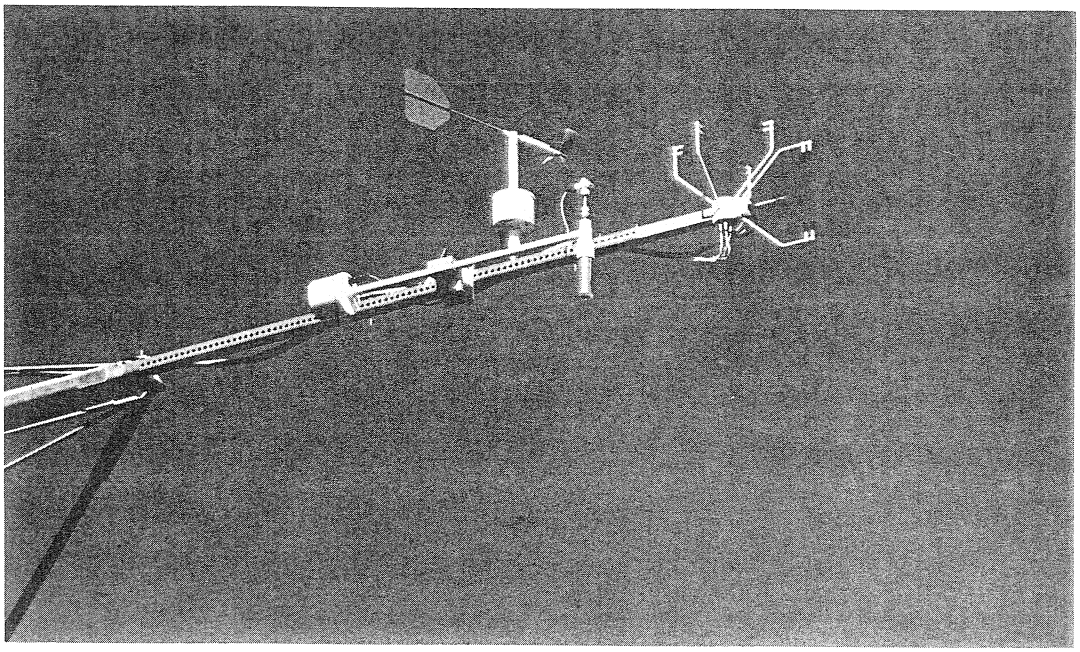

Figure 2.4--View of instruments on the SSE boom during the September 1978 "PHOENIX" experiment. The three-axis sonic anemometer is shown with the fast-response temperature probe mounted in the vertical array. The propeller-vane anemometer and the slow-response quartz thermometer (in the aspirated radiation shield) are mounted farther back on the boom.

The BAO tower is a guyed open-lattice structure of galvanized steel. It has a constant triangular cross section with 3-m spacing between the legs. The eight fixed levels of instrumentation on the tower are at heights 10, 22, 50, 100, 150, 200, 250, and 300 m. Sensors are mounted on two retractable 4-m booms at each level. Each boom is attached to a large hinged support with fine adjustments for precise leveling.

The eight levels are instrumented identically. A three-axis sonic anemometer mounted at the end of the SSE boom (Fig. 2.4) measures the mean and turbulent fluctuations of the wind along three orthogonal axes. A fine platinum wire probe attached to the sonic vertical array measures fluctuations in temperature. Mean temperature is measured by a quartz thermometer housed in an aspirated glass shield. The propeller-vane anemometer shown on the SSE boom in Fig. 2.4 was moved to the NNW boom between the first and second high-wind episodes discussed here. A cooled-mirror hygrometer (not shown) is mounted on the NNW boom for

measuring dew point temperatures. Further details of the instrumentation can be found in Kaimal (1978a).

The tower sensors of particular significance to this study are the sonic and the propeller-vane anemometers. The sonic anemometers include a mix of EG&G Model 198-2 two-axis probes and Ball Brothers[1] Model 125-198 two-axis and Model 125-197 single-axis probes. The sonic anemometer probes have a path length of 25 cm; their outputs are sampled at a 10-Hz rate. The propeller-vane anemometer is the "ruggedized" R.M. Young[2] Propvane Model 8002. Its polystyrene propeller has a distance constant of 2.5 m and a working range from 1 to 54 m/s. The speed and direction outputs from this sensor are sampled once per second.

The sonic anemometers on the tower use a fixed orthogonal array. Its two horizontal axes are aligned along and perpendicular to the boom (see Fig. 2.4); the vertical axis is mounted on the outer end of the array pointing away from the tower. Since the orientation of the anemometer axes is fixed with respect to the tower, the horizontal wind measurements are affected when the wind blows parallel to one of the axes.

An approximate functional form for the underestimation caused by the transducers is given by Kaimal (1980). Only the horizontal wind components are corrected for this error, since vertical wind inclination angles are seldom large enough to justify correcting the w component. Each data point sampled is corrected in real time using an algorithm that determines the magnitude of the correction from the ratio of the wind components measured along the two horizontal axes. The maximum correction for the winds along either axis is 13%, decreasing linearly with angle to zero at 75 deg.[3] The net effect of this correction is a

[1]The three-axis version of this array and associated electronics are now available commercially from Applied Technology, Inc., Boulder, Colorado.

[2]R. M. Young Company, 2801 Aeropark Drive, Traverse City, Michigan.

[3]This correction is a function of the transducer diameter-to-path-length ratio and may vary with probe design. The ratio in this probe is 1:25.

7% to 8% increase in variance spread uniformly over the entire spectral bandwidth.

Acquisition of data from the sensors is controlled by a PDP 11/34 computer at the BAO site. Real-time computations of means, variances, covariances, and Obukhov lengths are made for each consecutive 20-min period and recorded both on a line printer and a digital magnetic tape unit. The raw data from the sensors are also recorded on tape. To minimize tape storage only 10-s averages and 10-s grab samples (last sample in each 10-s period) are transmitted to Boulder for archiving. The high-frequency information lost by not saving the entire time series is preserved, however, in the form of smoothed spectral estimates, block-averaged to yield approximately seven logarithmically spaced estimates per decade. This spectral information is also transmitted along with other data for use in reconstructing the high-frequency end of spectra computed later from the 10-s averaged data points.

The information transmitted through phone lines feeds into a larger multiuser computer system centered on a PDP 11/70 in Boulder, where it is stored temporarily on disk for immediate use and later (a few days to a week) archived on magnetic tape.

The archiving scheme is designed for easy and rapid retrieval of data. Standard programs are available for inspection of the data. Some print numerical summaries, and others produce graphs. The search procedure for archived data is facilitated by a descriptor file in the computer. The descriptor, which consists of low-resolution (20-min averaged summary) data from all channels, with accompanying defect codes indicating the quality of information in each channel, is stored permanently in the computer. Details of the interactive access to the BAO data are given by Lawrence and Ackley (1979).

The data sets used in this report were prepared from the raw data tapes where the full time resolution of the system is retained. All the analyses described were performed on the PDP 11/70 computer using programs and subroutines specially developed for this project.

3.0 DESCRIPTION OF DATA

The two cases chosen for this study are fairly typical of the downslope wind storms observed along the Front Range of the Rocky Mountains. Several such high-wind episodes occur throughout the year, although they tend to be more frequent during the winter months. The two cases designated A and B in this report were associated with widely different static stabilities. The mean profiles of wind speed, wind direction, and temperature in Fig. 3.1 show how different conditions were for the two cases.

Case A occurred on 11 September 1979 during the PHOENIX Experiment conducted at the BAO. High winds persisted for over 24 h starting at about 1000 MST. Four hours of this episode were selected for analysis. Figure 3.2 shows the 20-min averaged speeds and directions for two heights for the entire period. (Data points represent averages for the following 20 min.) The temperature lapse rate stayed near-neutral during this period.

Case B, which occurred during the early hours of 5 December 1979, was a much shorter wind storm than the one observed in September. The wind speeds were higher, and, despite the strong mixing that the winds produced, a strong inversion persisted below 100 m (see Fig. 3.1). The speed and direction plots in Fig. 3.3 reveal a highly nonstationary period which includes a 20-deg shift in wind direction[1] and a near-sinusoidal rise and fall in wind speed.

The synoptic conditions associated with the two wind storms were not unusual for the time of year they occurred. Case A represents a typical chinook produced by an intensification of east-west pressure gradient over the mountains, which often accompanies the passage of a cold front. Upper-air flow was from the southwest. The pressure

[1]The direction shift occurred gradually over the 20-min period, so the shift reflected in Fig. 3.2 is a fair representation of the actual rate of change in direction.

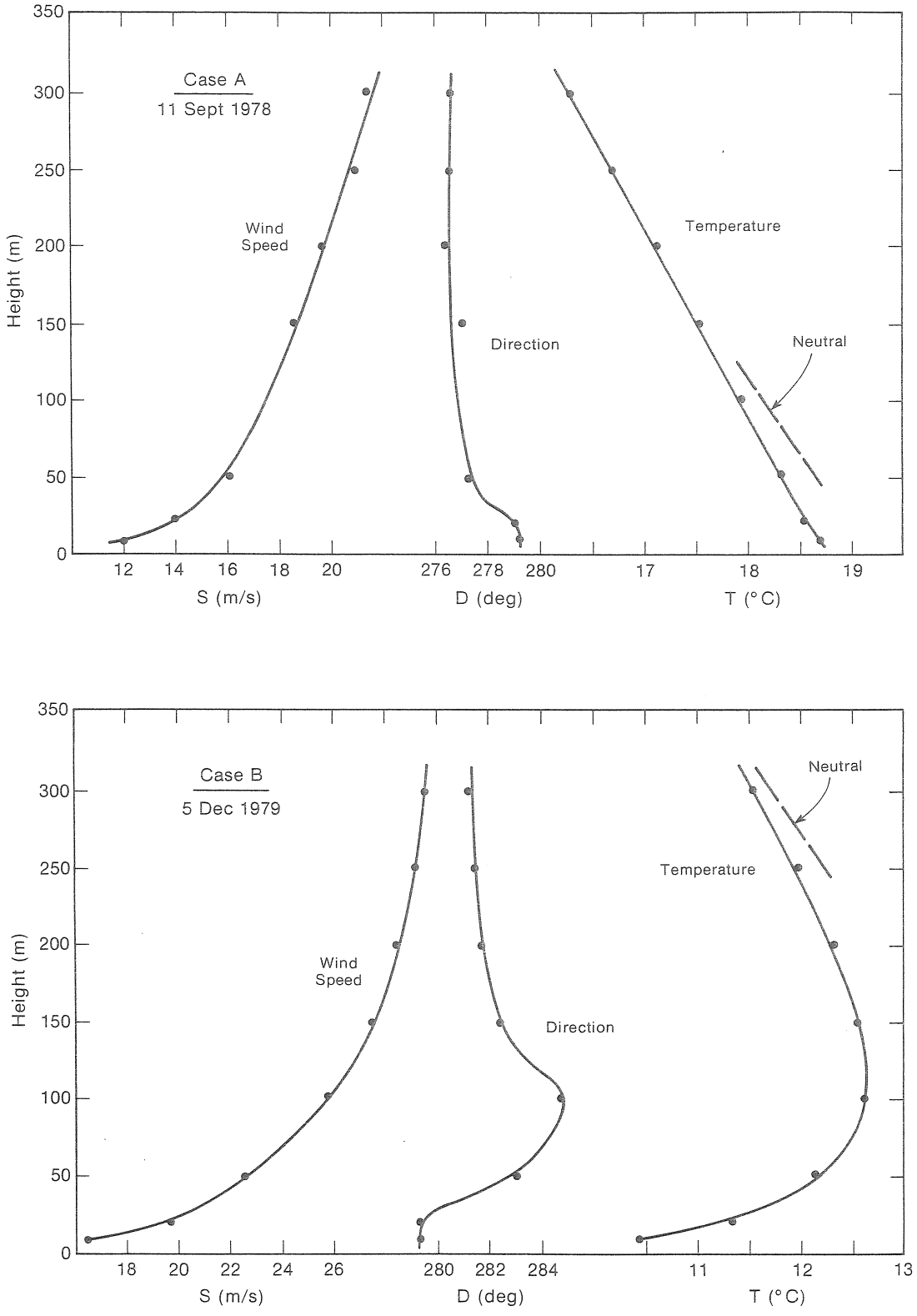

Figure 3.1--Mean wind speed, wind direction, and temperature profiles for two high-wind episodes observed at the BAO. Cases A and B represent different but fairly typical conditions associated with high winds along the Front Range of the Rocky Mountains. (Case A duration: 1600-2020 MST; Case B duration: 0040-0400 MST.)

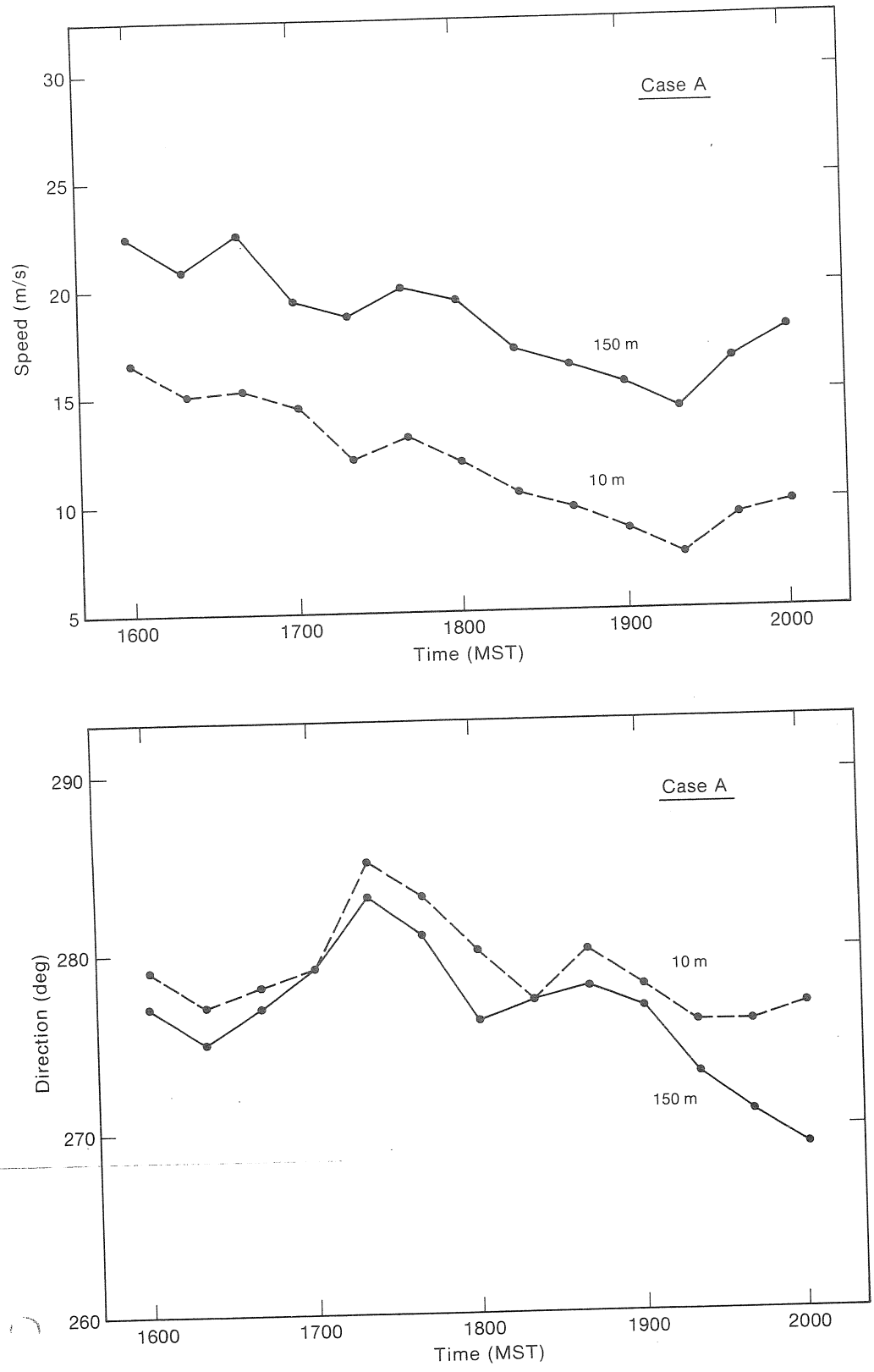

Figure 3.2--Plots of 20-min averaged wind speeds and directions at 10-m and 150-m levels for Case A. Each data point represents average for the succeeding 20-min interval.

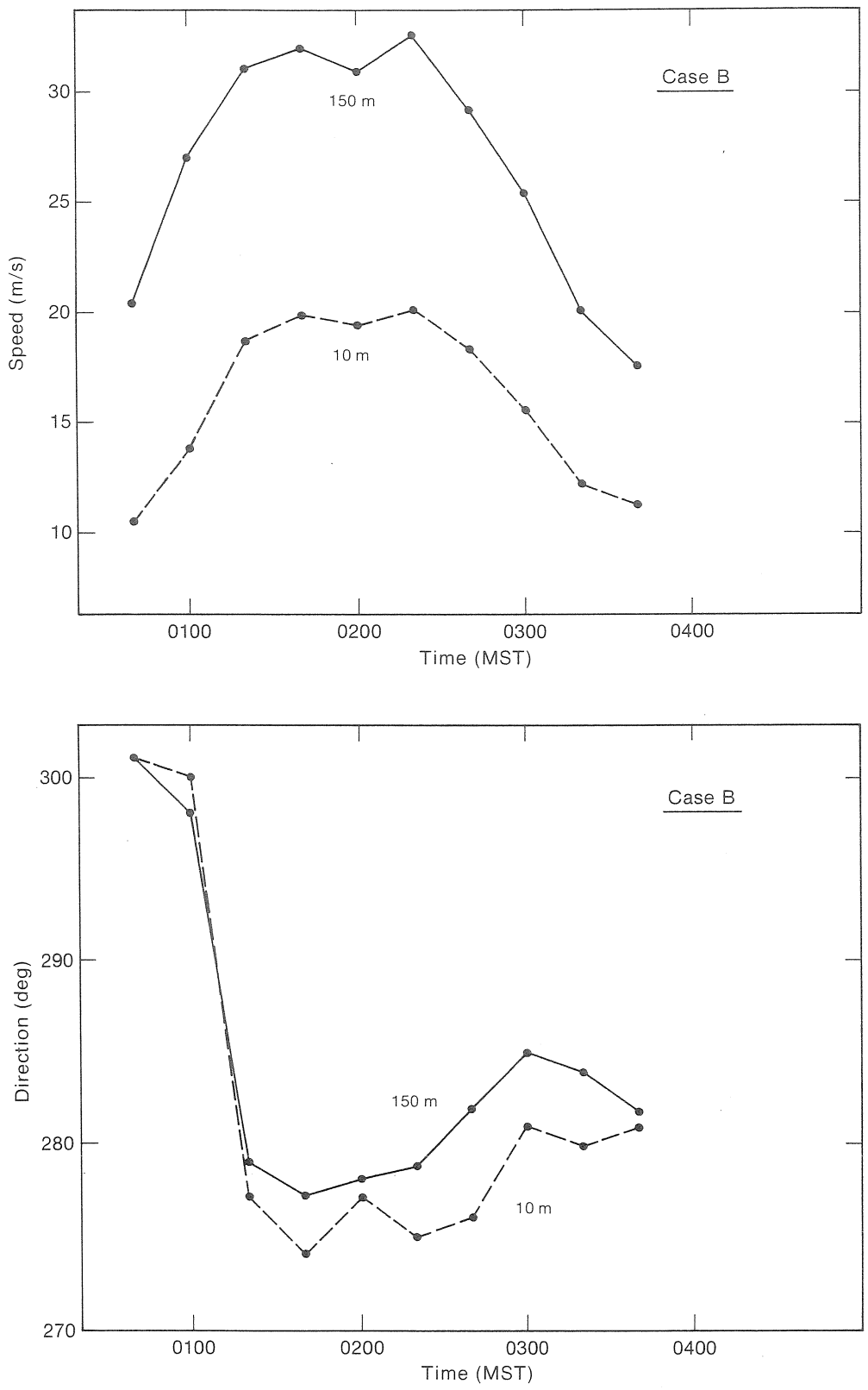

Figure 3.3--Plots of 20-min averaged wind speeds and directions at 10-m and 150-m levels for Case B. Each data point represents average for the succeeding 20-min interval.

pattern moved very slowly westward, causing the storm to persist for a long period. By contrast, Case B was more typical of a bora, which is a cold downslope wind of short duration. The winds in this case were caused by an upper air jet dipping down as it crossed the mountains. A surface low had formed in eastern Colorado, and the jet was drifting southward rapidly. Upper air winds were predominantly from the northwest, and account for the cold temperatures and stable stratification near the ground.

The data set for Case A consists of sonic anemometer outputs sampled 10 times a second from the four lowest levels: 10, 22, 50, and 150 m. (The 100-m measurements were not used because of suspected noise contamination in one of the axes.) For Case B, only the propeller-vane data are used since the combination of cold temperatures and high winds introduced noise spikes in the sonic anemometer data. Compatibility between the propeller-vane and sonic anemometer statistics was established by comparing results from both types of instruments. When subjected to the same filtering, the variances, skewness, and kurtosis from the two instruments showed very little difference. The compatibility was further enhanced by subjecting the sonic anemometer measurements to a 1-s nonoverlapping average to produce a time series similar to that obtained from the propeller-vane anemometer.

Sonic anemometers and propeller-vanes provide different types of information. The former yield wind components, and the latter yield wind speed and direction. Since the wind turbine generators are designed to face the mean wind, speed and direction are obviously the wind parameters they respond to. We therefore converted the sonic anemometer horizontal wind components to speed and direction for all the analysis described here. It is generally recognized that the spectral characteristics of speed and direction very closely approximate those of the longitudinal (u) and lateral (v) wind components. Powell and Connell (1980) report wind speeds to be only 3% greater than the u-component variance and the direction variance to be within 0.5% of that obtained by dividing the v-component variance by the square of the mean horizontal wind speed.

The spectra of speed and direction measured at 10 m and 150 m are shown in Fig. 3.4 (Case A) and Fig. 3.5 (Case B). Because of the higher sampling rate in the sonic anemometers, the spectra extend a decade higher in Case A than in Case B. The spectral behavior in this region is fairly predictable, so the high-frequency end in Case B may be approximated with reasonable certainty. The dashed lines in Fig. 3.5 follow the -5/3 power law predicted by Kolmogorov for the inertial subrange. (In our spectral representation, this power law appears as a -2/3 slope.) Included in Fig. 3.4 are the vertical velocity (w) spectra for 10 m and 150 m; this information is available from the sonic anemometers for Case A but not for Case B.

The inertial subrange represents the region of the spectrum where turbulent energy is neither produced nor destroyed, but handed down from the larger to the smaller eddies. In this region, all three components of velocity follow the -5/3 power law. Also, the turbulent field is locally isotropic (i.e., no preferred direction for eddies on that scale) with vanishing covariance between the different velocity components. The limiting wavelength on the low-frequency side is controlled by stability and the height above ground. The spectral maximum, farther down on the frequency scale, represents the region where energy is being produced by mechanical and buoyant forces, while farther up the scale, beyond the range of our spectral computations, energy is dissipated in the form of heat. Where turbulent energy is being produced, the spectrum slope tends to be shallower than in the inertial subrange, whereas in the region where energy is being dissipated, the slope tends to be steeper. The higher spectral energy in the w component, compared with the speed spectrum within the inertial subrange, is a consequence of isotropy. In our one-dimensional spectral representation (i.e., spatial cut of the turbulent field along the streamwise direction), the inertial subrange energy in the crosswind components (w and v) will appear 4/3 as high as the energy in the streamwise component (u). To the extent that the speed spectrum approximates the u spectrum, this condition is satisfied with respect to w in Fig. 3.4 at wavelengths $\lambda \leq 0.5z$, where λ is the wavelength ($\simeq \bar{u}/n$) and z is the height above ground.

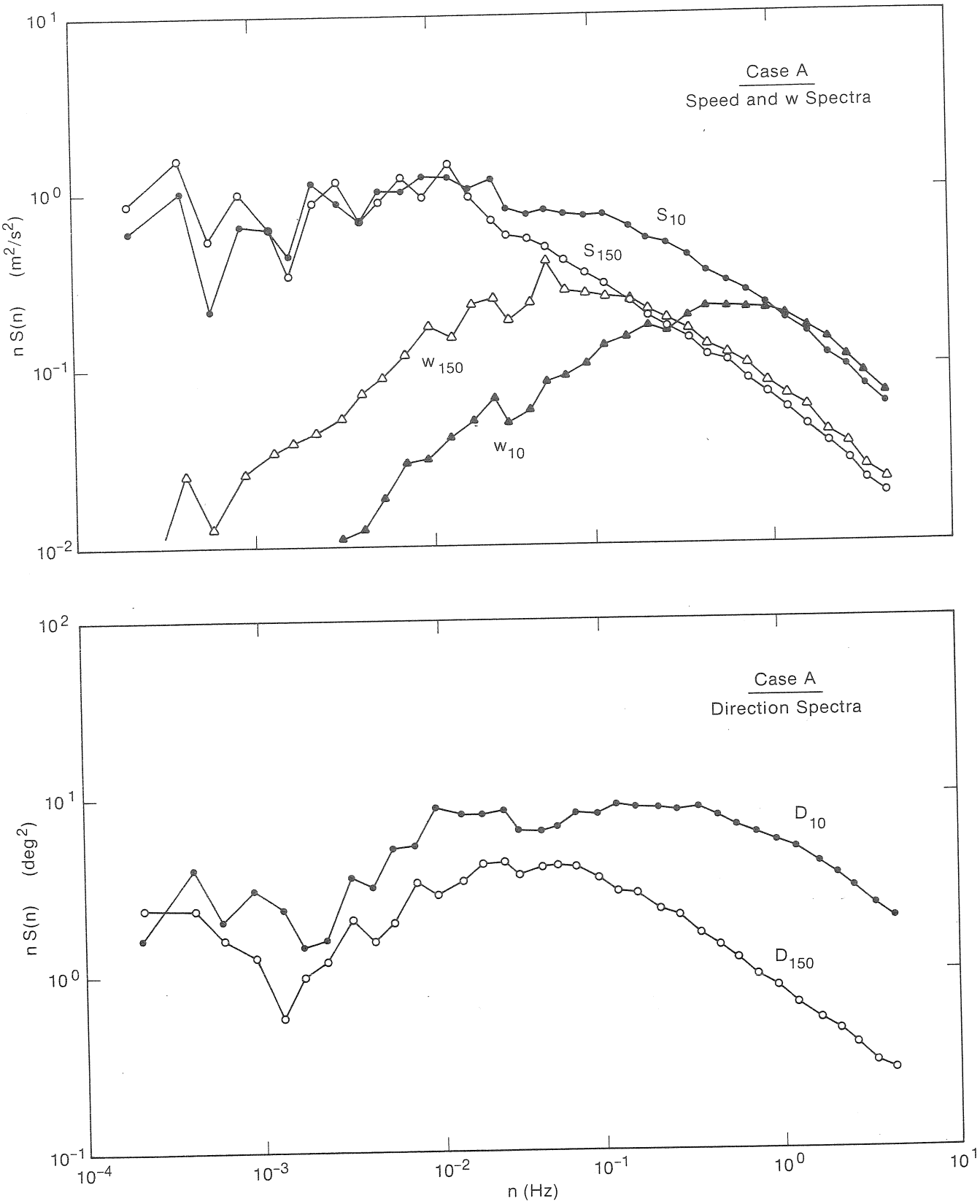

Figure 3.4--Logarithmic spectra of wind speed, w, and direction at 10-m and 150-m levels for Case A.

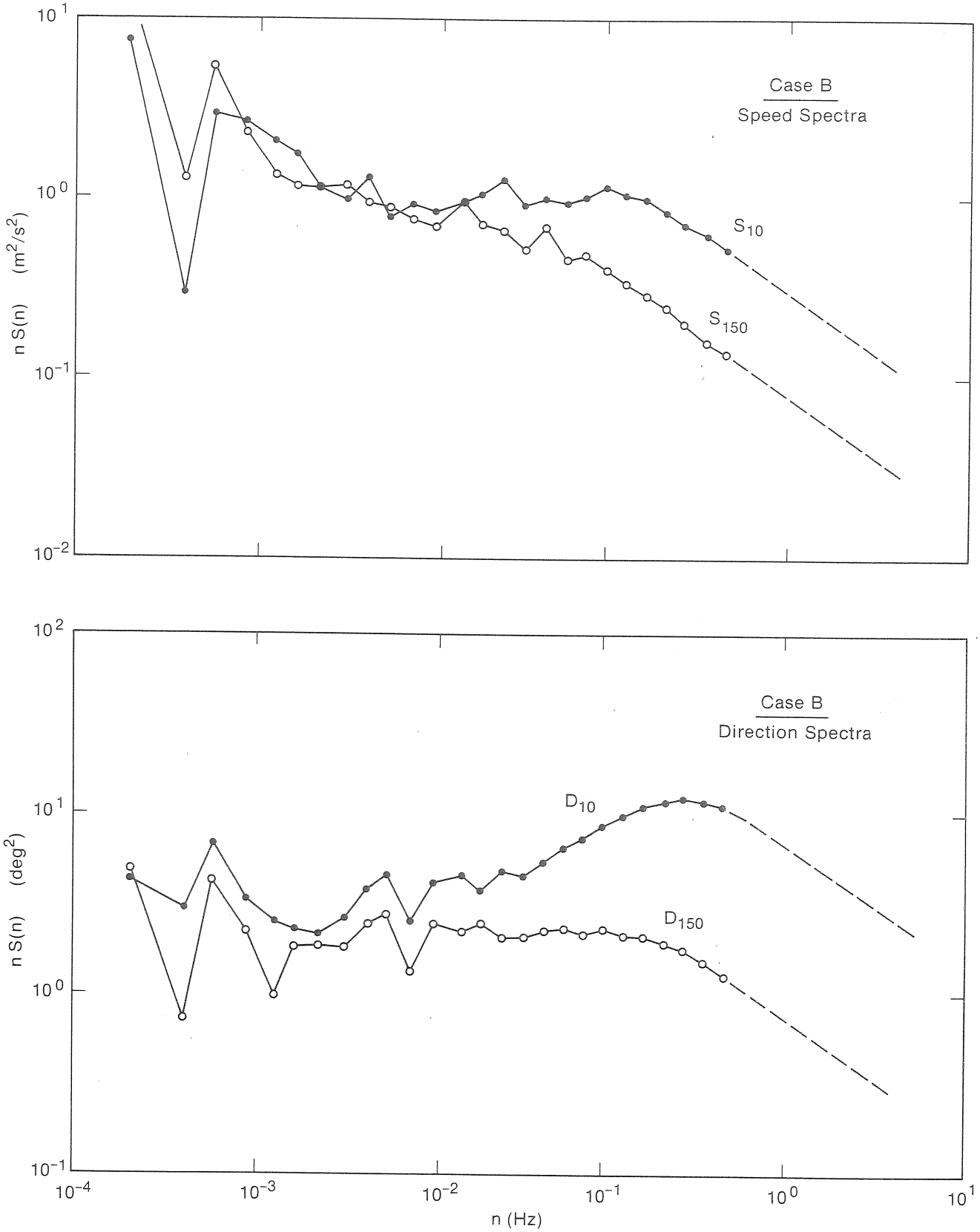

Figure 3.5--Logarithmic spectra of wind speed and direction at 10-m and 150-m levels for Case B.

The limiting wavelength λ_i for the inertial subrange normally approaches 0.5z only in an unstable boundary layer (Kaimal et al., 1972). As the atmosphere becomes stably stratified, λ_i becomes a function of stability as well (Kaimal, 1973). Another feature of the spectra in Fig. 3.4 that suggests a slightly unstable lapse rate is the constancy in the speed spectral peak with height. The wavelength at the spectral maximum, λ_m, remains constant at about 1.8 km between 10 and 150 m. In a convectively unstable boundary layer, λ_m for u and v scales with the height of the boundary layer (Kaimal, 1978b), but in the absence of a conventional boundary layer in Case A it is difficult to verify that relationship. The wavelength of the peaks observed here is typical for a daytime boundary layer roughly one 1 km deep.

In contrast to the indications provided by the speed spectrum, the peaks of the w and direction spectra in Fig. 3.4 behave as if the atmosphere is slightly stable (almost neutral). Here, λ_m for w is smaller than the usual value of 5.9z observed in an unstable atmosphere, and λ_m for direction varies with height as in a slightly stable layer. We find $\lambda_m \approx 2z$ and 5z, respectively, for w and direction.

An interesting point to note in Fig. 3.4 is the presence of a spectral gap centered around 10^{-3} Hz in both speed and direction. This gap indicates a separation between the scales associated with boundary layer turbulence and the larger mesoscale features of the wind field. The upward swing in the spectra below 10^{-3} Hz is produced by the downward trend in the time series (Fig. 3.2).

The trends are even more pronounced in Case B (Fig. 3.3), and their effect on the spectra extend to 10^{-2} Hz in Fig. 3.5. Consequently, the spectral gap is not as obvious as in Case A. However, the spectral peaks for at least the 10-m level can be identified and the relationship between λ_m and z examined. We find $\lambda_m = 10z$ and 3z respectively for speed and direction, corresponding to values one might expect in moderately stable layers ($z/L \sim 0.2$) under quieter conditions. Actual values of z/L ranged from 0.05 to 0.2 during the period.

No particular significance is attached to the peaks and valleys at the low-frequency end of the spectra in Fig. 3.5. These features are reproduced almost identically at all levels between 10 and 150 m. They reflect the finer details of the spectral content in the trends and cannot be attributed to computational uncertainties in the spectrum analysis.

For the reader interested in relating spectral behavior to the appearance of the actual time series, we present the first 20 min of the speed and direction fluctuations (deviations from the 20-min mean) in Figs. 3.6 and 3.7. In Case B, the amplitudes of the speed fluctuations are distinctly smaller than in Case A even though the direction amplitudes are larger, not an unusual occurrence in stable layers. However, the amplitudes of the speed fluctuations do increase with mean wind speed and approach their maximum values an hour later.

These descriptions of the two cases are intended to serve as background for interpreting the distributions and moments presented in this report. The spectral properties of the wind field, by themselves, appear to be of limited value in WECS design, although idealized spectral forms have been used for calculating the frequency of occurrence of gust events through Rice's equation (Powell and Connell, 1980). Bandpass filtering appropriate to the response characteristics of the device is the key to deriving parameters needed for the design of wind turbine generators. Our analysis therefore includes results for a range of filter options. These ranges can be identified in the spectral plots.

Not included in this report are the effects of wind shear on the propeller blades. Direction shears do not appear to be very significant, but the vertical speed gradients (5 m/s per 100 m for Case A and 7 m/s per 100 m for Case B) must seriously alter the spectral content of the wind field sensed by each propeller blade as it rotates. This problem is being addressed by Connell (1980) and Doran and Powell (1980).

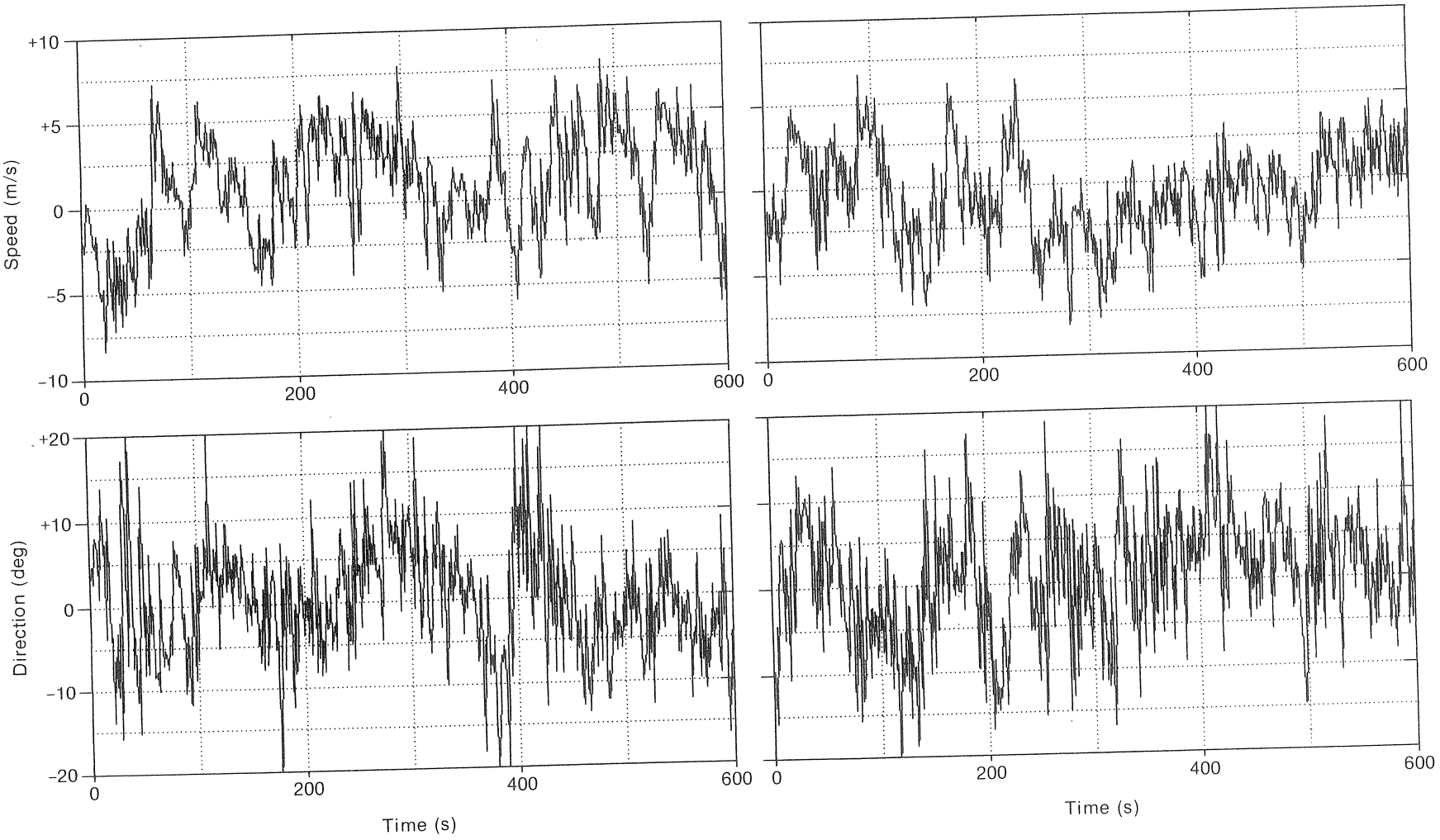

Figure 3.6--Plots of 1-s averaged data points of wind speed and direction fluctuations at 10 m for the first 20 min from Case A (1600-1620 MST).

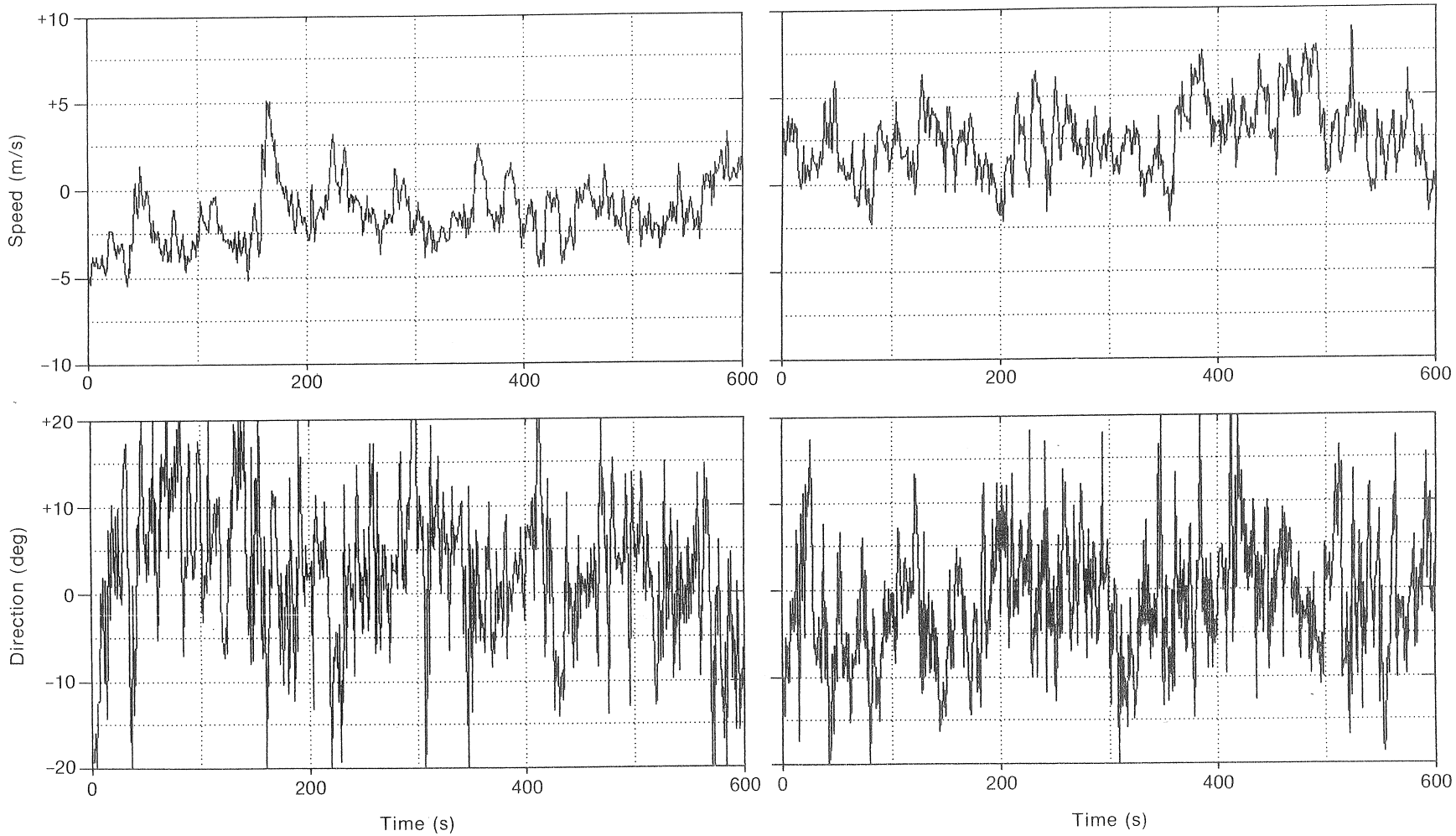

Figure 3.7--Plots of 1-s sampled data points of wind speed and direction fluctuations at 10 m for the first 20 min from Case B (0040-0100 MST).

4.0 OUTLINE OF ANALYSIS

The data set prepared for this study consists of wind speed and wind direction measurements from three heights (10, 50, and 150 m) in the form of discrete data points spaced 1 s apart. In Case A the original 10-Hz samples were block-averaged (see Chapter 3 for details) to achieve high-frequency smoothing comparable with the smoothing inherent in the 1-Hz propeller-vane data used in Case B. With the three heights chosen, we cover the wind field near the ground, at hub level, and near the top of the surface shear layer.

From these data several more time series were generated. The first set of operations performed involves bandpass filtering to simulate the response of the WECS to fluctuations in the wind speed and direction. Three passbands, each a decade wide, simulate the response of systems with slightly different characteristics. In Fig. 4.1 these filters are represented by designations 30/3, 50/5, and 100/10, where the first number in each group represents the half-power point on the highpass side of the filter and the second number the half-power point on the lowpass side. The numbers are the widths, in seconds, of the running means used in the highpass and lowpass filters, respectively. First, the original time series are averaged with a moving average filter of width τ_ℓ to remove frequencies higher than $1/\tau_\ell$ Hz (where τ_ℓ = 3, 5, or 10 s). The new time series thus created were then differenced from a moving average of width τ_h to remove frequencies smaller than $1/\tau_h$ Hz (where τ_h = 30, 50, or 100 s). The resulting time series are used for calculating the statistical properties of the WECS response. Doran and Powell (1980) give algorithms for this type of digital filtering.

The rationale for bandpass filtering to simulate WECS response stems from the assumption that fluctuations of very long and very short periods have little, if any, effect on the performance of the system. Spatial averaging of the wind fluctuations by the propellers diminishes WECS sensitivity to small-scale eddies, and the ability of the system to adjust to slow changes in wind speed and direction through blade pitch control

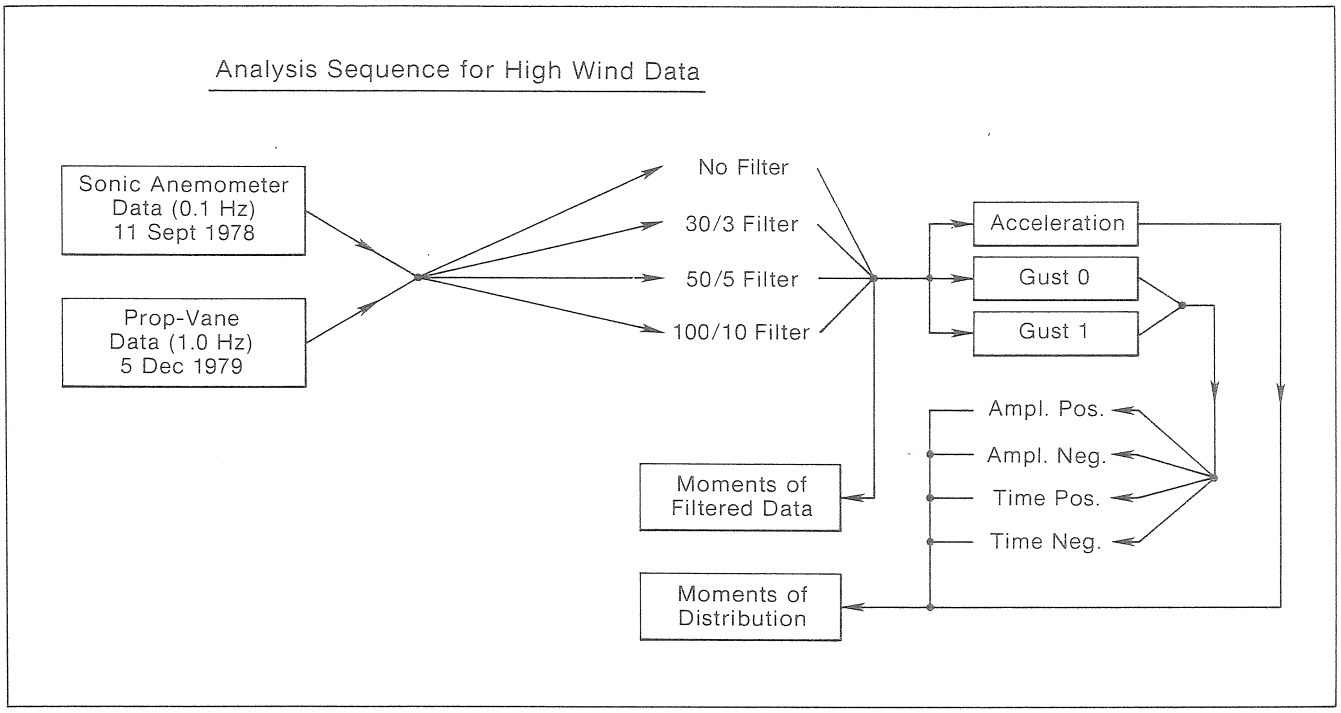

Figure 4.1--Flow chart showing analysis procedure for Case A and Case B data.

and rotation into the wind diminishes its sensitivity to the large eddies. Doran and Powell (1980) note that the gust statistics are relatively insensitive to highpass filtering for filter times longer than 100 s (probably the result of the spectral gap between 10^{-2} and 10^{-3} Hz). For moderately strong winds the averaging distance for a large propeller corresponds to roughly 3 s, which also happens to be the smallest convenient filter width for lowpass filtering. Our three bandpass filters are therefore confined to a window between 3- and 100-s periods. Centered within this window is the basic 50/5 filter of Powell and Connell (1980).

Each of the four sets of time series yields its own probability distributions, means, standard deviations, skewness, and kurtosis. In addition, the time series are converted to gust parameters appropriate to three gust models: 1) the acceleration (speed and direction difference) model, 2) the GUST 0 model, and 3) the GUST 1 model. Probability

distributions for each of the gust models are computed as well. The result is an enormous array of plots and tables. A major challenge the authors face is condensing the information in a way that makes it both accessible and useful to design engineers.

The acceleration model uses five distinct differencing intervals: Δt = 1, 3, 5, 10, and 30 s. Although all Δt intervals can be analyzed, only intervals equal to or larger than the lowpass interval τ_ℓ yield useful information; the moving average effectively filters out differences across intervals of shorter duration. The differenced time series available for analysis are listed in Table 4.1

Table 4.1--Differenced time series available for analysis

	Differencing Interval (s)				
Filter	1	3	5	10	30
none	x	x	x	x	x
30/3		x	x	x	x
50/5			x	x	x
100/10				x	x

The GUST 0 and GUST 1 models define gust events in terms of gust amplitudes and characteristic times. Definitions of amplitudes and times differ for the two models (see Fig. 4.2).

The GUST 0 model can be completely specified in terms of a positive peak amplitude $+A_0$, and the time interval $+T_0$ between zero crossings on either side. It can also be specified in terms of a negative peak amplitude $-A_0$ and the corresponding time interval $-T_0$. Both definitions are expected to yield similar statistics. Powell and Connell (1980) combine both positive and negative values into one set for their analysis.

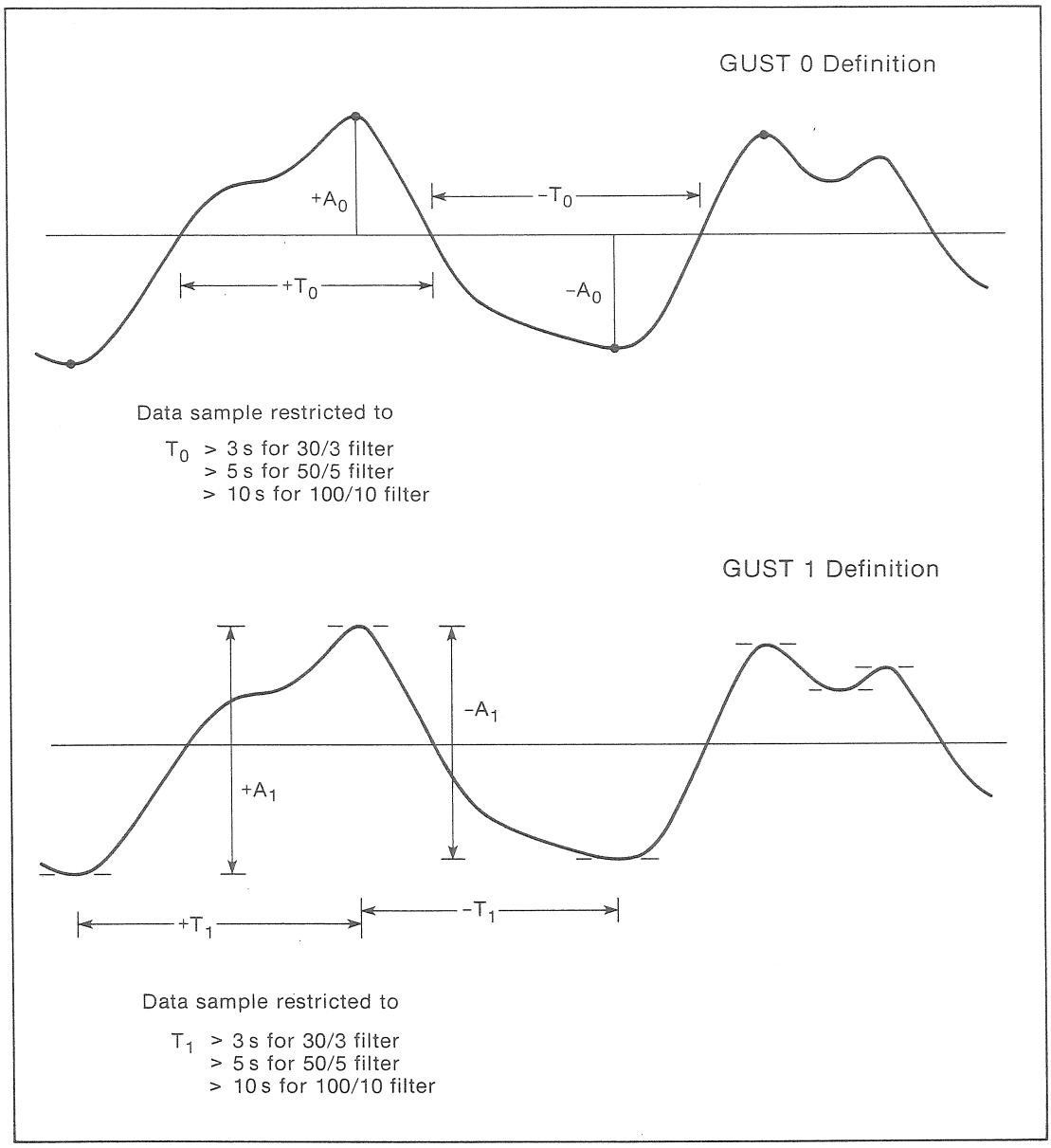

Figure 4.2--Definitions of GUST 0 and GUST 1 parameters.

The GUST 1 model can also be specified in terms of a positive amplitude $+A_1$ which is the peak-to-peak amplitude between adjacent minima and maxima, and a time interval $+T_1$ between the minima and the maxima; the positive sign indicates a positive rate of change in the variable. A comparable definition can be made in terms of amplitude

$-A_1$ and time $-T_1$, where the negative sign indicates a negative rate of change in the variable.

Thus, for each of these two discrete gust models, we have two subsets of events, defined in terms of positive and negative changes to describe the properties of the wind field. In preparing the subsets from the bandpass-filtered data, we imposed a lower limit for the time intervals, so that only T_0's and T_1's larger than τ_ℓ, the width of the lowpass moving average, were considered. This indirectly placed a lower limit on the A_0's and A_1's as well, since small amplitudes are more often than not associated with small time intervals. The parameters needed for WECS design are the root-mean-square values of the amplitudes and times. These are calculated from the means and standard deviations of A's and T's and listed as tables in subsequent chapters of this report.

5.0 EFFECT OF HEIGHT VARIATION AND CHOICE OF FILTER ON SPEED AND DIRECTION STATISTICS

Before we investigate the statistical properties of parameters mentioned in the previous chapter and their variation with height and filtering, it is important to understand how the basic time series themselves behave. Table 5.1 gives easy access to that information and permits direct comparisons between Case A and Case B.

The biggest variation, not surprisingly, is introduced by filtering. Between the unfiltered and filtered time series, the standard deviation drops a factor of 3 in wind speed and a factor of 2 in wind direction, the skewness drops to insignificant levels, and the kurtosis rises above 3, reaching values as high as 8.4 in Case B.

The drop in the standard deviation is obviously a consequence of removing contributions from large segments of the energy-containing region of the spectra. The smaller skewness values in the filtered data (indicative of a more symmetrical shape in the probability distribution) and the larger kurtosis values (indicative of a more peaked distribution) result from the exclusion of long-period fluctuations in the filtered time series.

Variations between filtered time series are not particularly significant. (The only exception to this observation is the behavior of the 150-m direction kurtosis in Case B; we interpret this as a reflection of the strong static stability present at the time.) On examining the variability with height, we find a small but systematic decrease in the standard deviations, but no such pattern can be found in the skewness or kurtosis. The 150-m direction kurtosis in Case B is an exception to that rule, but that level was clearly above the top of the surface inversion where the structure of the fluctuations can be expected to differ from the structure within the inversion.

Table 5.1--Variation in the statistical properties of speed and direction with height and choice of filtering. (All dimensions are in SI units.)

Statistical parameter	Variable	Height	Case A filters				Case B filters			
			None	30/3	50/5	100/10	None	30/3	50/5	100/10
Standard deviation	Speed	10	3.52	1.18	1.23	1.29	4.23	1.33	1.29	1.22
		50	3.68	0.97	1.08	1.22	4.88	1.17	1.17	1.14
		150	3.16	0.88	0.98	1.09	5.01	0.88	0.91	0.98
	Direction	10	7.34	3.76	3.62	3.53	7.60	3.66	3.13	2.69
		50	5.71	2.97	2.92	2.82	5.95	2.46	2.21	1.94
		150	5.04	2.58	2.57	2.45	5.15	1.95	1.90	1.84
Skewness	Speed	10	0.46	-0.05	0.01	0.07	-0.08	0.17	0.21	0.21
		50	0.41	-0.08	-0.03	0.02	-0.48	-0.15	-0.11	-0.04
		150	0.23	-0.10	-0.13	-0.14	-0.63	-0.16	-0.13	-0.10
	Direction	10	0.11	-0.02	0.01	-0.02	-0.16	-0.01	0.04	0.13
		50	0.20	0.05	0.06	0.09	-0.36	0.11	0.06	0.00
		150	0.17	-0.03	-0.11	-0.22	-0.19	0.13	0.05	-0.04
Kurtosis	Speed	10	2.66	3.60	3.53	3.56	2.59	3.38	3.34	3.15
		50	2.55	3.77	3.63	3.46	2.92	4.41	4.44	3.99
		150	2.52	3.88	3.81	3.57	2.44	5.44	4.86	4.24
	Direction	10	3.44	3.77	3.81	3.51	3.12	4.13	4.50	4.60
		50	3.27	3.51	3.55	3.66	2.86	5.12	5.16	4.62
		150	2.98	3.63	3.64	3.80	3.21	8.39	7.16	4.57

The frequency distribution plots presented in Figs. 5.1-5.12 offer a detailed view of how the large skewness and kurtosis values manifest themselves. For comparison, the true Gaussian distribution for the same variance is superimposed on the observed distribution. (Multiplication factor in parenthesis (e.g., x 10) converts numbers on the abscissa to SI units.) The asymmetry in the unfiltered time series is immediately apparent. That the distributions for Case A and Case B are skewed in opposite directions is not significant, being merely a consequence of the asymmetry in the long-term trend with respect to the overall mean value. Interestingly enough, the asymmetry in the frequency distribution is much less pronounced in the direction fluctuations than in the speed fluctuations. The absence of such asymmetry in the filtered distribution suggests that medium- and small-scale fluctuations are distributed evenly across both sides of their computed running means. Thus the assumption of a stationary Gaussian process, made in many gust models, has validity only for the filtered data, not for the unfiltered time series.

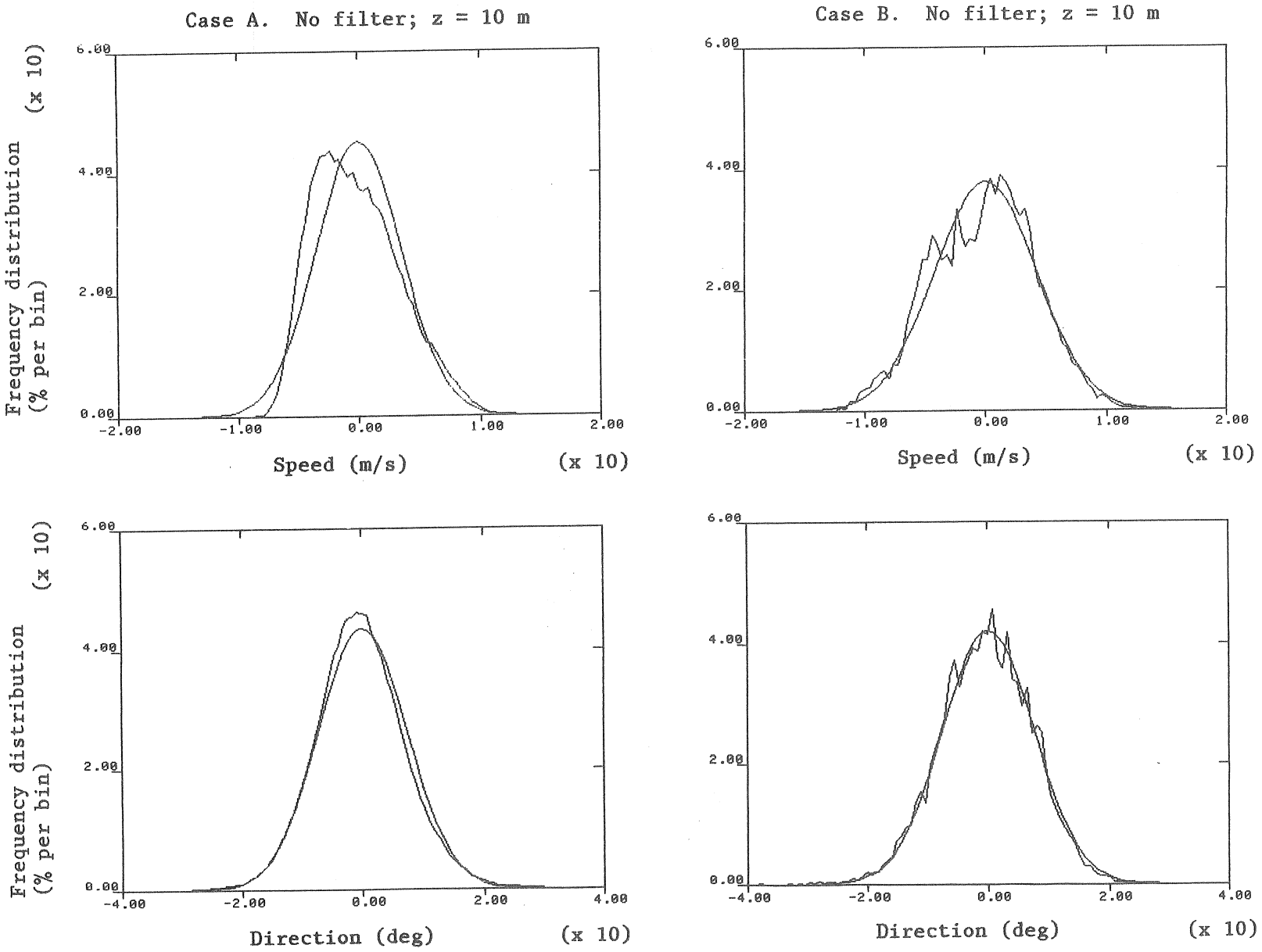

Figure 5.1--Distributions of speed and direction at 10 m (no filter). Bin sizes are ΔS = 0.4 m/s, ΔD = 0.8 deg. Superimposed for comparison are the ideal Gaussian distributions for the same variance.

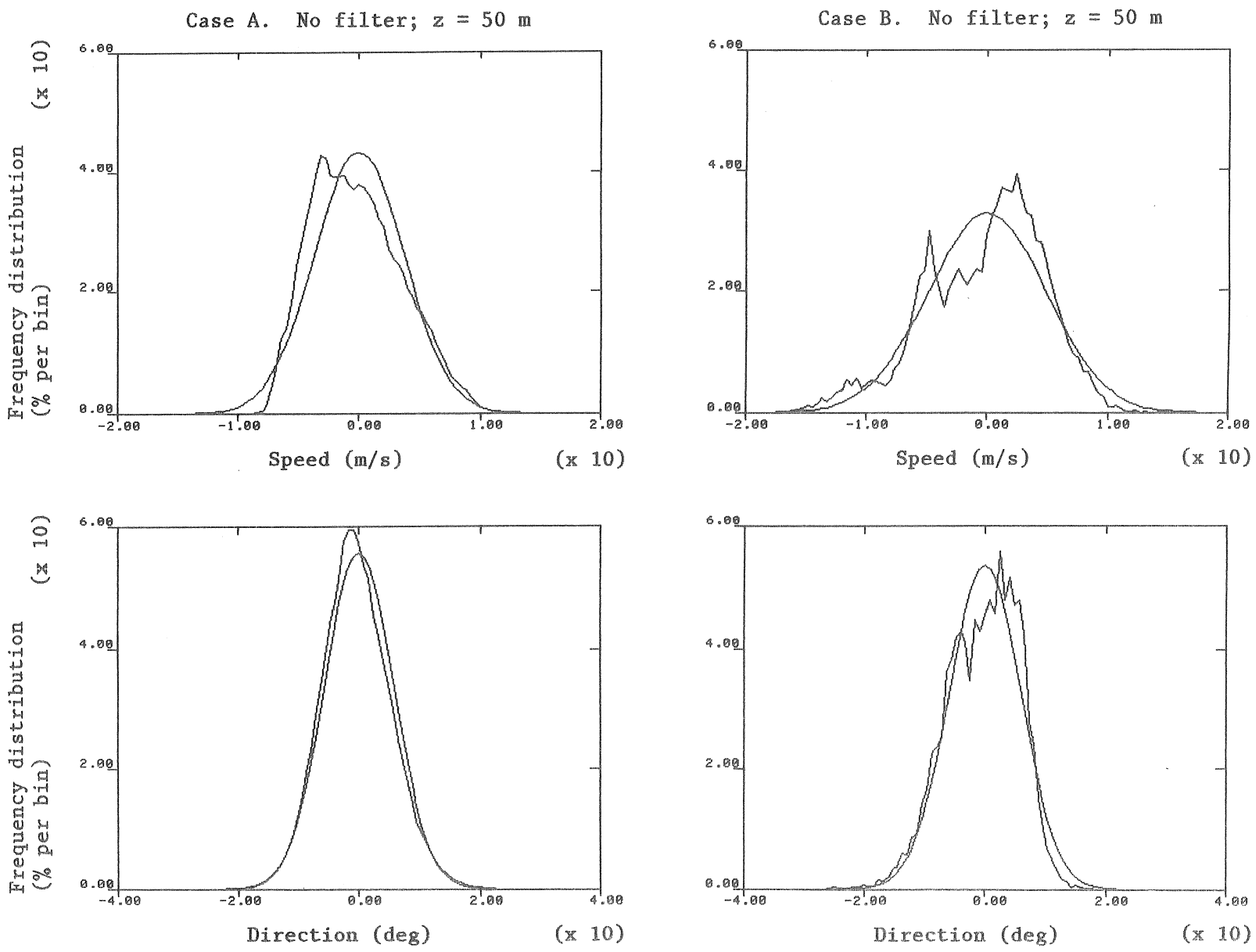

Figure 5.2--Distributions of speed and direction at 50 m (no filters). ΔS = 0.4 m/s; ΔD = 0.8 deg.

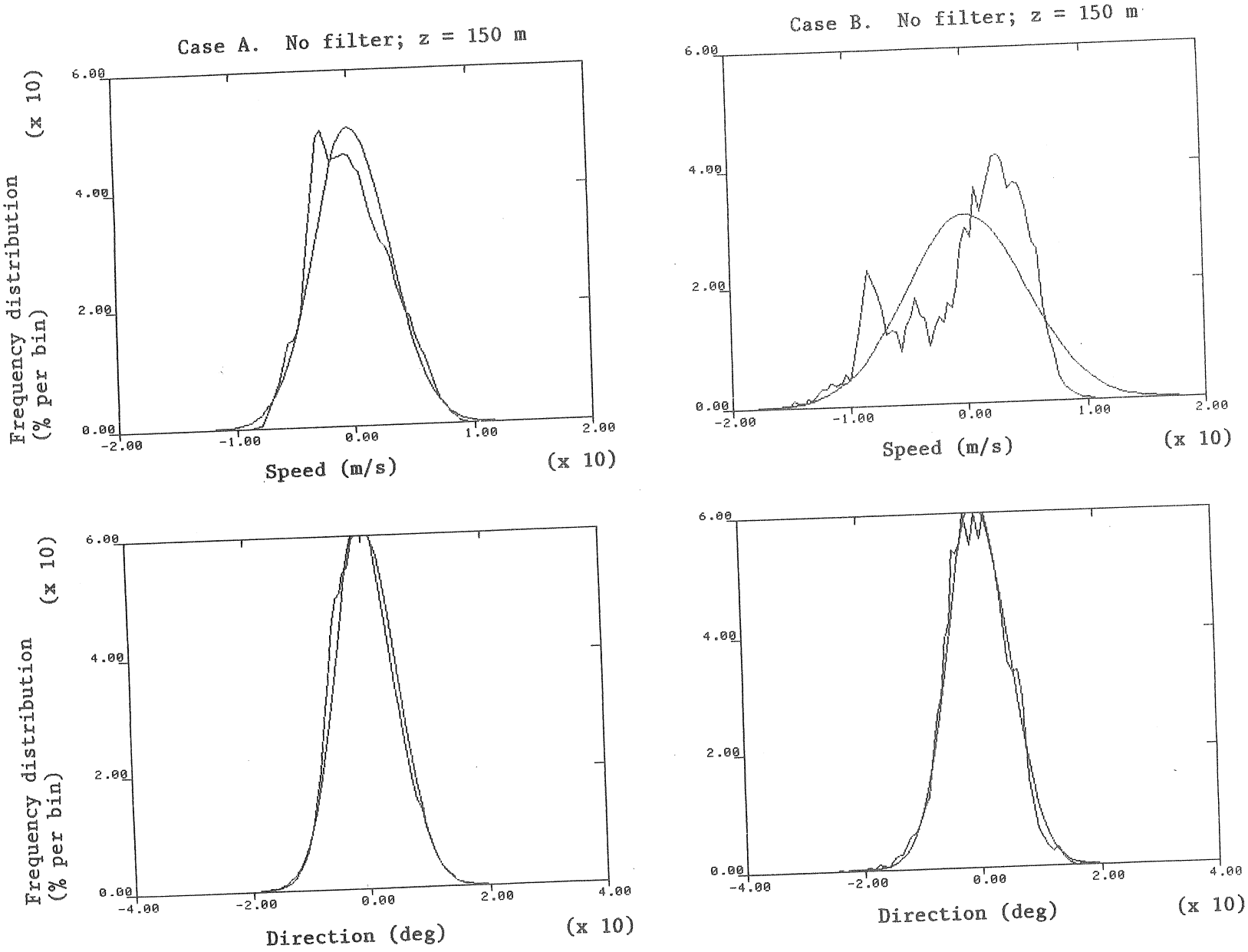

Figure 5.3--Distributions of speed and direction at 150 m (no filters). ΔS = 0.4 m/s; ΔD = 0.8 deg.

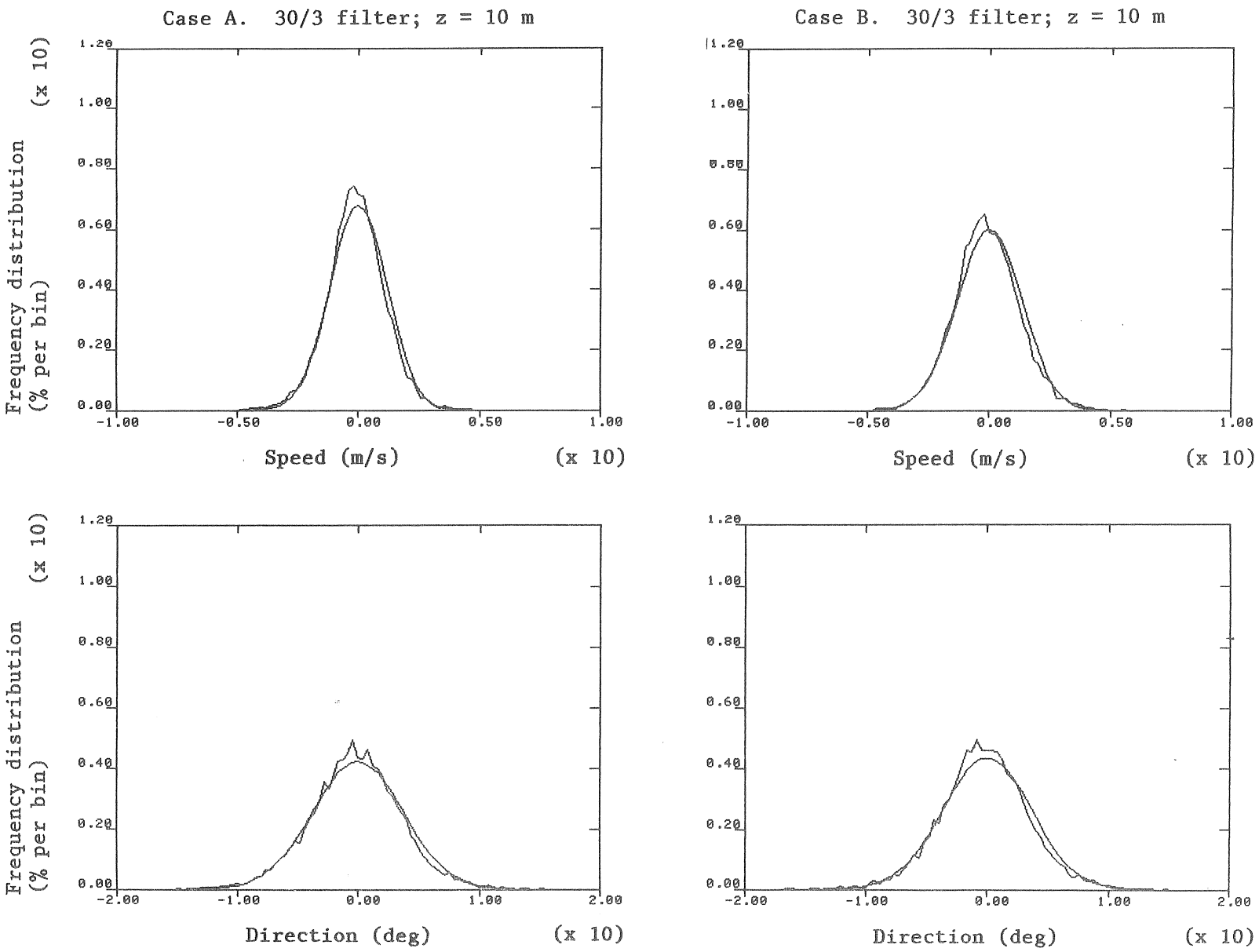

Figure 5.4--Distributions of speed and direction at 10 m (30/3 filter). ΔS = 0.2 m/s; ΔD = 0.4 deg.

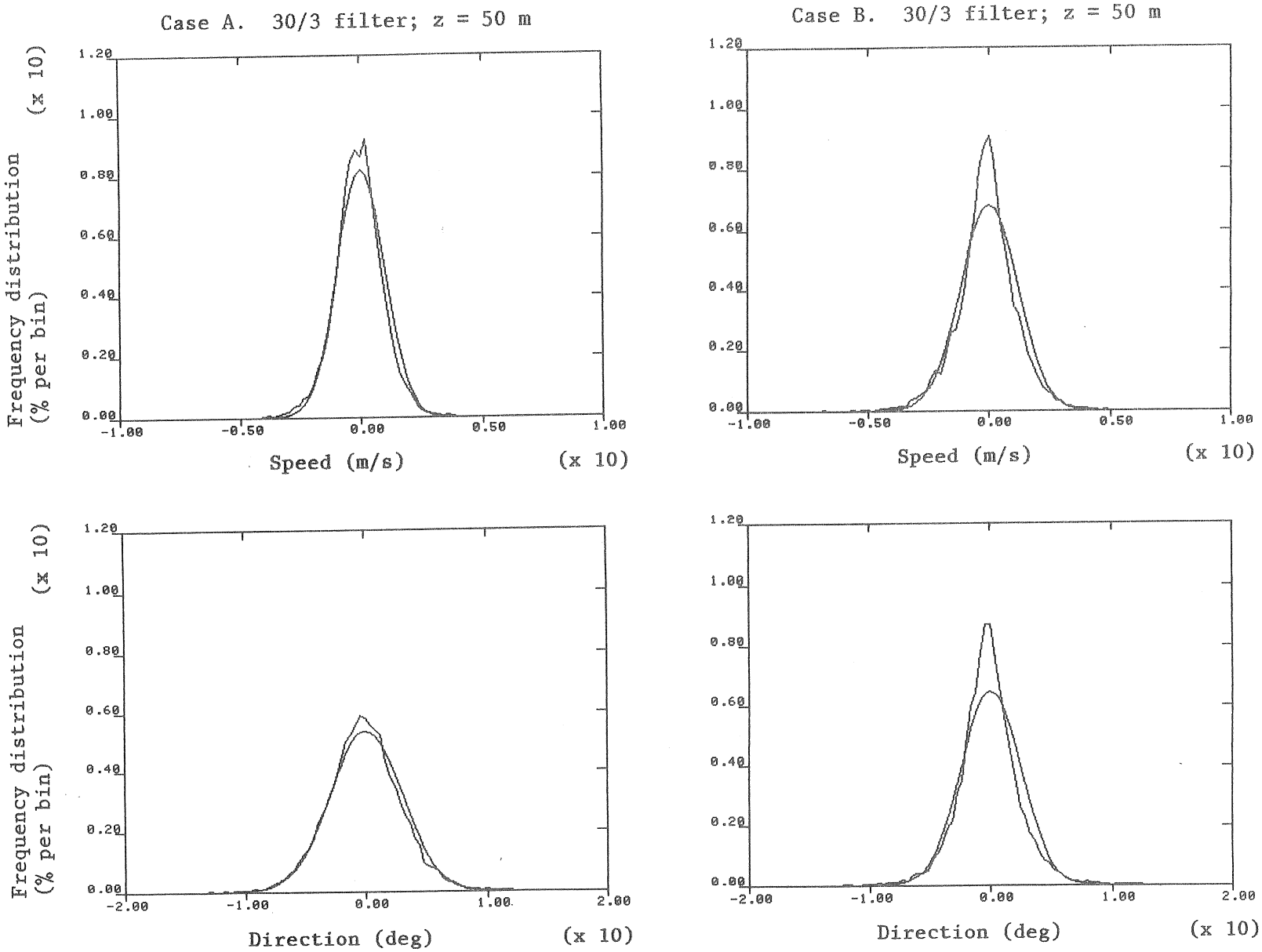

Figure 5.5--Distributions of speed and direction at 50 m (30/3 filter). ΔS = 0.2 m/s; ΔD = 0.4 deg.

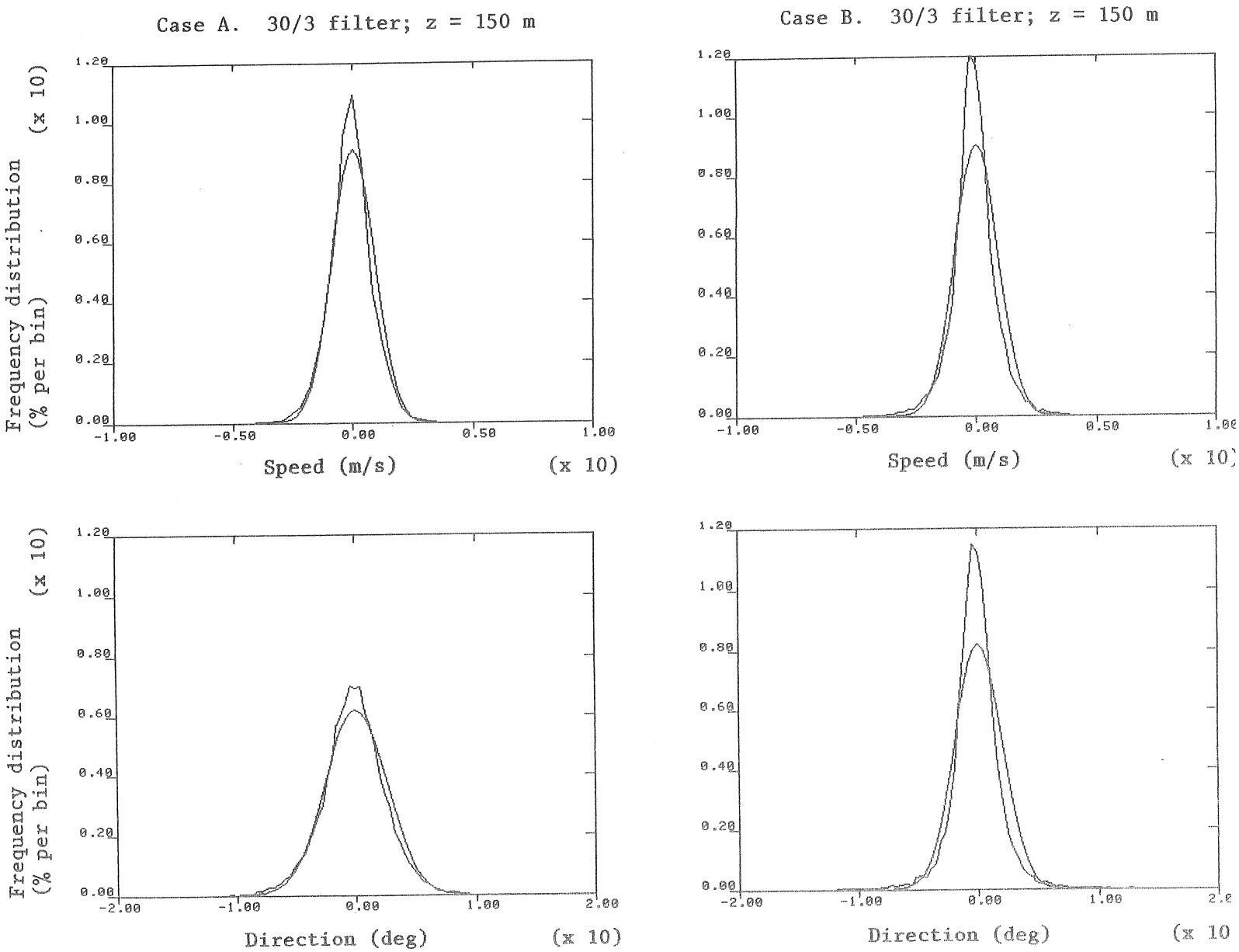

Figure 5.6--Distributions of speed and direction at 150 m (30/3 filter). ΔS = 0.2 m/s; ΔD = 0.4 deg.

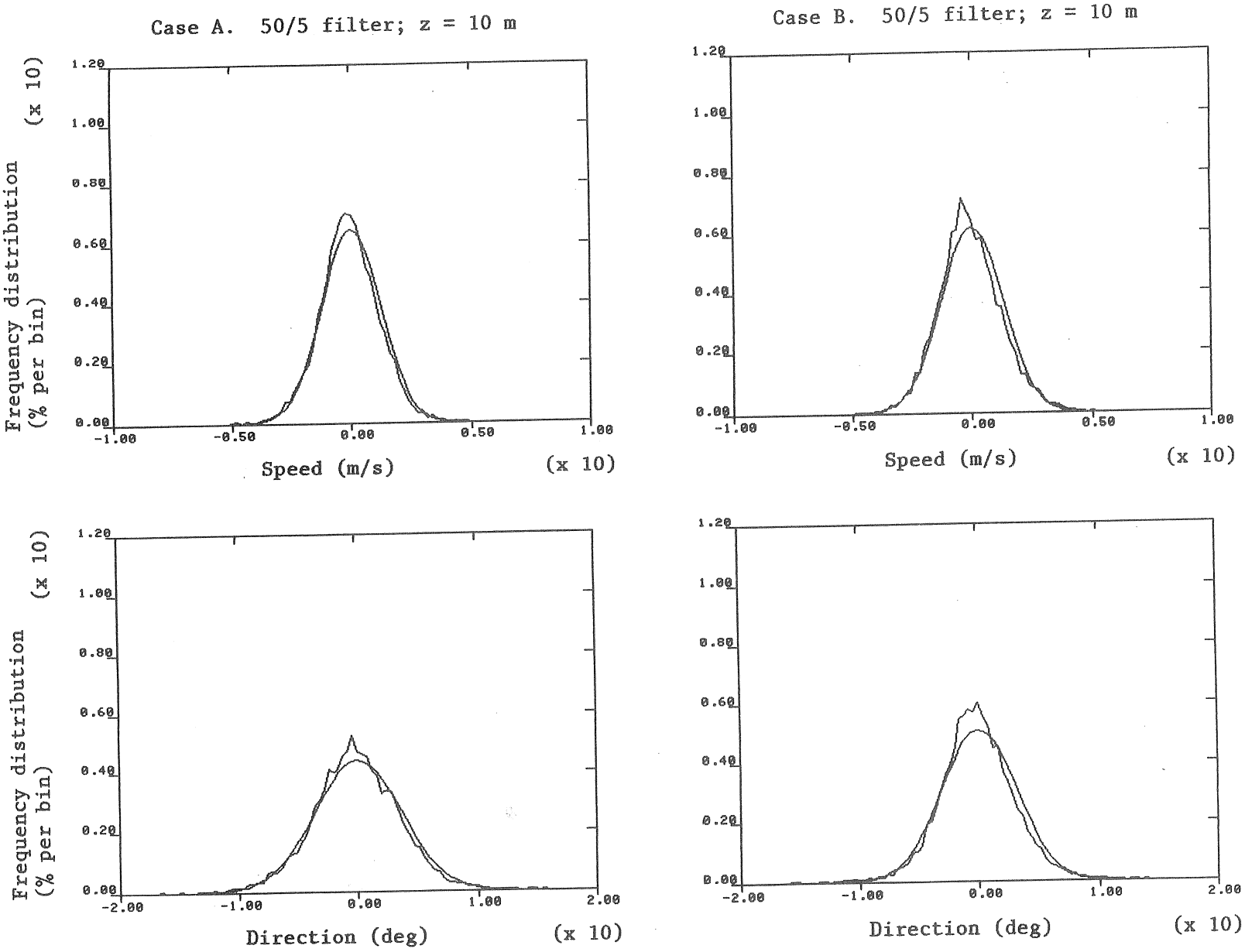

Figure 5.7--Distributions of speed and direction at 10 m (50/5 filter). ΔS = 0.2 m/s; ΔD = 0.4 deg.

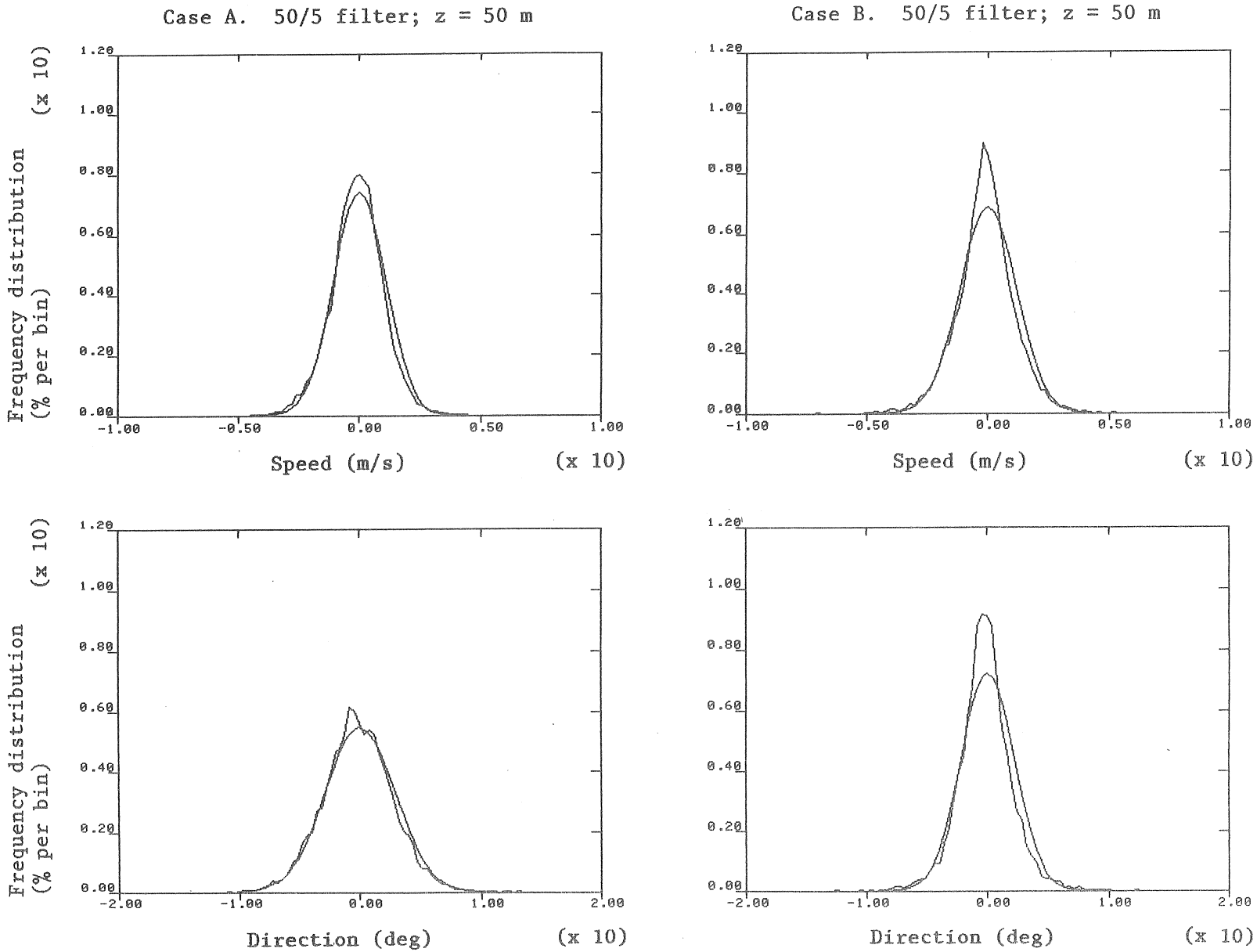

Figure 5.8--Distributions of speed and direction at 50 m (50/5 filter). ΔS = 0.2 m/s; ΔD = 0.4 deg.

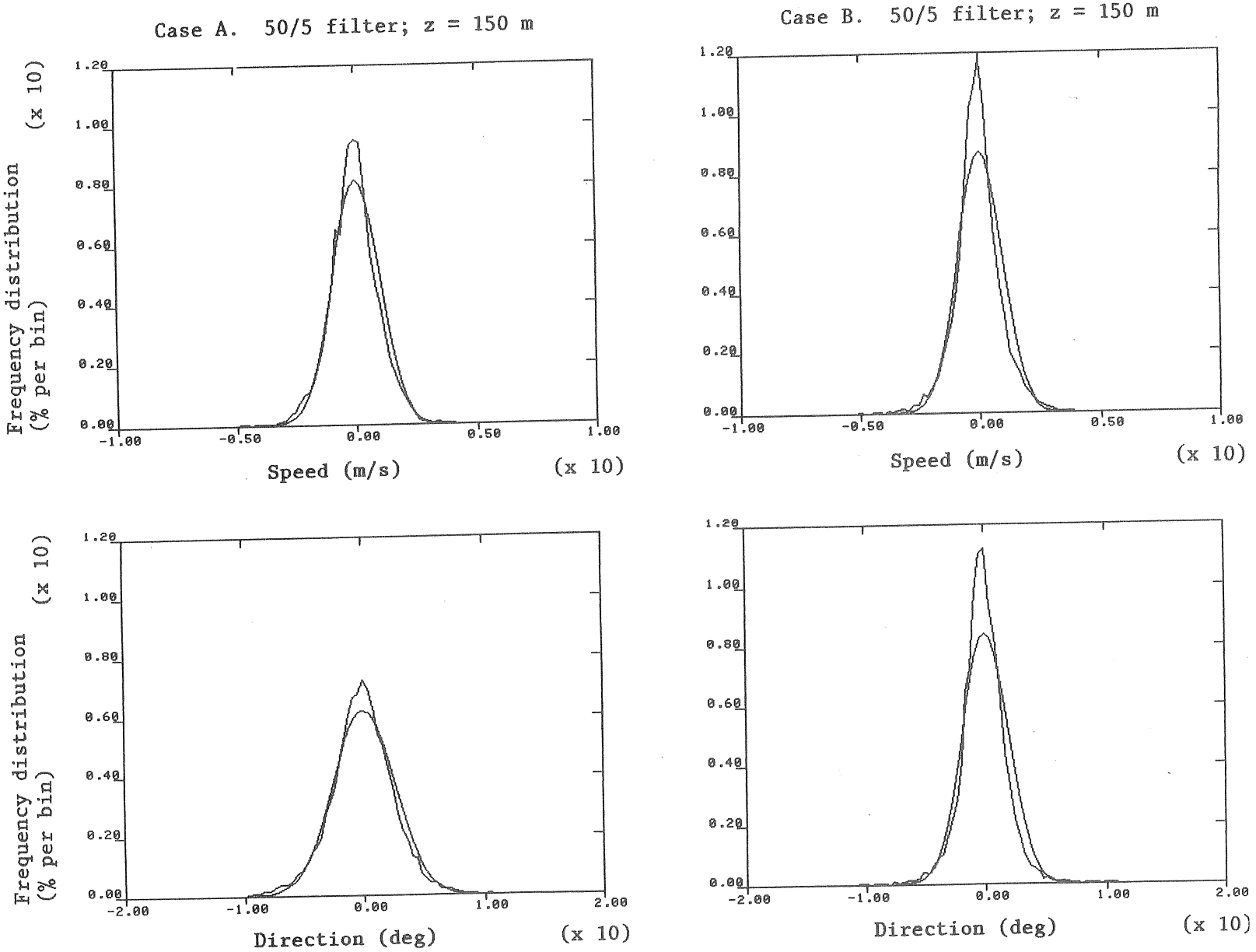

Figure 5.9--Distributions of speed and direction at 150 m (50/5 filter). ΔS = 0.2 m/s; ΔD = 0.4 deg.

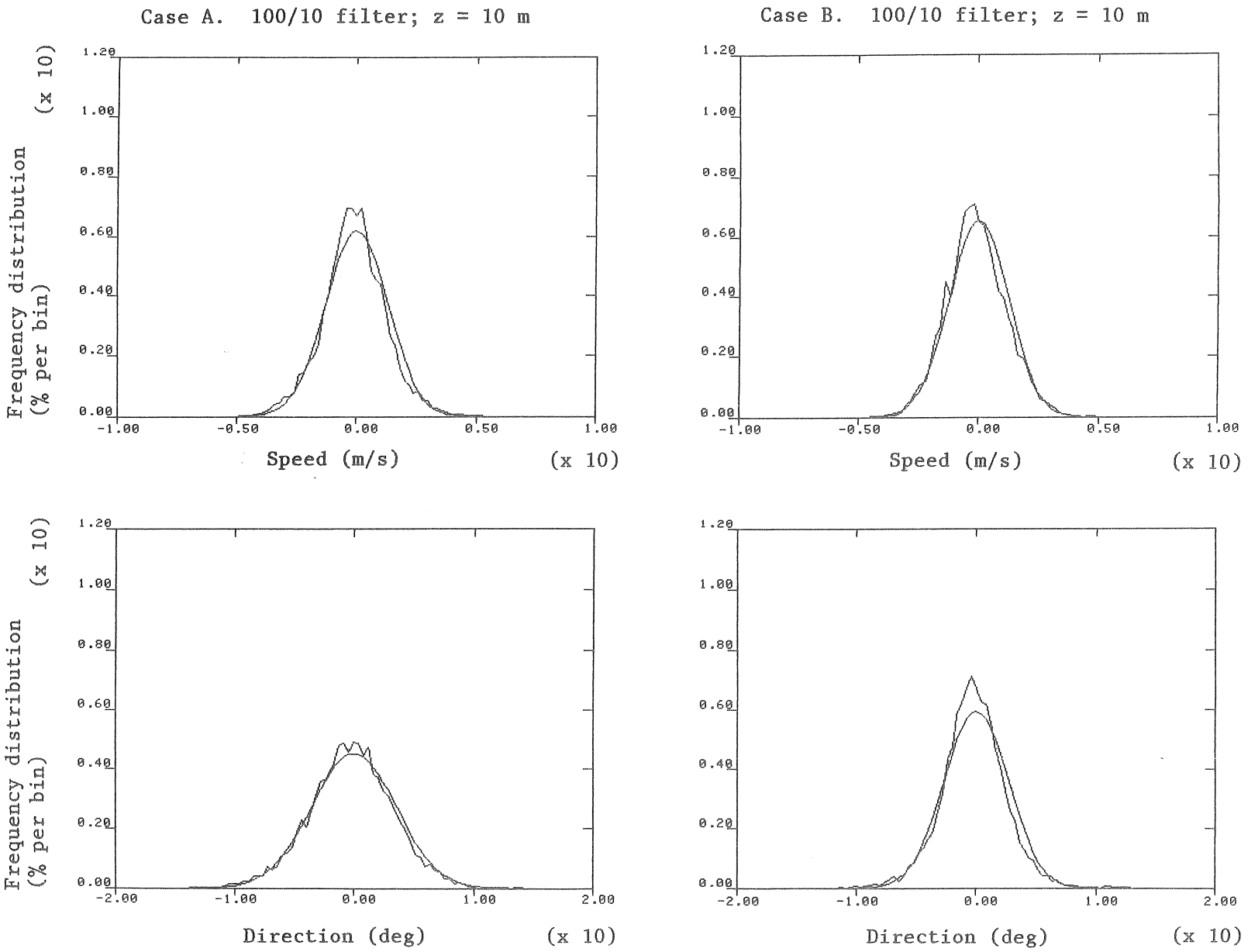

Figure 5.10--Distributions of speed and direction at 10 m (100/10 filter). ΔS = 0.2 m/s; ΔD = 0.4 deg.

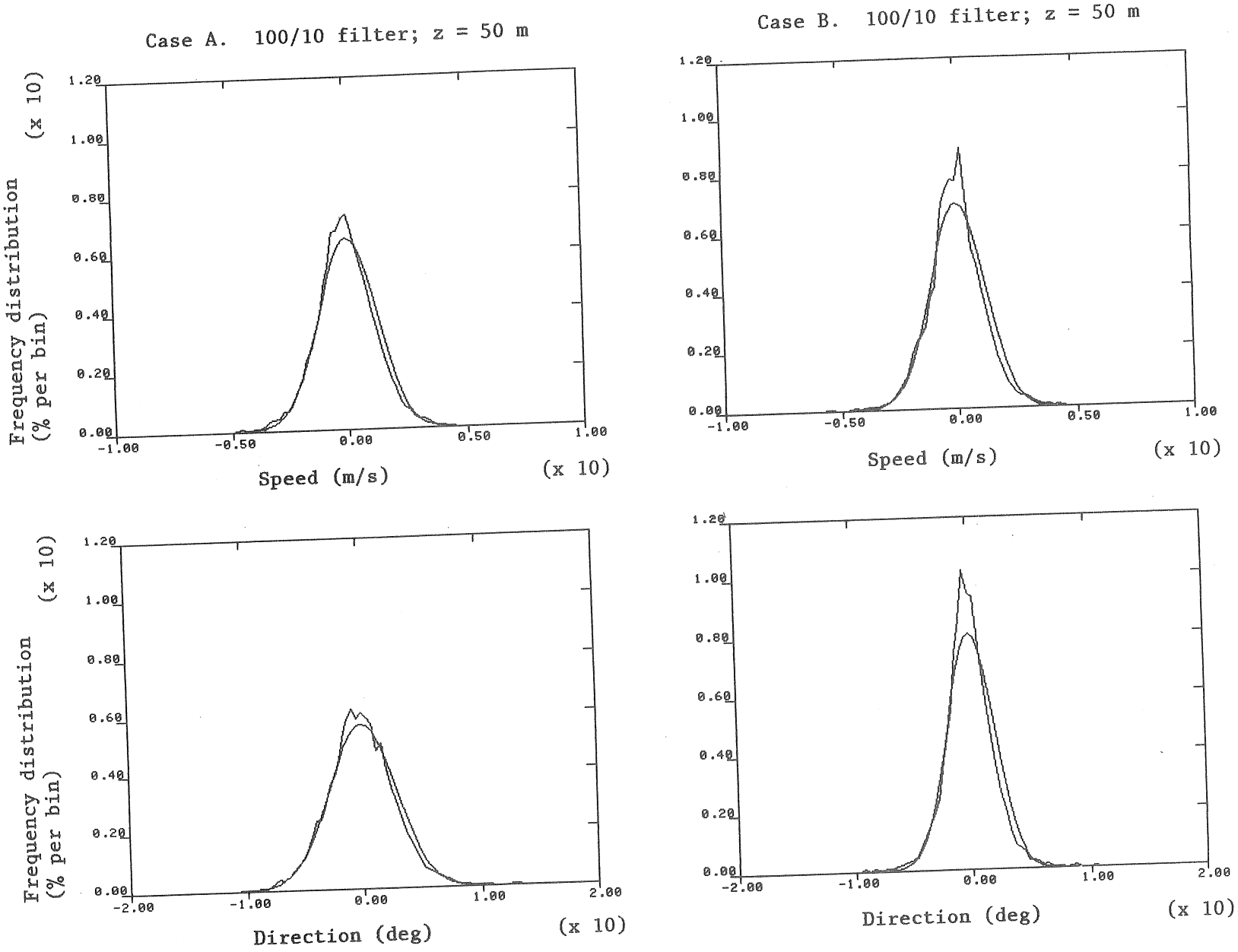

Figure 5.11--Distributions of speed and direction at 50 m (100/10 filter). ΔS = 0.2 m/s; ΔD = 0.4 deg.

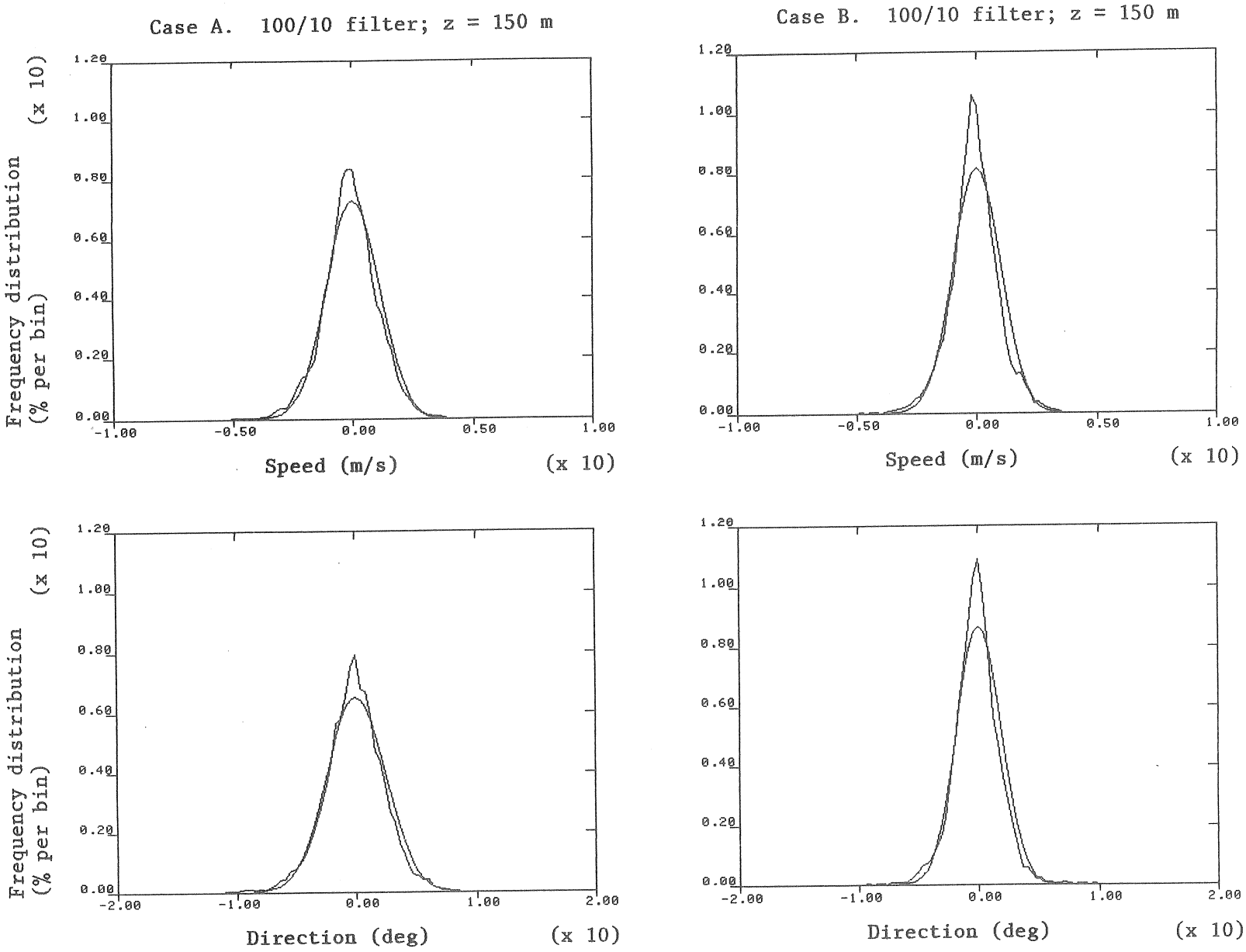

Figure 5.12--Distributions of speed and direction at 150 m (100/10 filter). ΔS = 0.2 m/s; ΔD = 0.4 deg.

6.0 ANALYSIS OF WIND ACCELERATION

All gust models define discrete gust events in terms of some aspect of turbulence. The time rate of change of the wind speed and wind direction are convenient parameters for defining gust events since they are a measure of the severity of the event. The Cliff-Fichtl (1978) and Huang-Fichtl (1979) models use speed difference information to create discrete gust events. Such models are sometimes referred to as gust-rise models, but in the case of the former model that definition incorrectly implies a preference for a positive speed change. Their main usefulness is in calculating the probabilities of extreme events, and they have also been found useful for fatigue calculations (Powell and Connell, 1980).

In both the Cliff-Fichtl (CF) and Huang-Fichtl (HF) models the wind speed time series is replaced by the speed difference computed across a time interval Δt. In the CF model, the discrete events are the actual values of speed differences measured across Δt. In the HF model the discrete events are the positive slope crossings of the speed difference function at level x. In contrast with the CF model, Δt in this model is made as small as possible to make the difference function appear continuous.

Another point of contrast between the models is their basic frequency factor. For the CF model this factor is a constant equal to $1/(2\Delta t)$, which is the Nyquist frequency for the differenced time series. For the HF model the frequency factor is calculated through an expression based on Rice's equation involving the filtered variance of the differenced time series and its power spectrum.

The choice of Δt for differencing is obviously a critical factor since an improper choice of Δt could result in the underestimation of the severity of the gust environment. In this chapter we examine the effect of varying Δt in the unfiltered and the three filtered time series. The plots in Figs. 6.1-6.6 show the standard deviations, skewness, and kurtosis for five Δt values: 1, 3, 5, 10, and 30 s. All three heights

(10, 50, and 150 m) are represented. In addition, the frequency distributions for Δt = 5, 10, and 30 are provided in Figs. 6.7-6.15. The following comments can be made regarding the response of the statistical parameters to the various operations performed on the time series.

6.1 STANDARD DEVIATION

The disparity between the filtered and the unfiltered standard deviations is not as large as in the undifferenced speed and direction time series. This is because differencing is inherently a high-pass process; the low-frequency contributions that contribute greatly to the high standard deviations and cause departures from Gaussian behavior in the skewness and kurtosis in the undifferenced time series are absent in the differenced time series.

The unfiltered standard deviations are smallest for Δt = 1 s, but rise rapidly between Δt of 1 and 5 s and more gradually between 5 and 30 s. The 30/3 and 50/5 time series show a distinct maximum at 10 s, whereas the 100/10 time series show the same rate of increase with Δt as the unfiltered data. If one considers the 50/5 filter the basic filter for WECS design, the optimum choice for Δt is 10 s.

6.2 SKEWNESS

The skewness values are not noticeably affected by filtering. They are small, and become even smaller for speed as Δt increases. Shown on an expanded scale, the direction skewness behaves more erratically, but the values are so small one may consider them zero for all practical purposes.

6.3 KURTOSIS

The kurtosis values show a definite decrease with increasing Δt, but, in contrast to the behavior of the standard deviations and the skewness, there is little similarity between the kurtosis plots of Case

A and Case B. In Case A, both the filtered and unfiltered kurtoses drop from numbers close to 5 at Δt = 1 s to about 3.5 at Δt = 30 s. In Case B the kurtosis values are larger, especially for direction and show a strong dependence on choice of filter.

6.4 FREQUENCY DISTRIBUTIONS

Only the 50/5 filtered distributions are shown here, but they amply demonstrate differences between the kurtosis Case A and Case B. In the strongly stable stratification of Case B, one can expect a higher preference for smaller fluctuations in the speed and direction signals, and this preference to be further accentuated in the differenced signals.

6.5 VARIATIONS WITH HEIGHT

The sensitivity to height variation in the statistical properties of these differenced time series is much more pronounced than in the original time series. The standard deviations decrease with height for all choices of Δt. The kurtosis increases sharply with height; the kurtosis of 8.5 found in the 50/5 filtered data with Δt = 10 s represents a significant departure from Gaussian.

Powell and Connell (1980) note that the theoretical usefulness of any of the gust models requires that the filtered turbulence or gust data be approximately Gaussian. The degree to which the kurtosis departs from 3 has serious implications for the theoretical model. However, large kurtosis is often the result of stationarity in the signal. Differencing of the signal, by removal of the large low-frequency oscillations in the signal, increases the kurtosis. We believe the departure of the kurtosis from 3 is not an important factor in the engineering design so long as the filter passband approximates the WECS response.

Departures from Gaussian behavior notwithstanding, certain consistent patterns emerge as one normalizes the standard deviations of the differenced data with the standard deviations of the corresponding undifferenced filtered time series. As seen in Table 6.1 the ratios stay surprisingly constant from one level to another and from one case to the other. The only significant variations are those introduced by filter choice and differencing interval. Denoting the standard deviation of the undifferenced filtered time series by $[\sigma(X)]_F$, where X is the variable and F denotes filtered data, and the standard deviation of the differenced time series by $[\sigma(\Delta X)]_F$, we can express the relationship between the two for the 50/5 filtered data differenced across 10 s (our optimum differencing interval) as

$$\left[\frac{\sigma(\Delta X)}{\sigma(X)}\right]_F = \begin{cases} 1.47 \text{ for Case A speed} \\ 1.52 \text{ for Case B speed} \\ 1.52 \text{ For Case A cirection} \\ 1.51 \text{ for Case B direction .} \end{cases} \qquad (6.1)$$

Thus, the standard deviation of the differenced signal can be approximated with a high degree of confidence from the standard deviation of the basic filtered time series.

In the CF and HF models, the rms value of the differenced data (which is the same as the standard deviation in the absence of a mean) is related to the rms value of the undifferenced data through a function f involving the wind speed S, the integral length scale L, and Δt:

$$\left[\frac{\sigma(\Delta S)}{\sigma(S)}\right]_F = \sqrt{2}\, f(S, L, \Delta t) \; . \qquad (6.2)$$

The form of f is different for the two models, but our results in Table 6.1 suggest that the effect of varying speed and integral length scale (as between Case A and Case B) is not very significant.

Table 6.1--Normalized standard deviations for speed and direction differences (SI units)

Parameter	Height	Filter	Case A Differencing Interval(s) 5	Case A Differencing Interval(s) 10	Case A Differencing Interval(s) 30	Case B Differencing Interval(s) 5	Case B Differencing Interval(s) 10	Case B Differencing Interval(s) 30
Speed difference	10	30/3	1.43	1.63	1.42	1.46	1.61	1.44
		50/5	1.18	1.49	1.46	1.26	1.50	1.43
		100/10		1.21	1.62		1.32	1.58
	50	30/3	1.38	1.65	1.41	1.45	1.63	1.41
		50/5	1.05	1.46	1.45	1.23	1.52	1.38
		100/10		1.14	1.63		1.28	1.55
	150	30/3	1.35	1.65	1.39	1.41	1.67	1.41
		50/5	1.08	1.47	1.44	1.18	1.53	1.44
		100/10		1.17	1.61		1.22	1.54
Direction difference	10	30/3	1.47	1.60	1.40	1.51	1.57	1.42
		50/5	1.27	1.49	1.41	1.40	1.52	1.40
		100/10		1.26	1.60		1.37	1.56
	50	30/3	1.45	1.64	1.42	1.50	1.56	1.40
		50/5	1.24	1.52	1.42	1.35	1.50	1.39
		100/10		1.29	1.59		1.35	1.60
	150	30/3	1.43	1.67	1.42	1.45	1.65	1.39
		50/5	1.21	1.54	1.40	1.24	1.51	1.39
		100/10		1.34	1.58		1.28	1.57

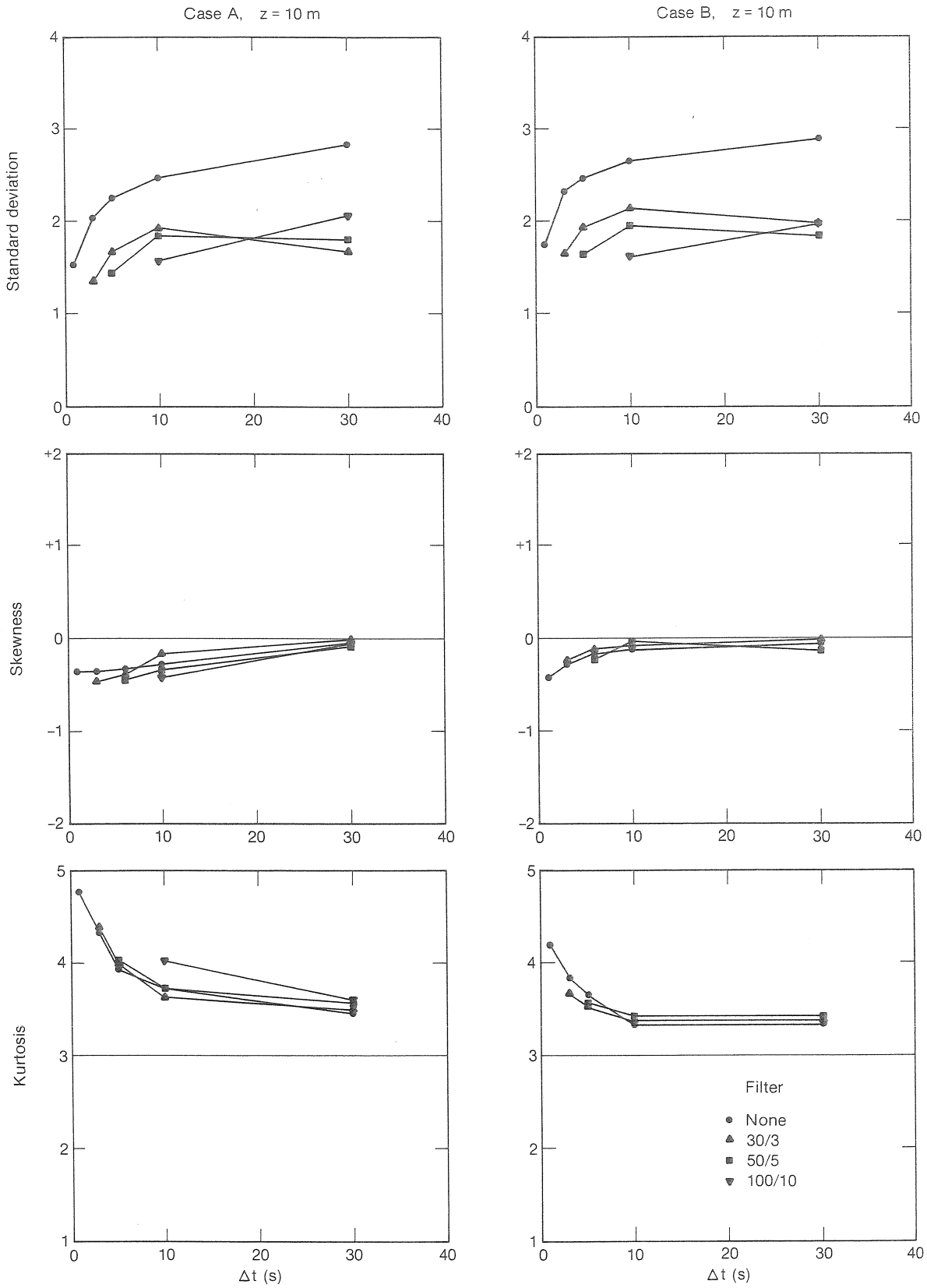

Figure 6.1--Speed difference statistics at 10 m shown as a function of differencing interval. Standard deviations are in m/s.

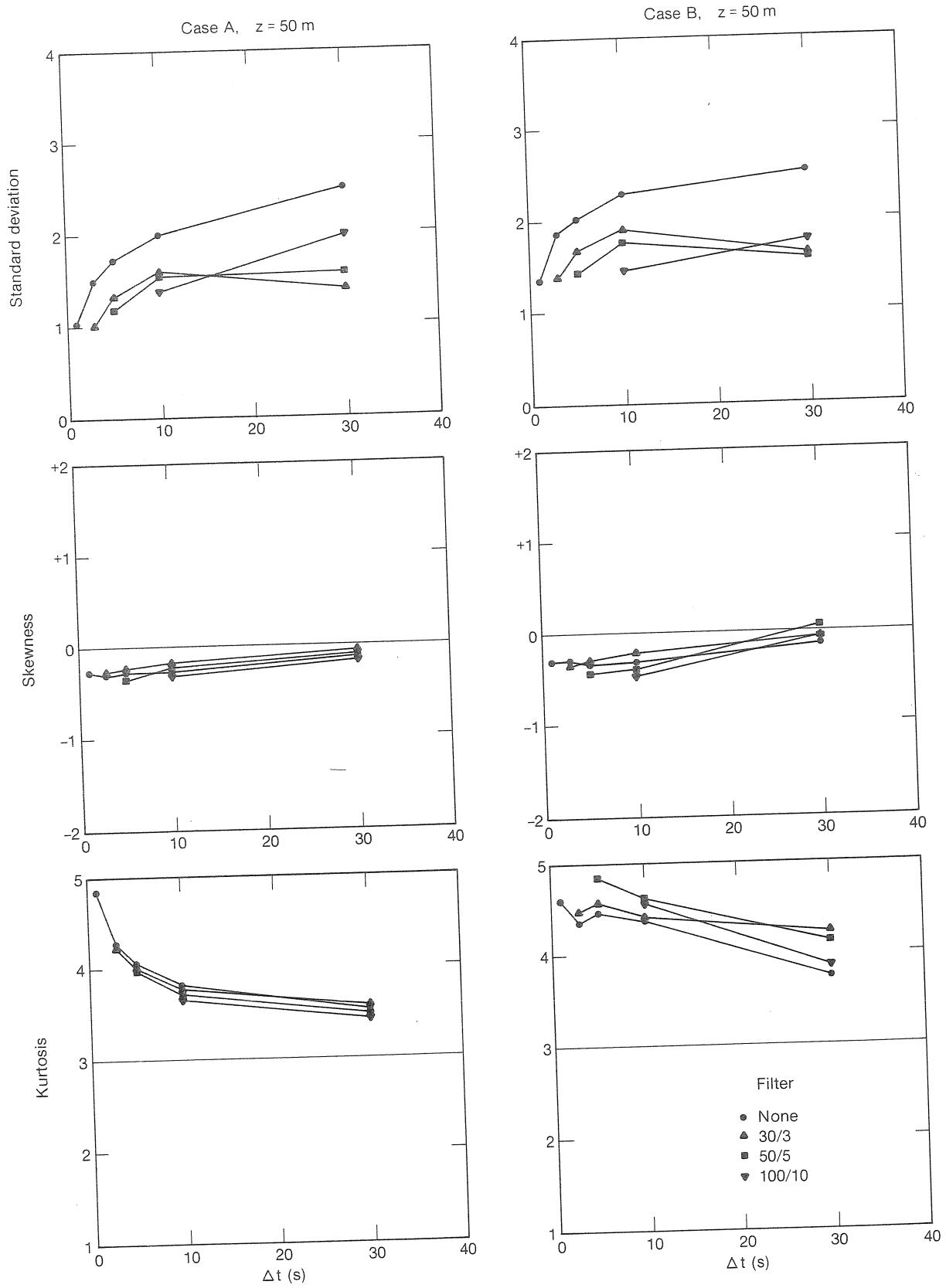

Figure 6.2--Speed difference statistics at 50 m shown as a function of differencing interval. Standard deviations are in m/s.

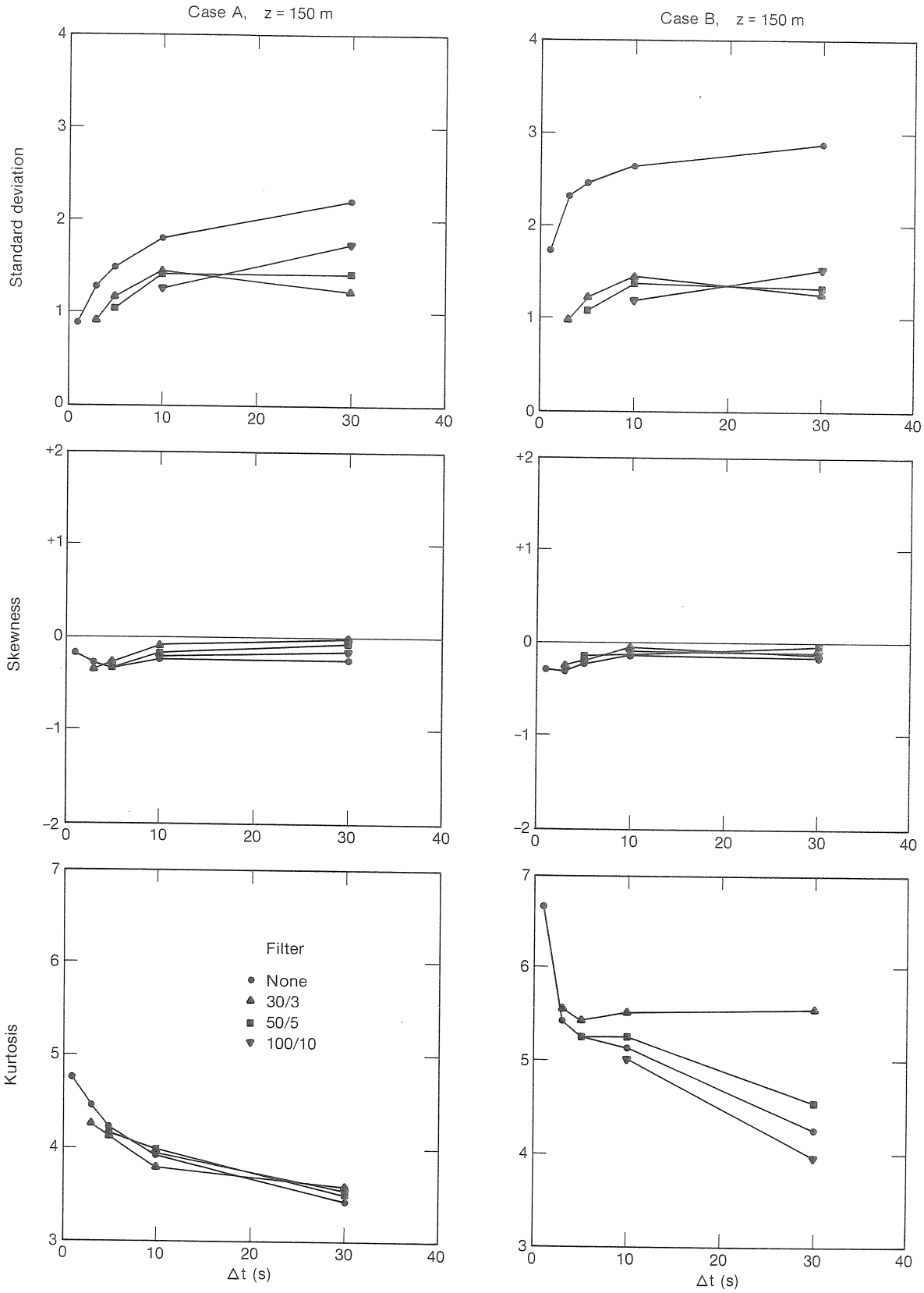

Figure 6.3--Speed difference statistics at 150 m shown as a function of differencing interval. Standard deviations are in m/s.

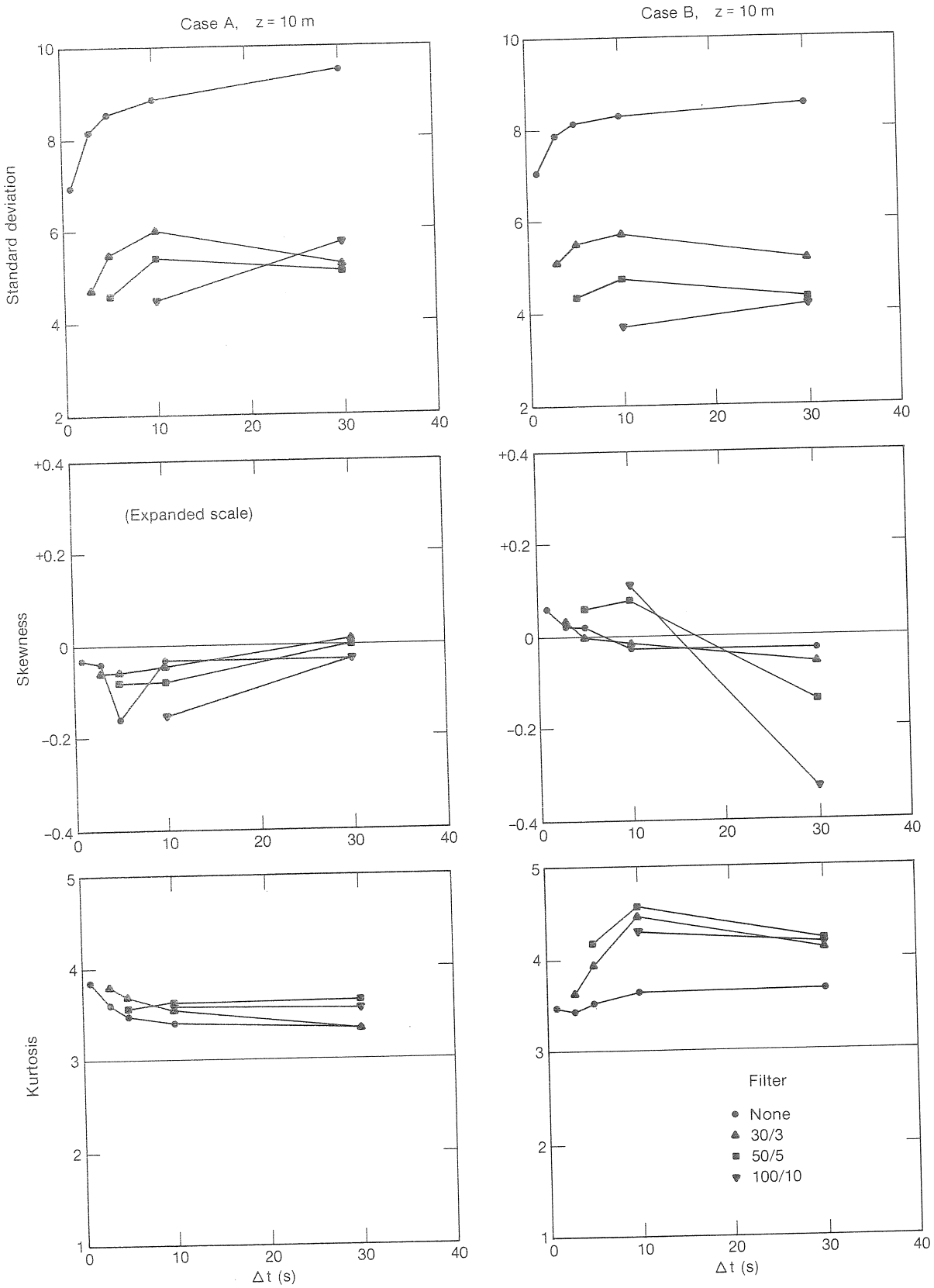

Figure 6.4--Direction difference statistics at 10 m shown as a function of differencing interval. Standard deviations are in degrees.

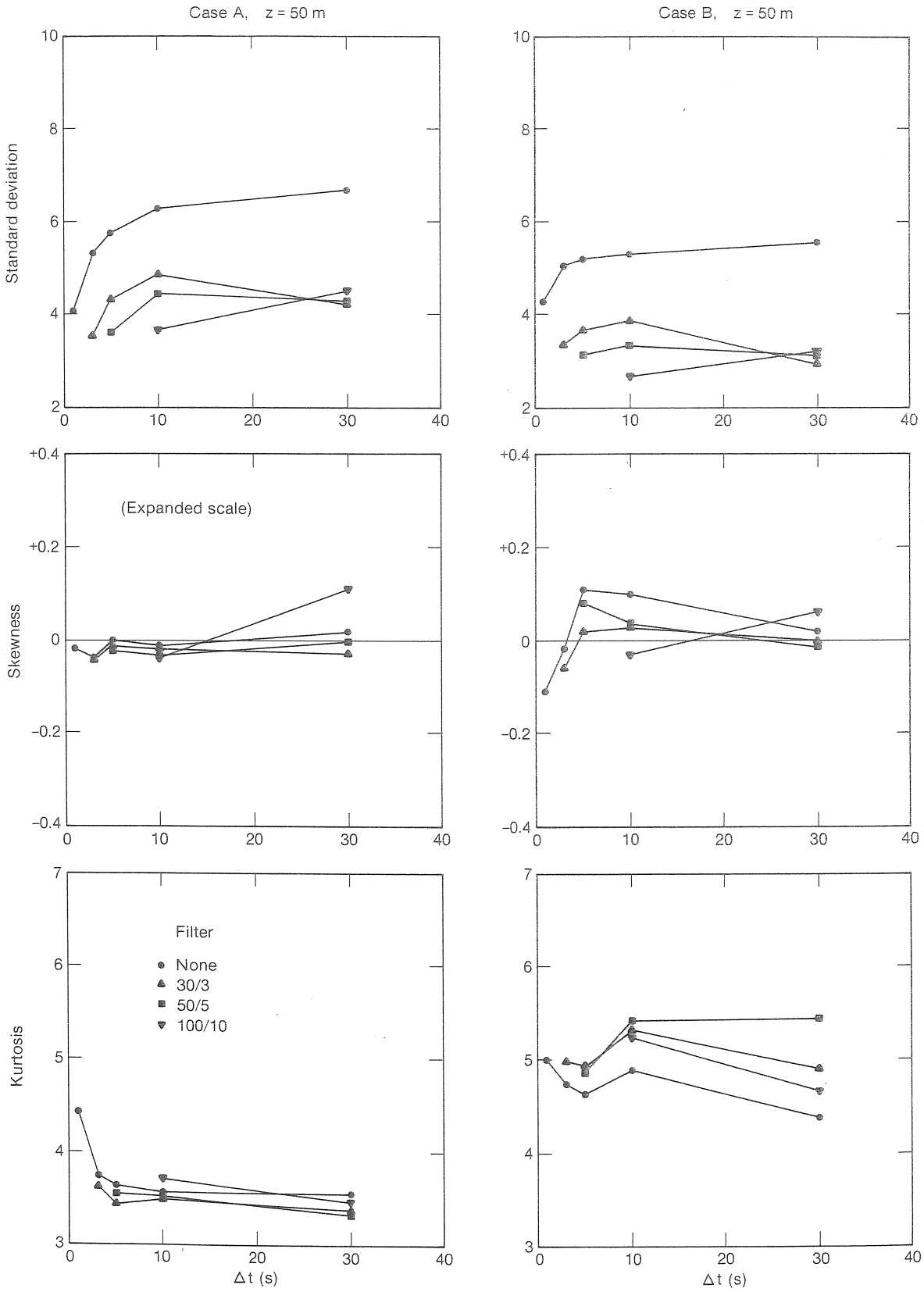

Figure 6.5--Direction difference statistics at 50 m shown as a function of differencing interval. Standard deviations are in degrees.

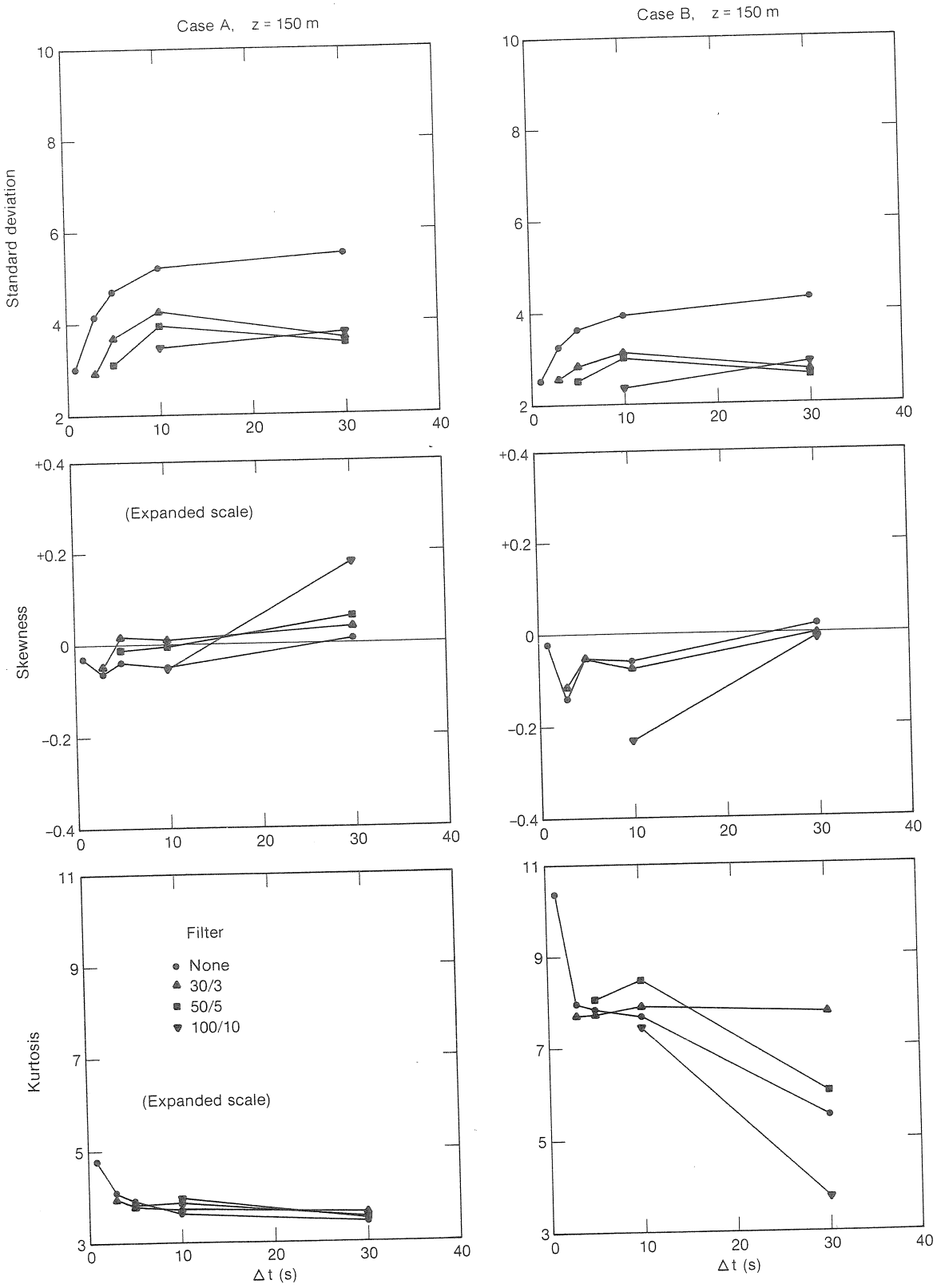

Figure 6.6--Direction difference statistics at 150 m shown as a function of differencing interval. Standard deviations are in degrees.

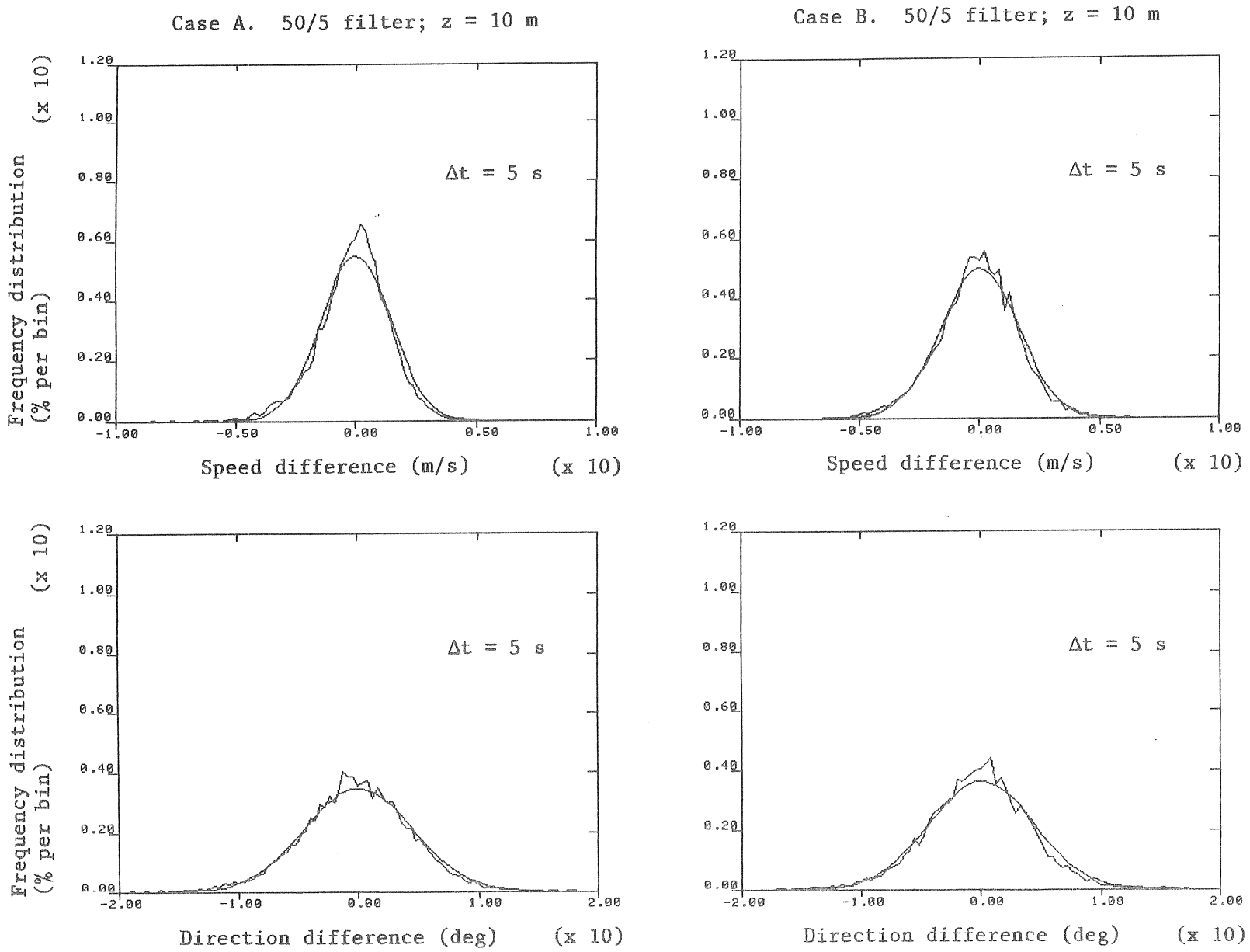

Figure 6.7--Distributions of speed and direction differences at 10 m with 50/5 filter and Δt = 5 s. ΔS = 0.2 m/s; ΔD = 0.4 deg.

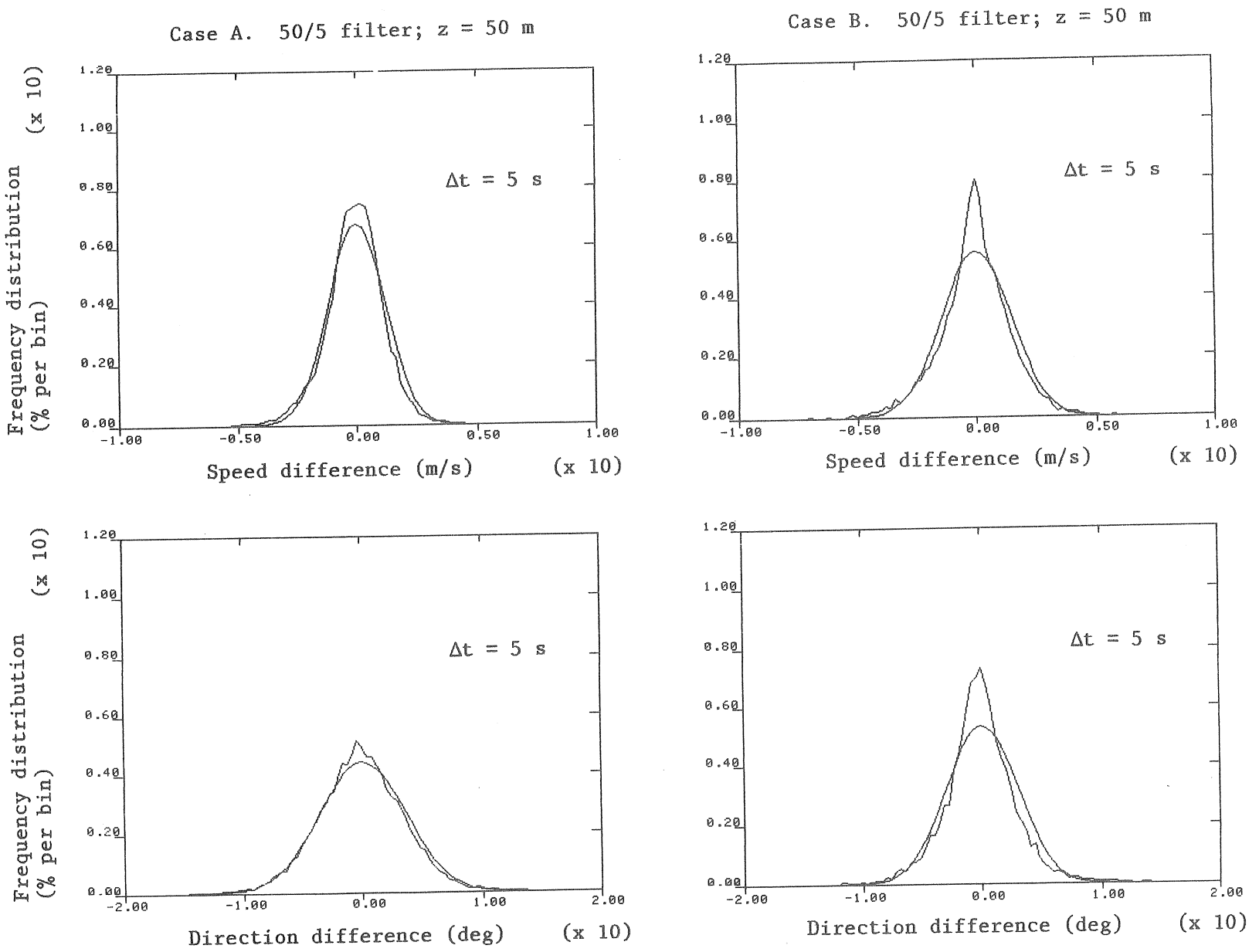

Figure 6.8--Distributions of speed and direction differences at 50 m with 50/5 filter and Δt = 5 s. ΔS = 0.2 m/s; ΔD = 0.4 deg.

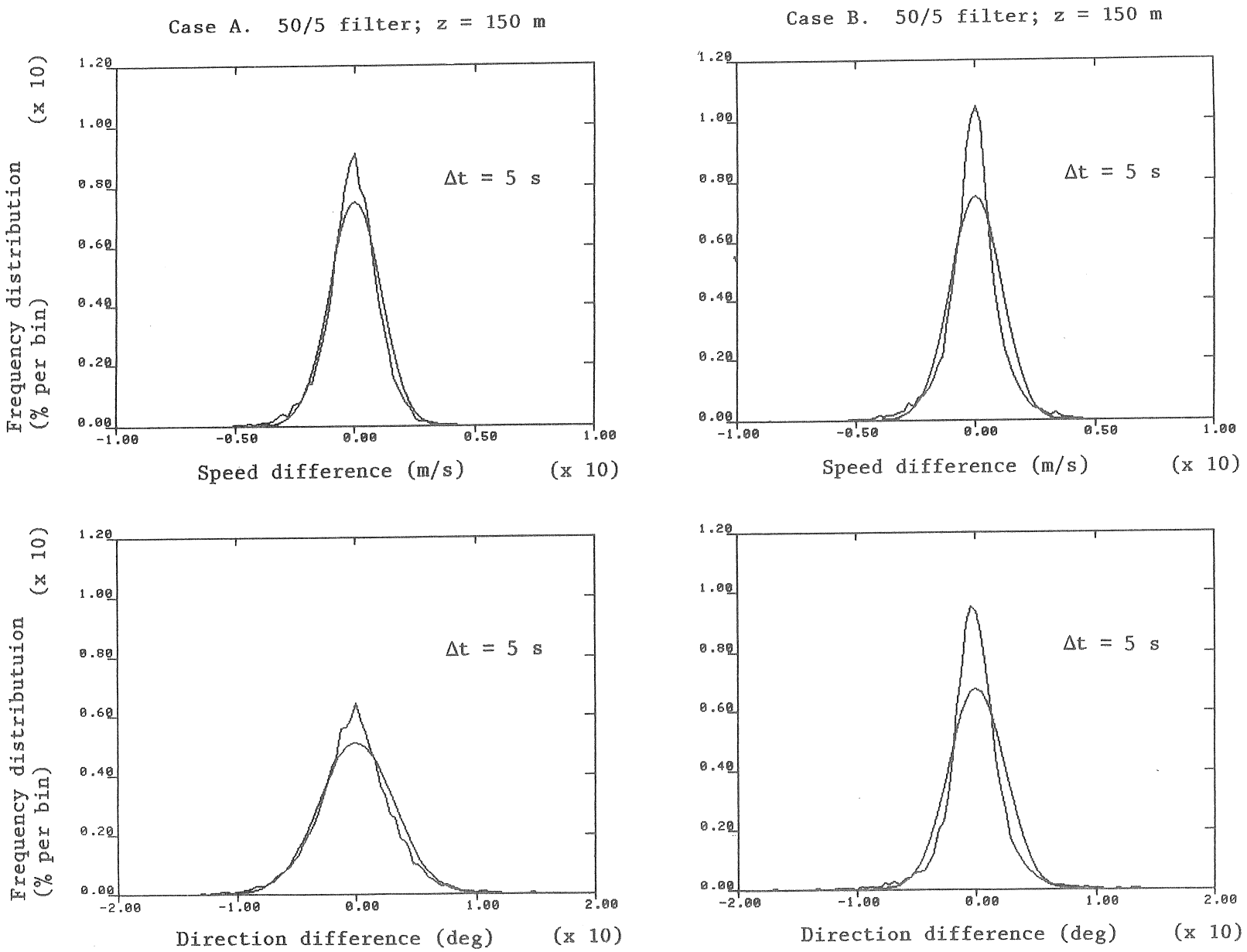

Figure 6.9--Distributions of speed and direction differences at 150 m with 50/5 filter and Δt = 5 s. ΔS = 0.2 m/s; ΔD = 0.4 deg.

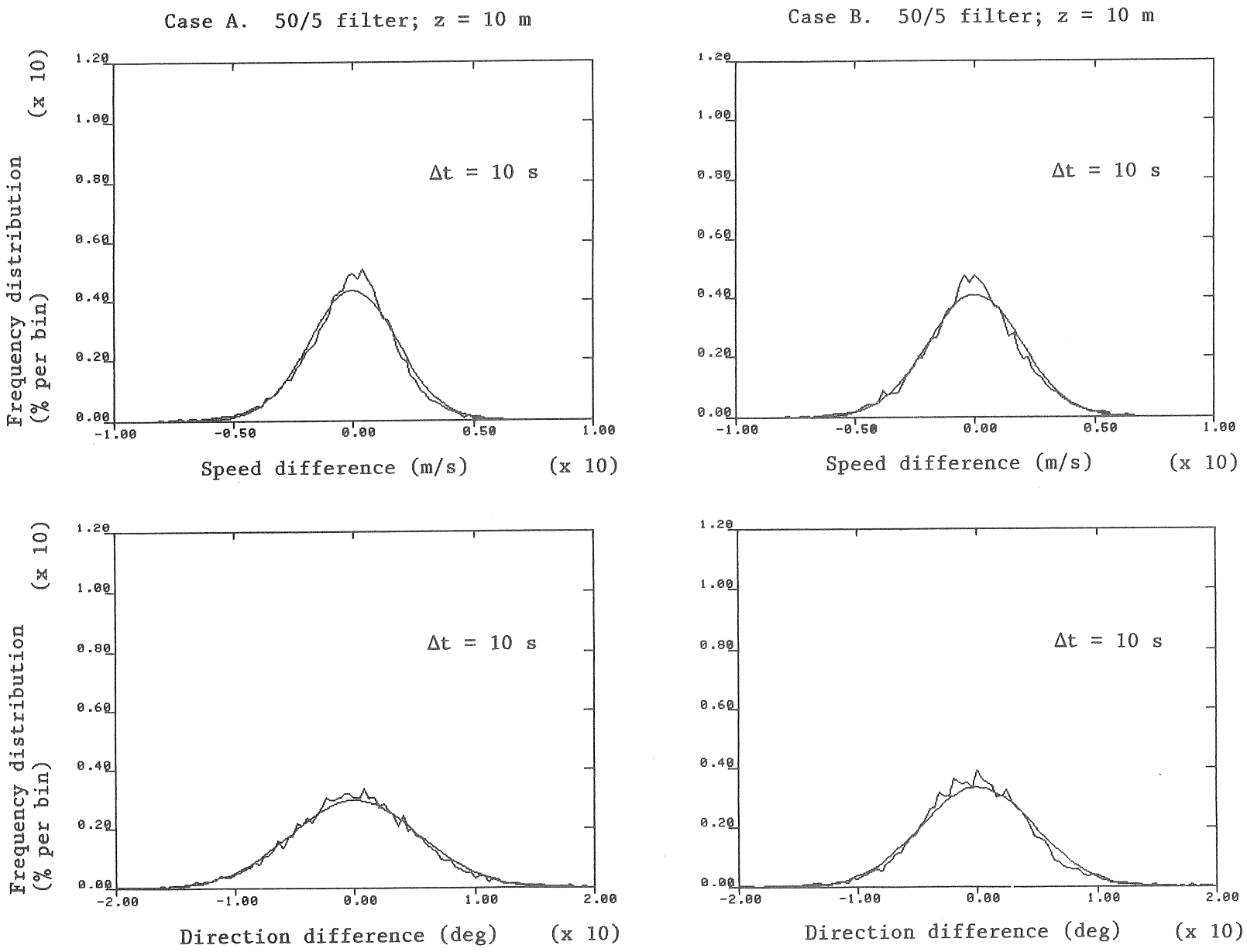

Figure 6.10--Distributions of speed and direction differences at 10 m with 50/5 filter and Δt = 10 s. ΔS = 0.2 m/s; ΔD = 0.4 deg.

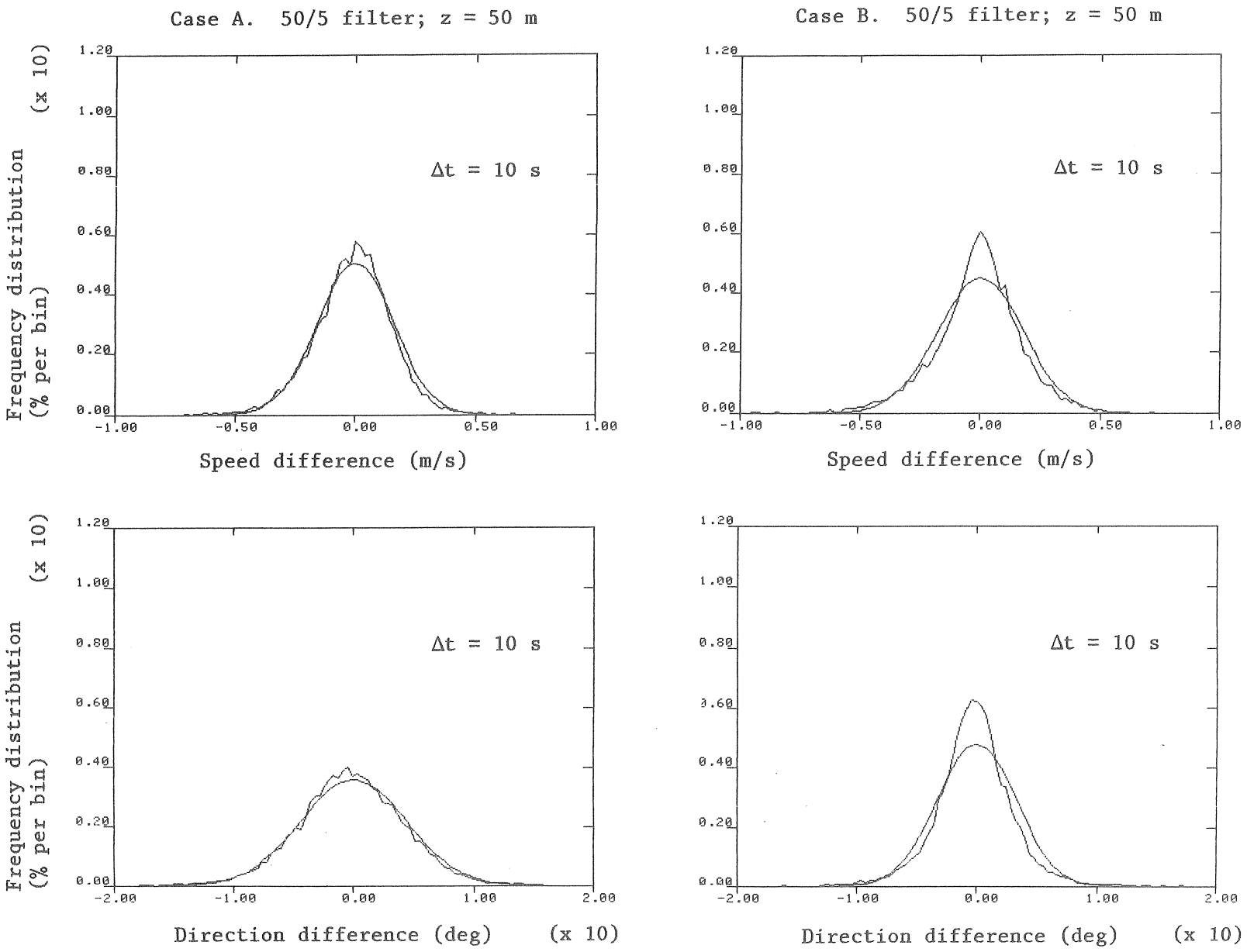

Figure 6.11--Distributions of speed and direction differences at 50 m with 50/5 filter and Δt = 10 s. ΔS = 0.2 m/s; ΔD = 0.4 deg.

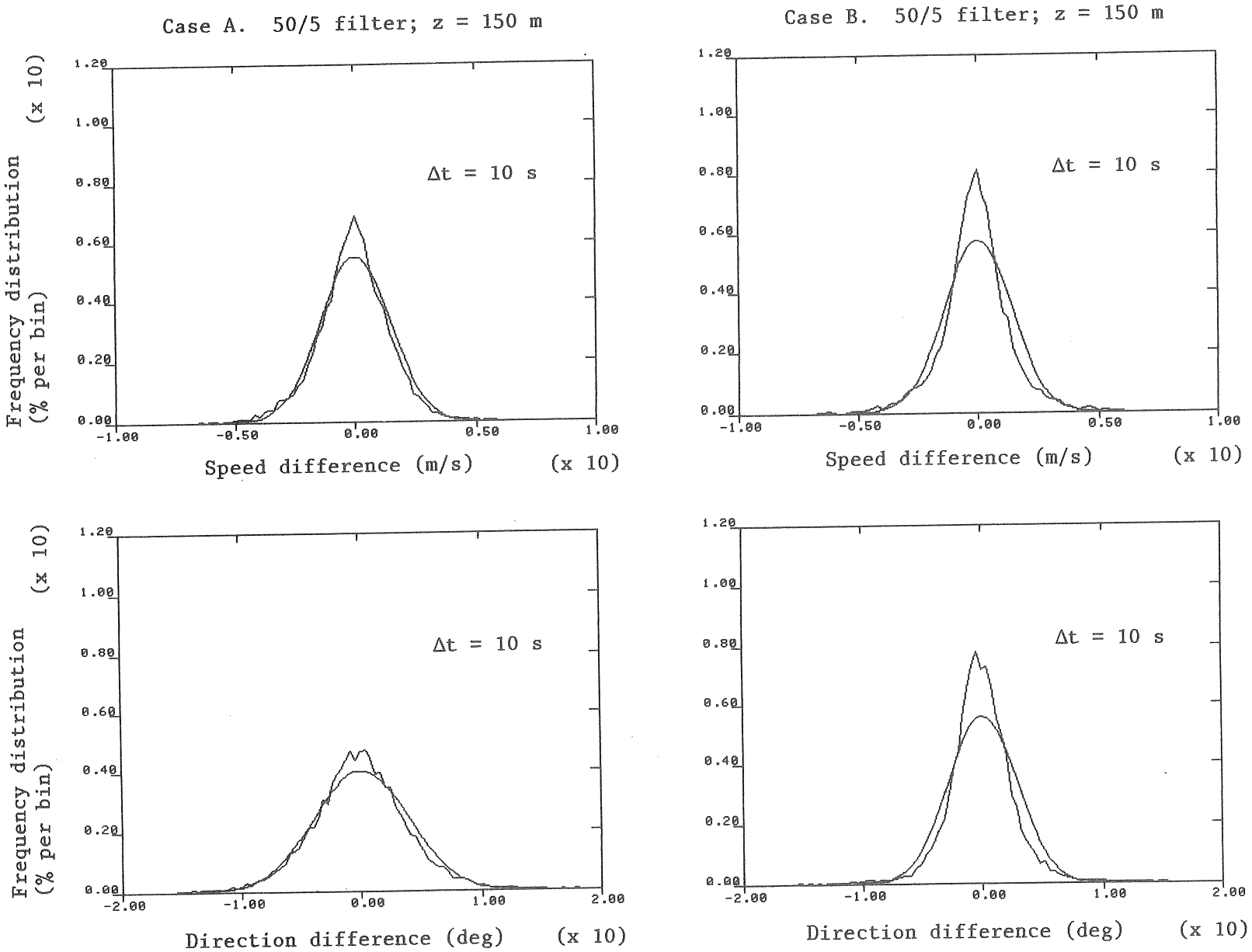

Figure 6.12--Distributions of speed and direction differences at 150 m with 50/5 filter and Δt = 10 s. ΔS = 0.2 m/s; ΔD = 0.4 deg.

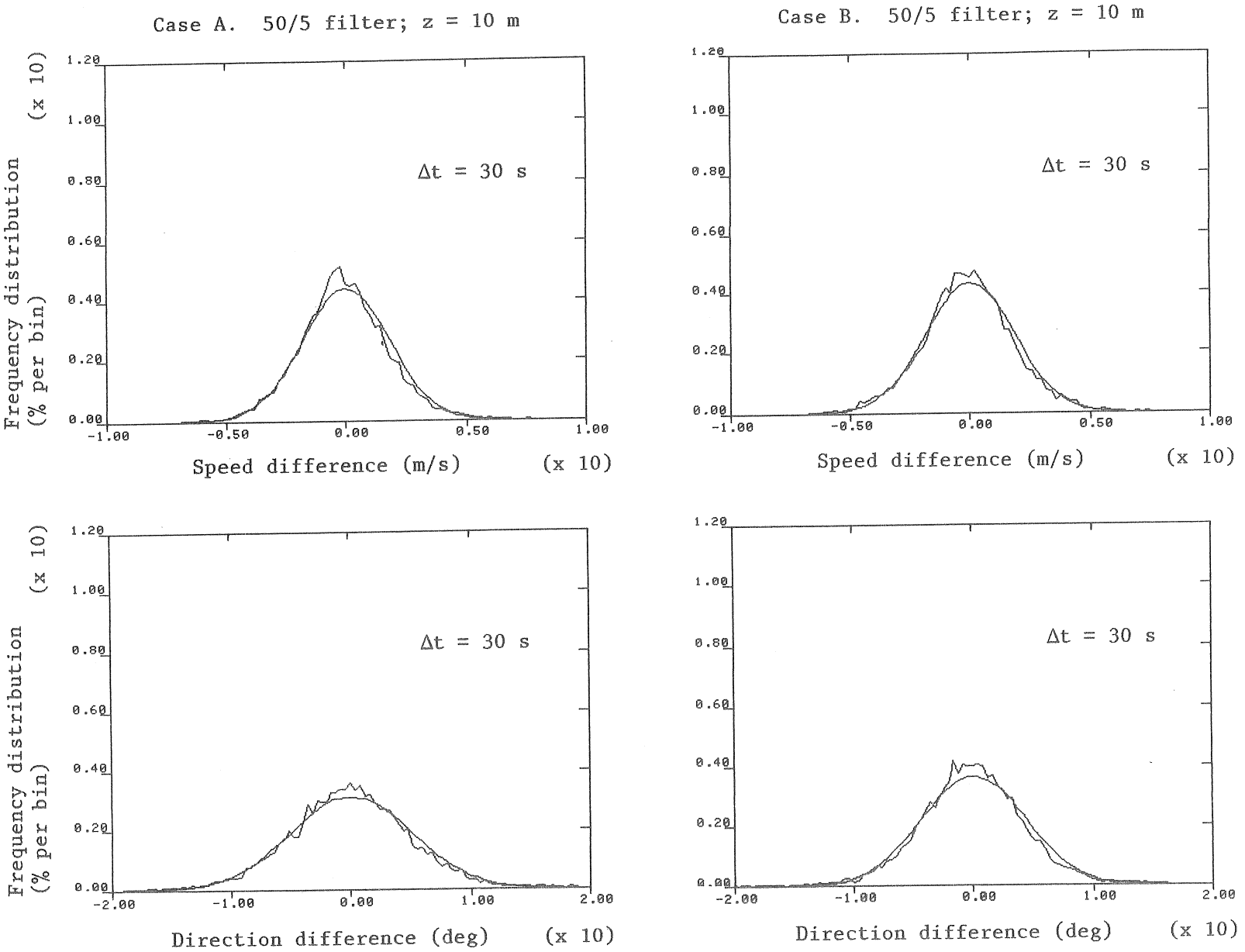

Figure 6.13--Distributions of speed and direction differences at 10 m with 50/5 filter and Δt = 30 s. ΔS = 0.2 m/s; ΔD = 0.4 deg.

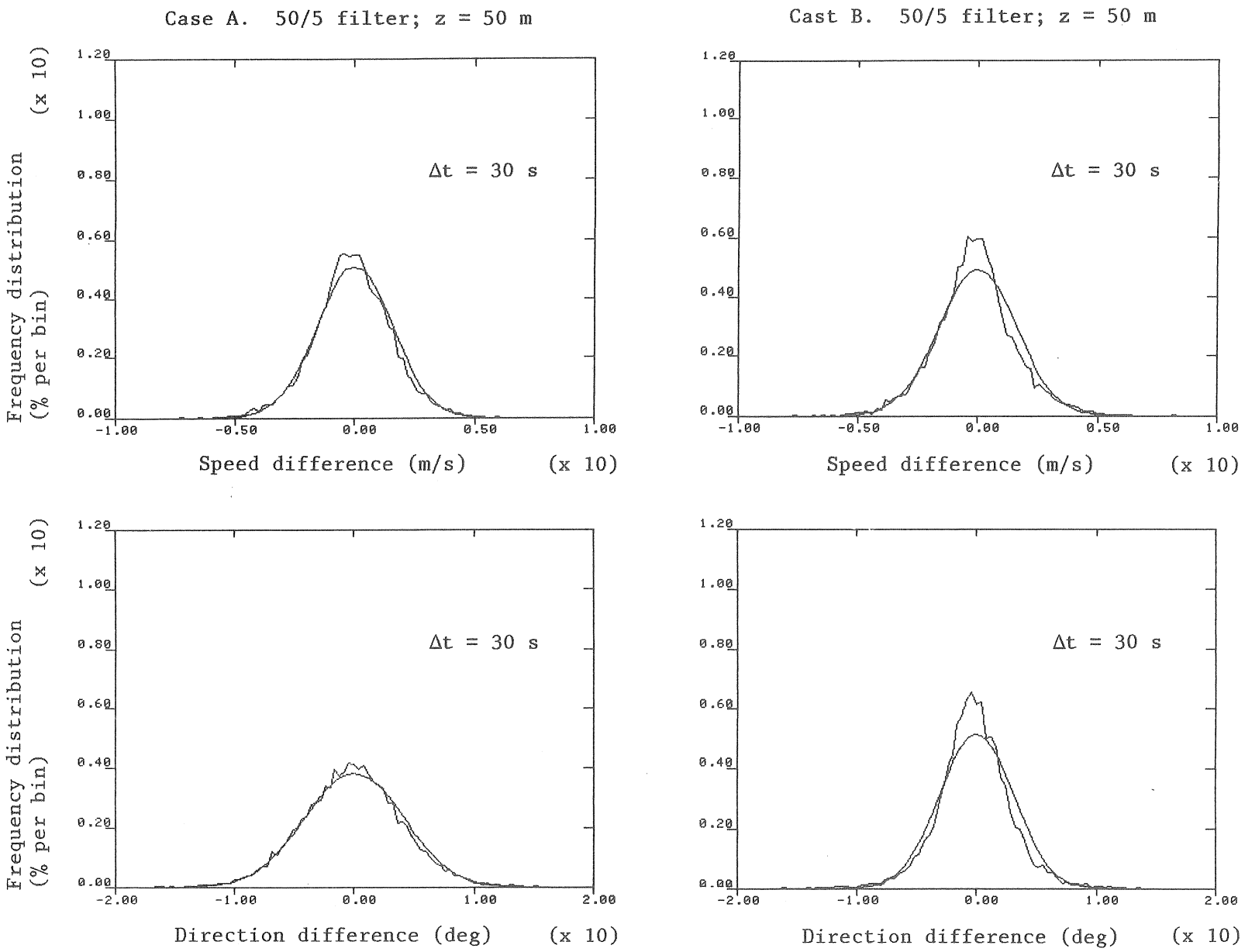

Figure 6.14--Distributions of speed and direction differences at 50 m with 50/5 filter and Δt = 30 s. ΔS = 0.2 m/s; ΔD = 0.4 deg.

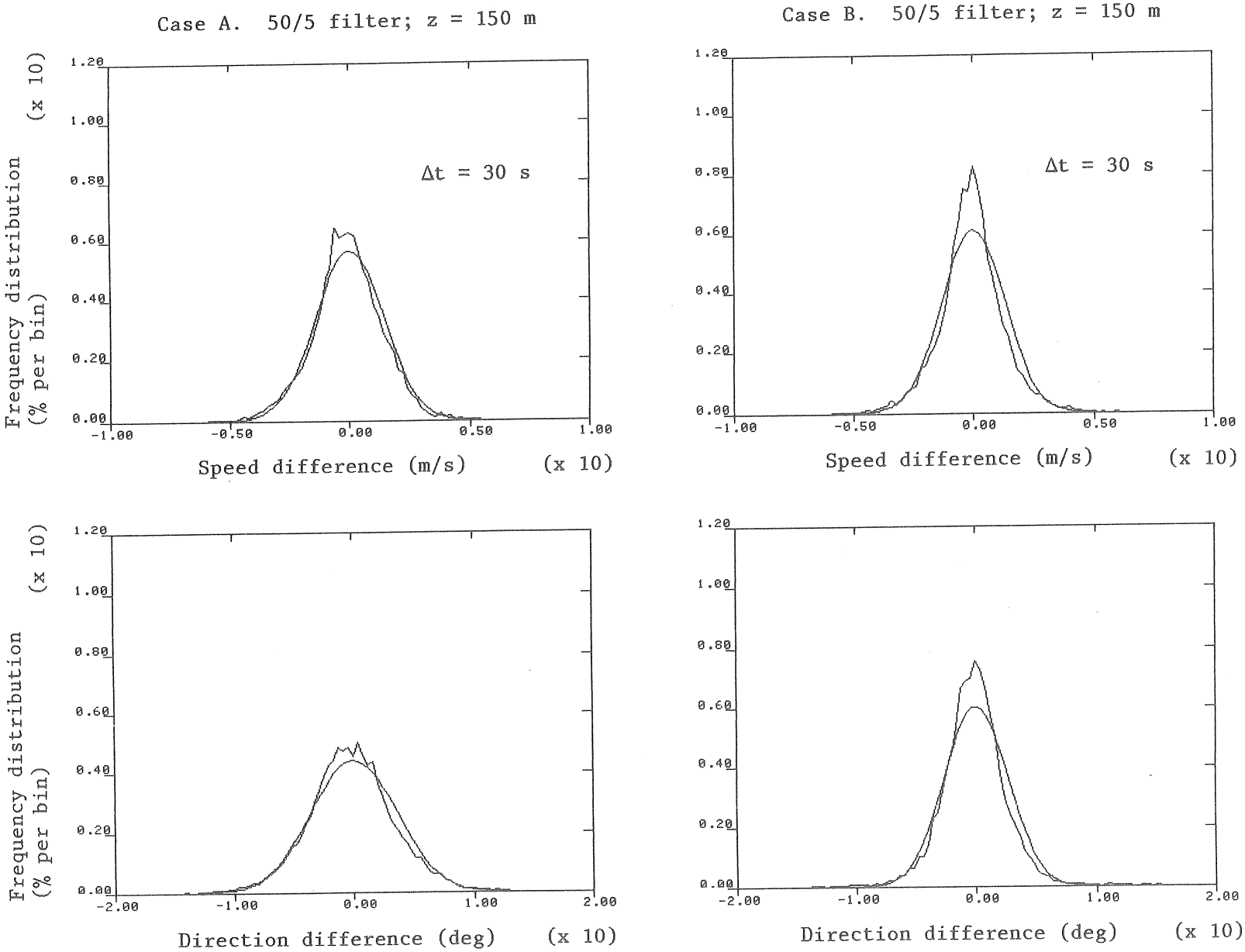

Figure 6.15--Distributions of speed and direction differences at 150 m with 50/5 filter and Δt = 30 s. ΔS = 0.2 m/s; ΔD = 0.4 deg.

7.0 ANALYSIS OF GUST 0 PARAMETERS

The GUST 0 definition of Powell and Connell (1980) contains the two elements essential to the definition of a discrete gust event: an amplitude definition and a time definition. These events, designated A_0 and T_0, are the maximum amplitudes and the time intervals between zero-crossings bracketing those peaks respectively. In studies reported so far, positive and negative values of A_0 and T_0 have been grouped for analysis. Positive and negative gusts have been treated as equivalent. This assumption is clearly not valid for the unfiltered data because of the degree of skewness in the original time series, but it is not an unreasonable one for filtered data. The statistical results presented in Figs. 7.1-7.3 are therefore confined to $+A_0$ and $+T_0$. Figures 7.4-7.9 offer a direct comparison of the positive and negative gust distribution events in the 50/5 filtered data. The scatter plots of amplitudes and time given in Figs. 7.10-7.13 provide yet another representation of their positive and negative distributions. The symmetry in the gust behavior is confirmed in these figures.

The GUST 0 statistics plotted in Figs. 7.1 and 7.2 show standard deviations of the gust amplitudes decreasing with height, and those of the gust times increasing with height. Sensitivity to filtering is much more pronounced in the gust times than in the gust amplitudes. The effect of height variation in the GUST 0 kurtosis is not as systematic as in the standard deviations. In general, the tendency is for the kurtosis to increase with height. The variation is somewhat less systematic in the cross correlation coefficients of Fig. 7.3, but the tendency of the cross correlation to decrease with height is apparent.

In the theoretical development of the GUST 0 model it is assumed that the A_0's and T_0's have distributions that approach Gaussian. Powell and Connell (1980) expect such a distribution for data subjected to a bandpass filter approximately a decade wide. If the bandwidth is significantly smaller or larger than a decade, they expect both the gust amplitudes and gust times to lose their Gaussian character. These

expectations are satisfied in their experimental results. Their data, which include both positive and negative values, with no distinction of sign, fit a half-Gaussian distribution reasonably well. No limiting value is imposed on the amplitudes or the times. In our analysis we treat positive and negative values separately but impose the condition that $|T_0| > \tau_\ell$, the lowpass filter time. Even though indications of a full Gaussian distribution are strong in our distribution plots, the absence of values close to zero (imposed partly by the limit on T_0 and partly by the lowpass cutoff in the pass band) makes exact comparisons difficult.

Another significant point of difference between our results and those of Powell and Connell (1980) is the magnitude of the A_0 T_0 correlation coefficients. Our correlations are almost a factor of 2 smaller. The scatter in Fig. 7.3 confirms this point. A correlation coefficient between 0.7 and 0.8 would have produced a tighter grouping of the data points.

As mentioned earlier the relevant parameters for WECS design are not the standard deviations but the rms values of the A_0's and T_0's. Conversion from one to the other requires knowledge of their mean values. For example,

$$\sigma^2_{rms}(+A_0) = \sigma^2(+A_0) + (+\bar{A}_0)^2 \ , \qquad (7.1)$$

where $\sigma_{rms}(+A_0)$ and $\sigma(+A_0)$ denote rms and standard deviation of $+A_0$, and the overbar denotes mean value.

In Table 7.1 we present the average values of A_0's and T_0's for Cases A and B. The corresponding rms values are given in Table 7.2. For a Gaussian distribution the ratio of the rms to average value should be $\sqrt{\pi}/2$ (≈ 1.25). The numbers in the two tables almost satisfy this condition.

Table 7.1--Average GUST 0 amplitudes and times (SI units)

Parameter	Height	Filter	Case A				Case B			
			$+\bar{A}_0$	$+\bar{T}_0$	$-\bar{A}_0$	$-\bar{T}_0$	$+\bar{A}_0$	$+\bar{T}_0$	$-\bar{A}_0$	$-\bar{T}_0$
Speed	10	30/3	1.49	7.42	-1.53	-7.55	1.80	6.55	-1.74	-6.87
		50/5	1.67	12.19	-1.67	-12.96	1.87	10.59	-1.72	-11.18
		100/10	1.76	21.30	-1.70	-23.81	1.89	19.03	-1.77	-21.11
	50	30/3	1.22	8.37	-1.25	-8.08	1.42	7.07	-1.50	-6.97
		50/5	1.35	13.34	-1.42	-12.96	1.53	11.42	-1.58	-11.49
		100/10	1.66	24.08	-1.65	-23.84	1.52	20.79	-1.63	-20.61
	150	30/3	1.07	8.53	-1.09	-8.29	1.04	7.84	-1.08	-7.76
		50/5	1.25	13.90	-1.25	-12.97	1.13	12.39	-1.18	-12.48
		100/10	1.39	23.93	-1.48	-23.81	1.26	21.95	-1.33	-22.94
Direction	10	30/3	4.91	6.60	-5.00	-6.41	4.96	5.47	-4.89	-5.44
		50/5	5.05	10.69	-5.01	-10.62	4.69	8.96	-4.54	-8.92
		100/10	4.98	20.12	-5.12	-20.42	4.15	16.20	-4.16	-16.99
	50	30/3	3.86	7.08	-3.81	-7.04	3.22	5.68	-3.11	-5.81
		50/5	3.90	11.06	-3.88	-11.11	3.11	9.52	-3.08	-9.96
		100/10	4.00	19.97	-3.96	-19.53	2.93	18.54	-2.89	-18.70
	150	30/3	3.25	7.64	-3.27	-7.58	2.30	6.84	-2.34	-6.93
		50/5	3.35	11.96	-3.44	-11.44	2.46	11.72	-2.45	-11.43
		100/10	3.35	19.87	-3.57	-19.07	2.56	22.32	-2.62	-20.58

Table 7.2--Root-mean-square GUST 0 amplitudes and times (SI units)

Parameter	Height	Filter	Case A				Case B			
			$\sigma_{rms}(+A_0)$	$\sigma_{rms}(+T_0)$	$\sigma_{rms}(-A_0)$	$\sigma_{rms}(-T_0)$	$\sigma_{rms}(+A_0)$	$\sigma_{rms}(+T_0)$	$\sigma_{rms}(-A_0)$	$\sigma_{rms}(-T_0)$
Speed	10	30/3	1.71	8.34	1.77	8.46	2.05	7.30	1.94	7.73
		50/5	1.88	13.60	1.89	14.67	2.07	11.75	1.91	12.62
		100/10	2.01	23.71	1.93	26.22	2.09	20.96	1.93	23.50
	50	30/3	1.41	9.40	1.46	9.06	1.68	7.98	1.80	7.82
		50/5	1.57	15.08	1.63	14.40	1.77	12.69	1.85	12.96
		100/10	1.89	26.83	1.87	26.51	1.75	23.63	1.87	23.24
	150	30/3	1.26	9.68	1.30	9.31	1.28	8.82	1.35	8.71
		50/5	1.44	15.60	1.47	14.43	1.36	13.94	1.44	13.85
		100/10	1.59	27.03	1.71	26.81	1.49	24.72	1.58	26.07
Direction	10	30/3	5.61	7.43	5.72	7.29	5.60	6.10	5.52	6.05
		50/5	5.68	11.90	5.64	11.92	5.25	9.81	5.09	9.84
		100/10	5.57	22.91	5.70	22.71	4.66	18.00	4.60	18.94
	50	30/3	4.42	7.91	4.36	7.84	3.85	6.35	3.68	6.51
		50/5	4.42	12.37	4.39	12.41	3.63	10.63	3.59	11.14
		100/10	4.47	22.58	4.38	22.04	3.34	20.91	3.34	21.07
	150	30/3	3.75	8.49	3.81	8.48	2.94	7.74	2.96	7.86
		50/5	3.83	13.34	3.93	12.65	3.04	13.33	3.02	13.00
		100/10	3.75	22.42	4.05	20.87	3.01	25.19	3.05	23.39

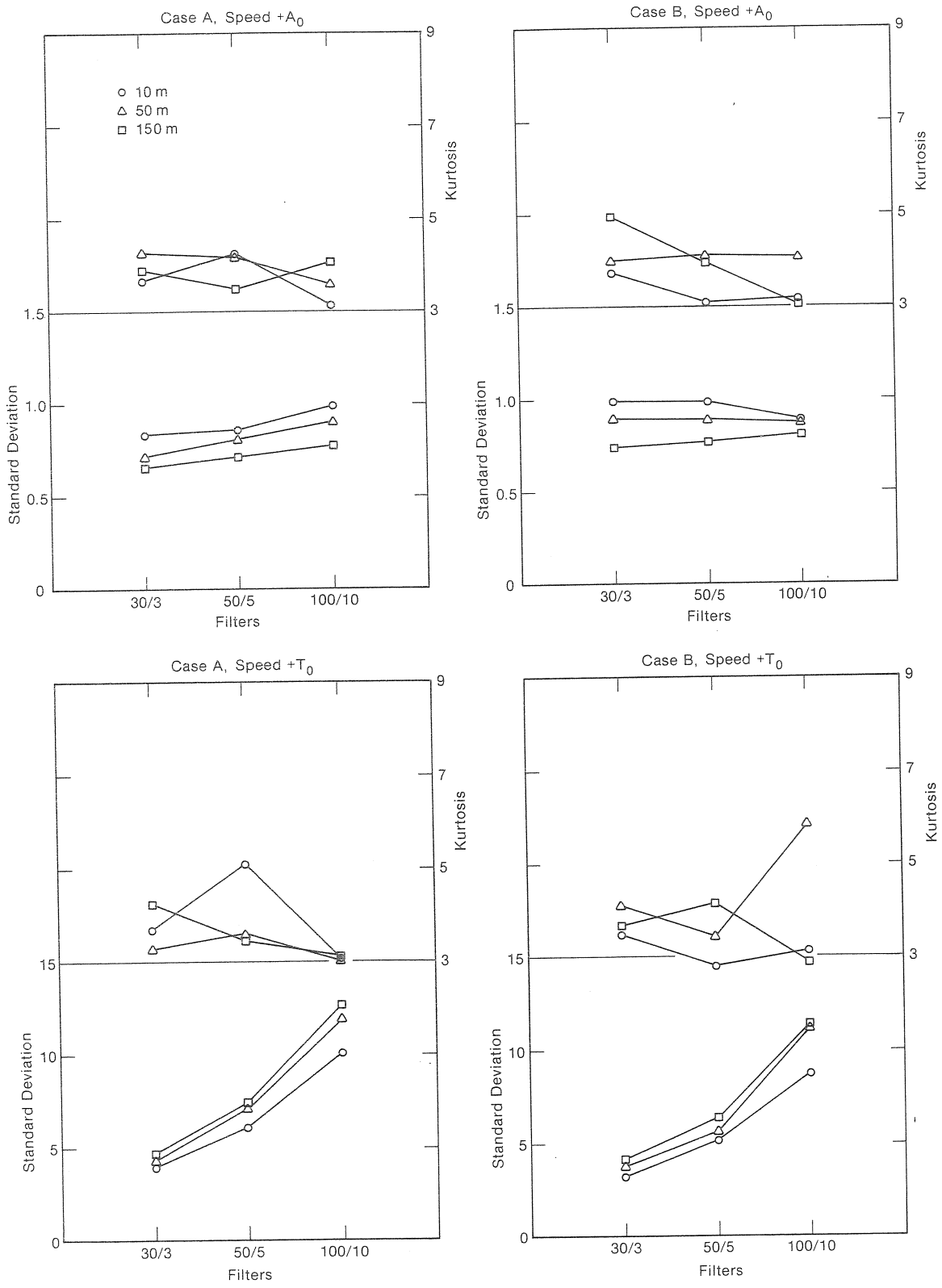

Figure 7.1--GUST 0 speed $+A_0$ and speed $+T_0$ kurtosis (upper part of frame) and standard deviation (lower part) as a function of bandpass filtering. Standard deviations are in m/s and degrees.

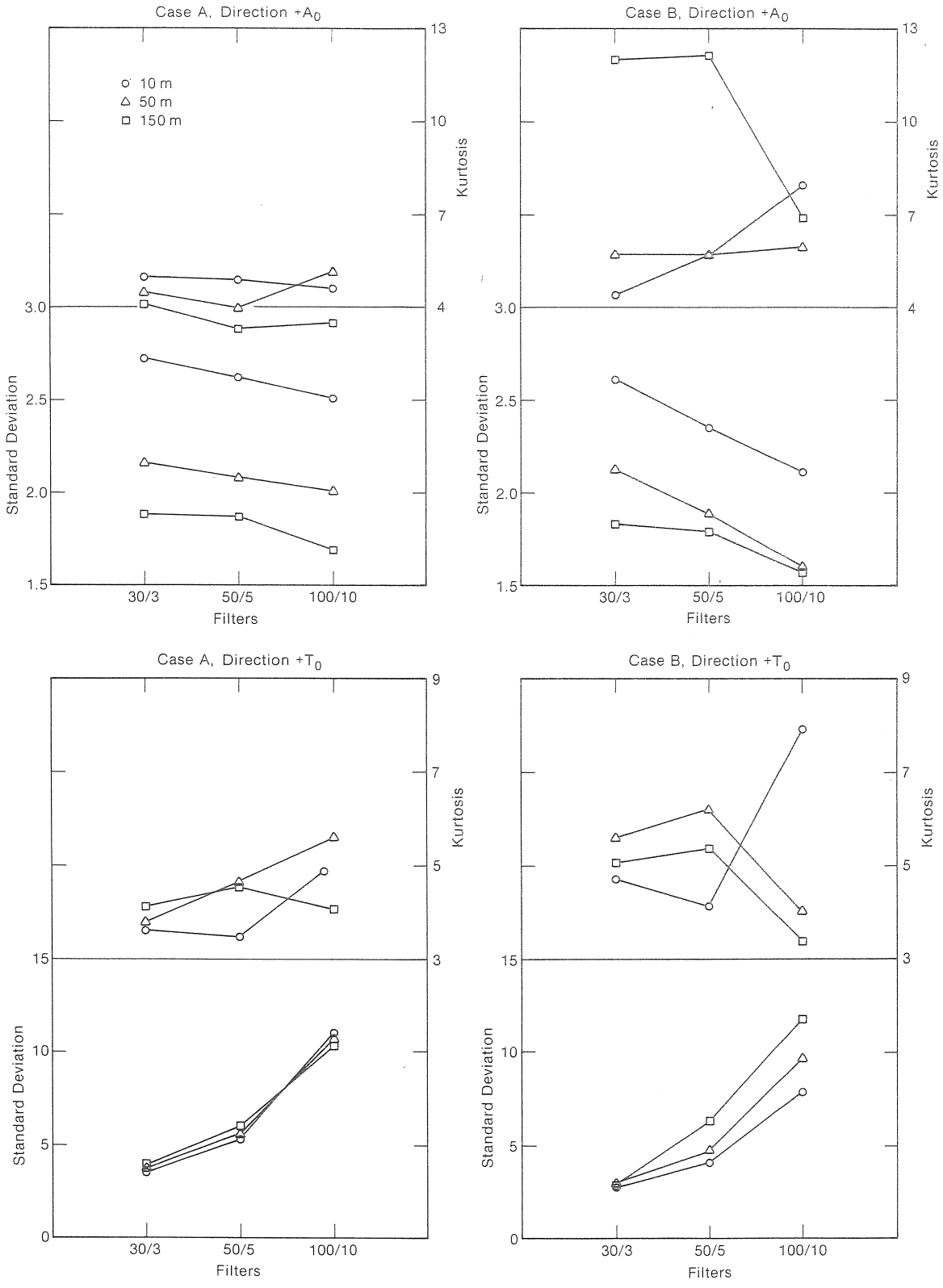

Figure 7.2--GUST 0 direction $+A_0$ and direction $+T_0$ statistics as a function of bandpass filtering. Standard deviations are in m/s and degrees.

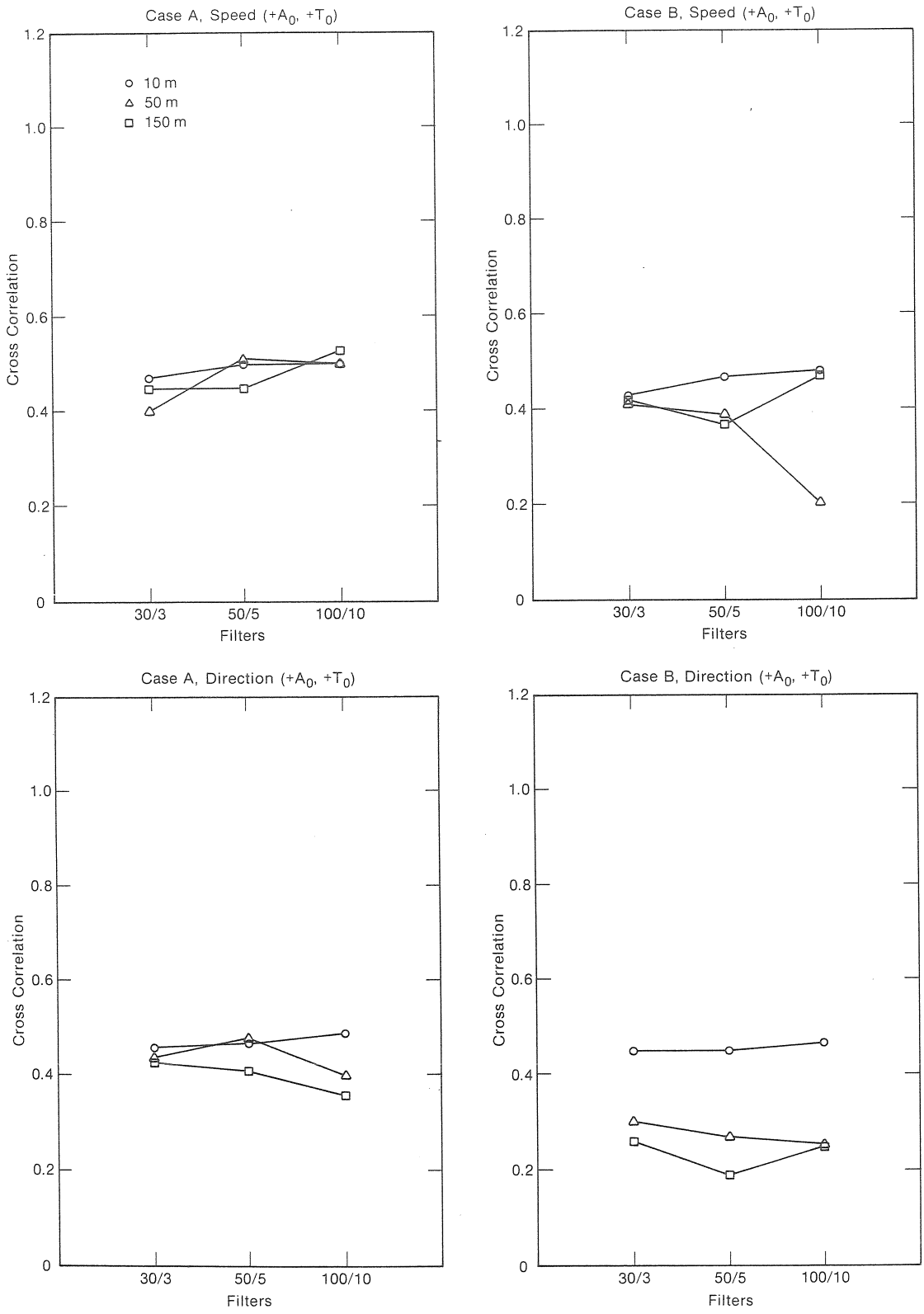

Figure 7.3--GUST 0 amplitude-time cross correlation coefficients as a function of bandpass filtering.

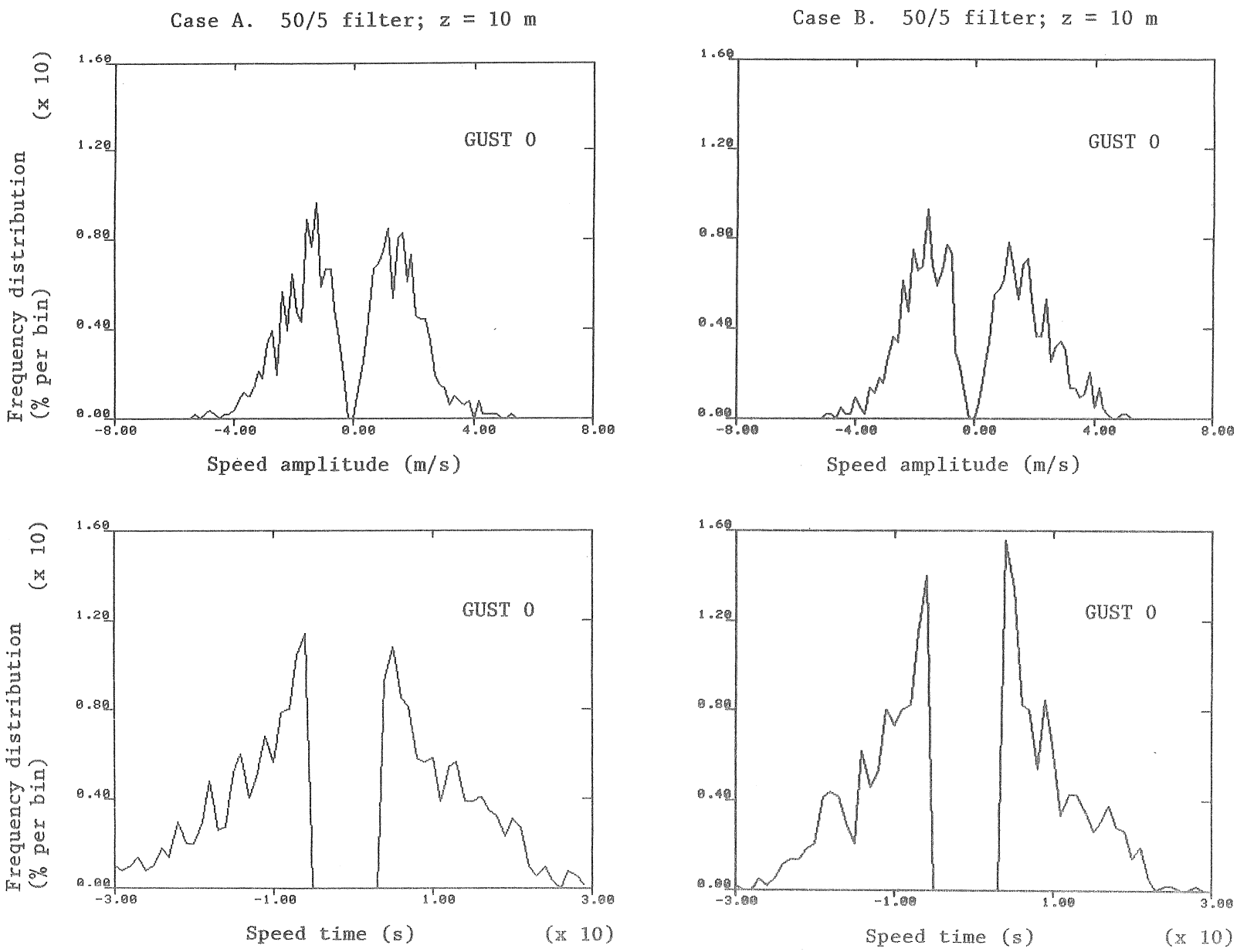

Figure 7.4--GUST 0 speed A_0 and speed T_0 distributions for 50/5 filter at 10 m. ΔA_0 = 0.16 m/s; ΔT_0 = 0.6 s.

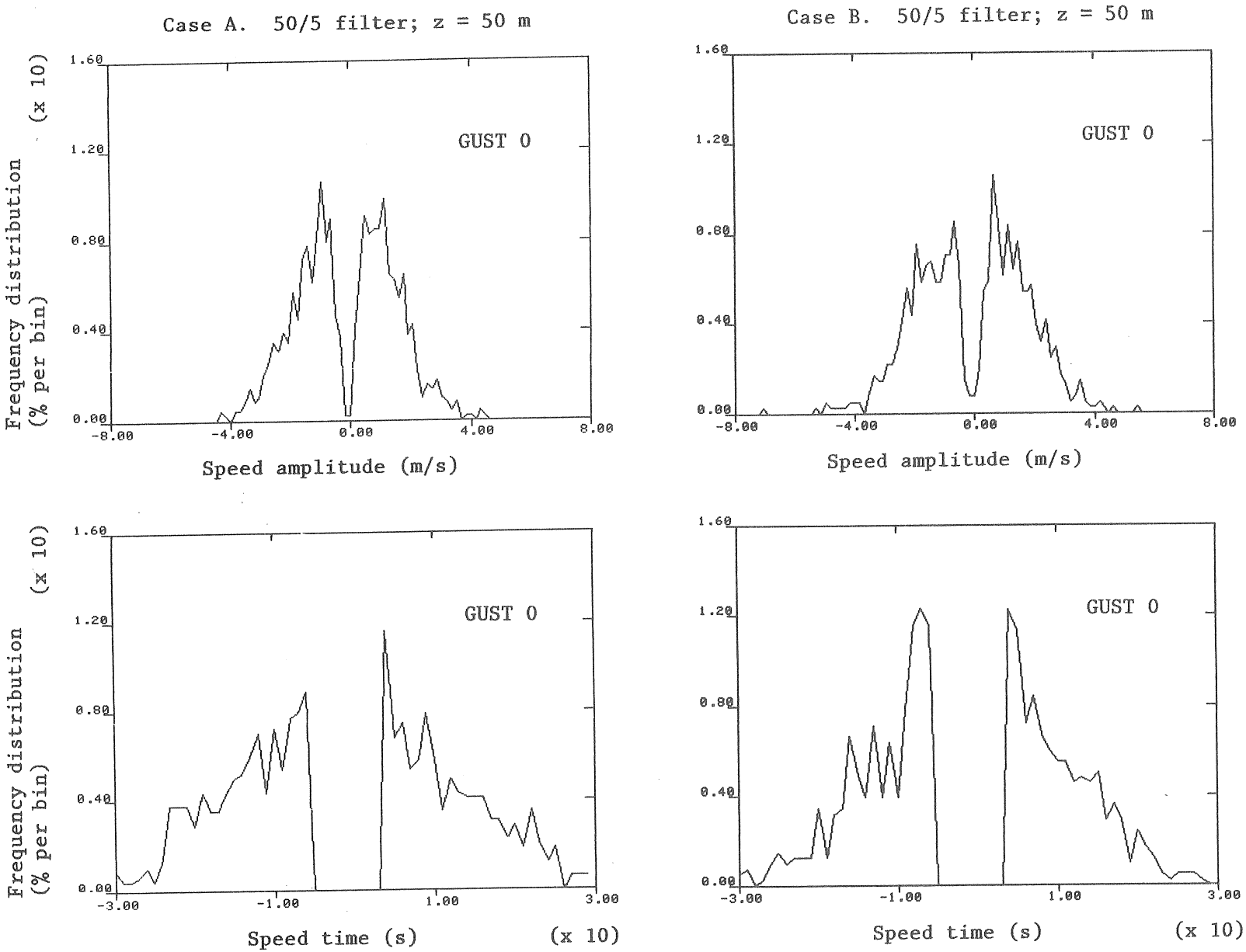

Figure 7.5--GUST 0 speed A_0 and speed T_0 distributions for 50/5 filter at 50 m. ΔA_0 = 0.16 m/s; ΔT_0 = 0.6 s.

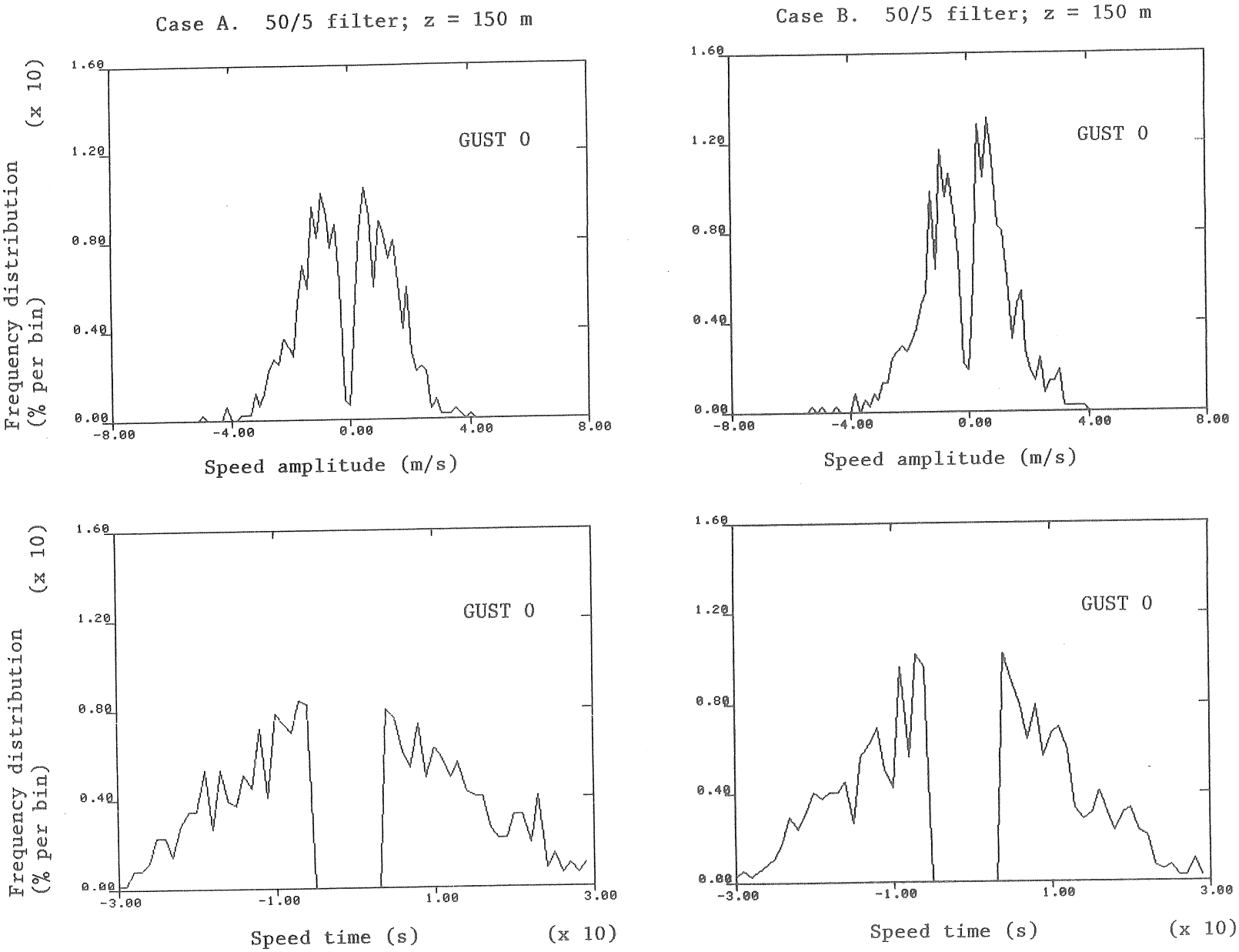

Figure 7.6--GUST 0 speed A_0 and speed T_0 distributions for 50/5 filter at 150 m. ΔA_0 = 0.16 m/s; ΔT_0 = 0.6 s.

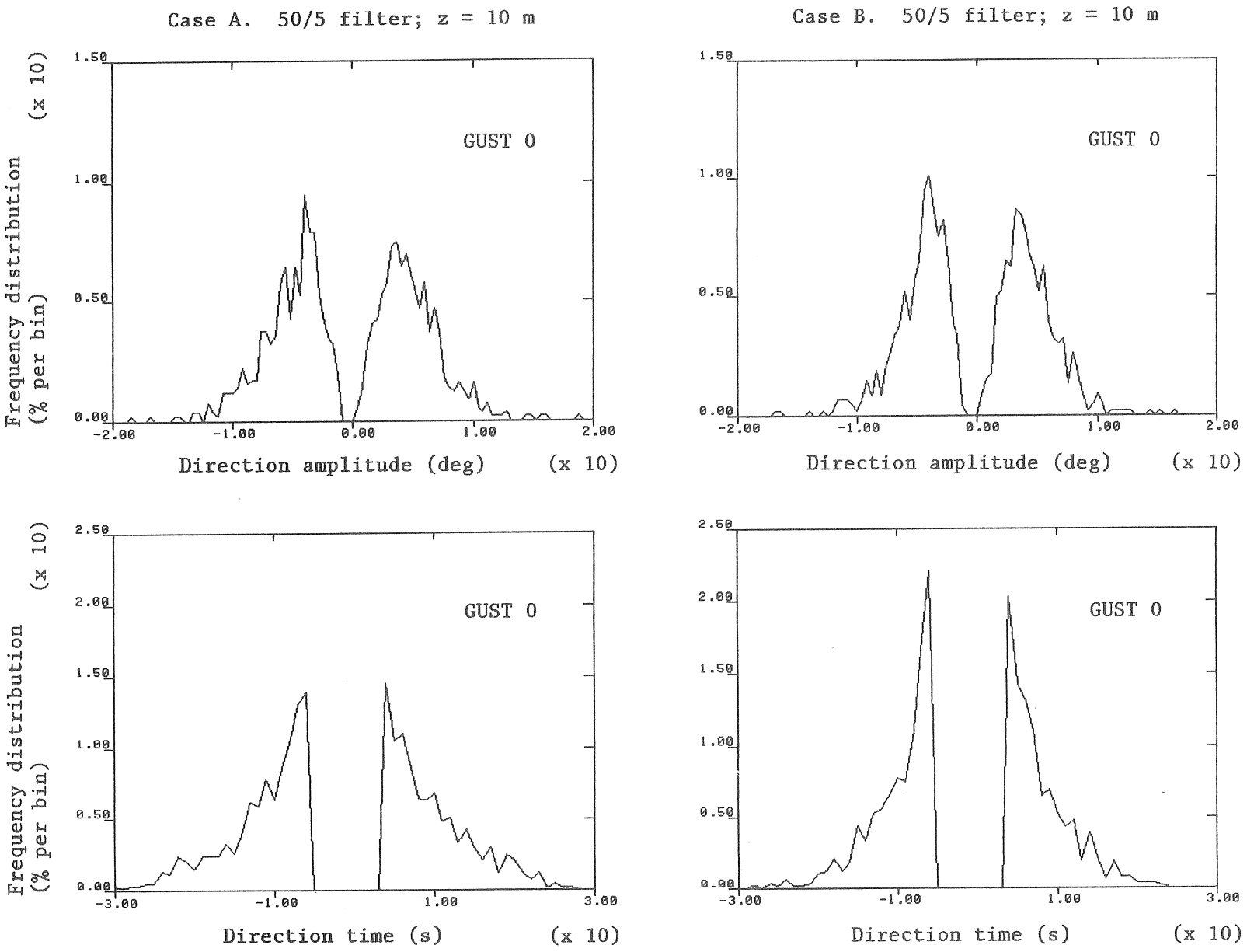

Figure 7.7--GUST 0 direction A_0 and direction T_0 distributions for 50/5 filter at 10 m. ΔA_0 = 0.4 deg; ΔT_0 = 0.6 s.

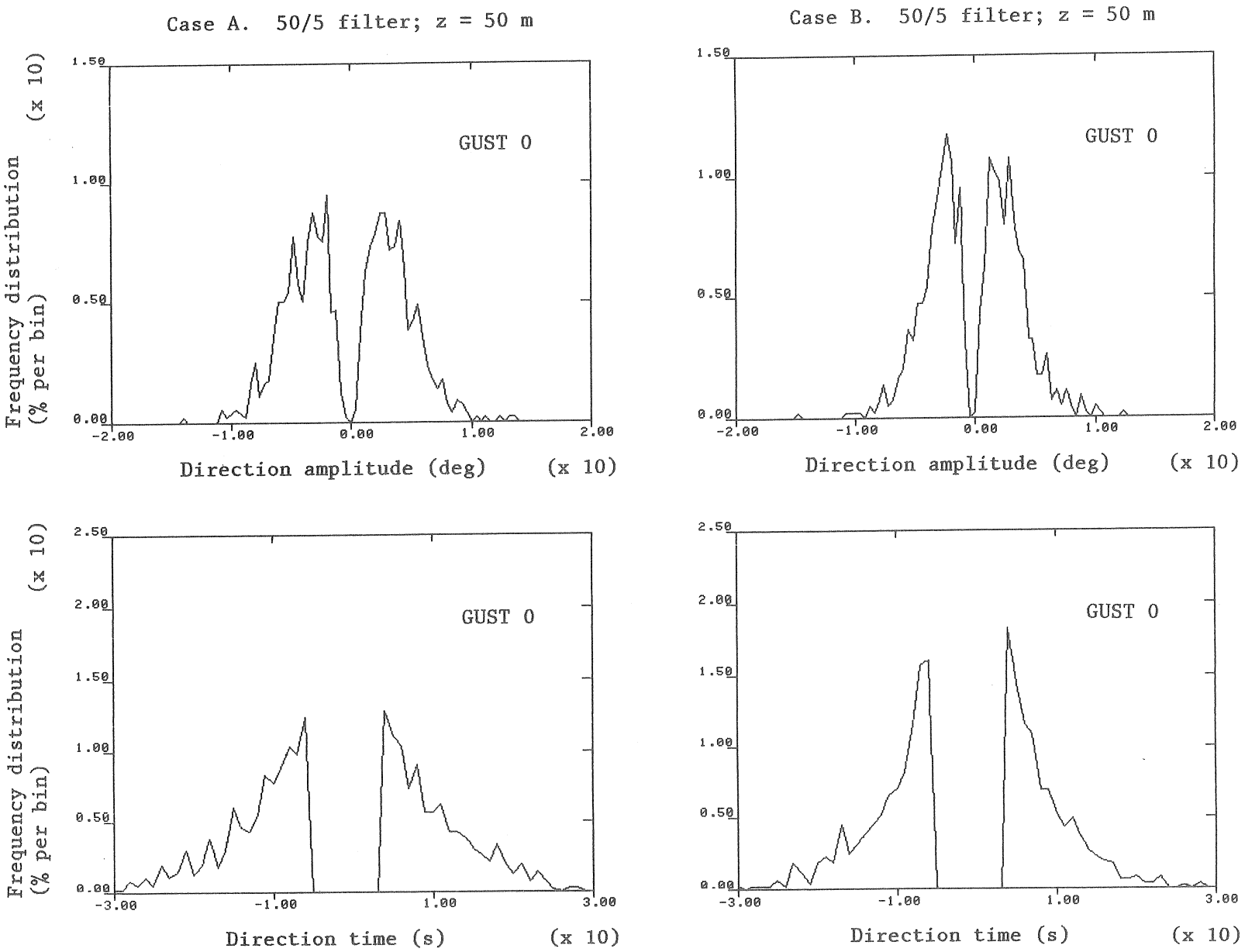

Figure 7.8--GUST 0 direction A_0 and direction T_0 distributions for 50/5 filter at 50 m. ΔA_0 = 0.4 deg; ΔT_0 = 0.6 s.

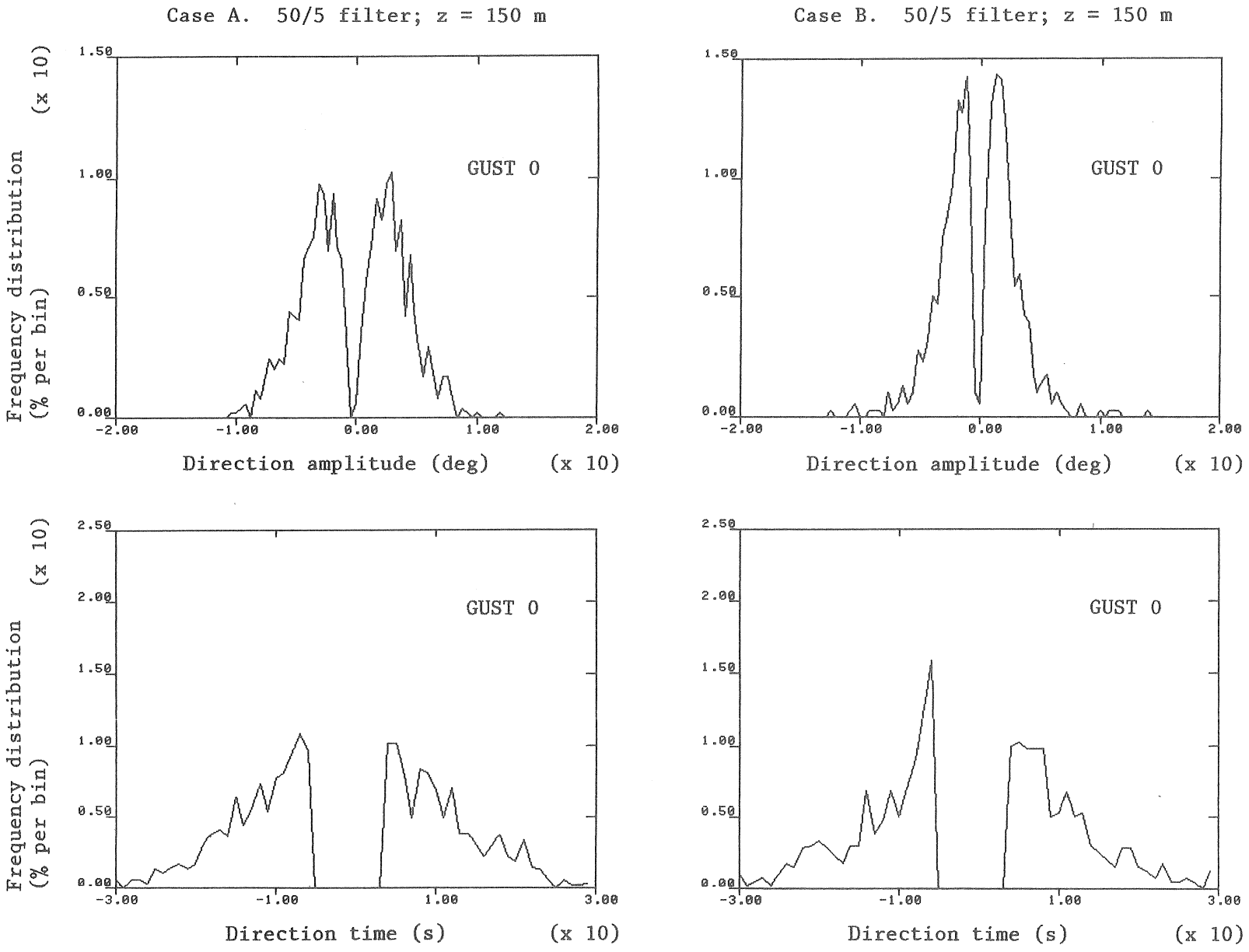

Figure 7.9--GUST 0 direction A_0 and direction T_0 distributions for 50/5 filter at 150 m. ΔA_0 = 0.4 deg; ΔT_0 = 0.6 s.

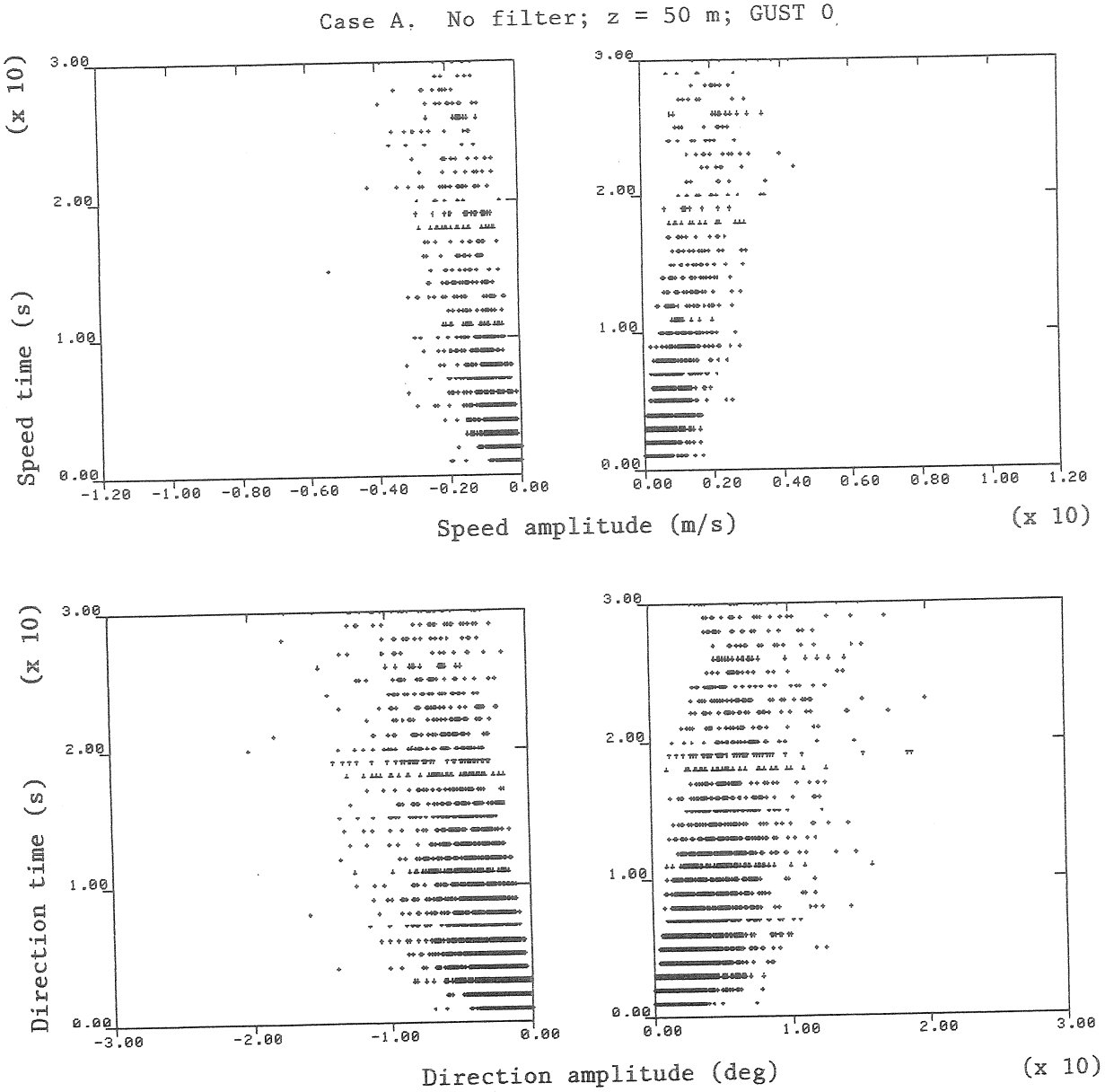

Figure 7.10--Plots of GUST 0 amplitudes vs. times for Case A at 50 m (no filter).

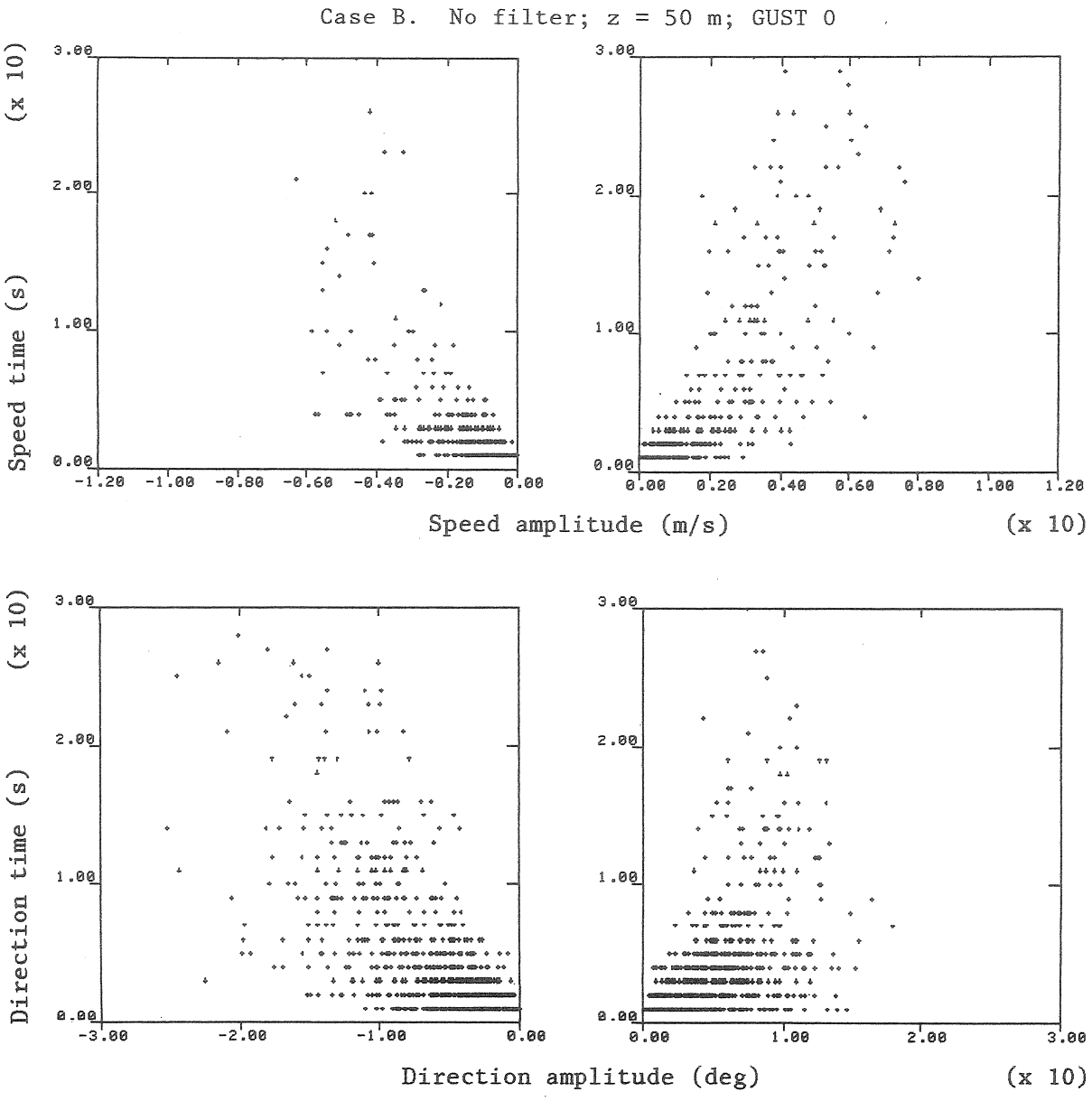

Figure 7.11--Plots of GUST 0 amplitudes vs. time for Case B at 50 m (no filter).

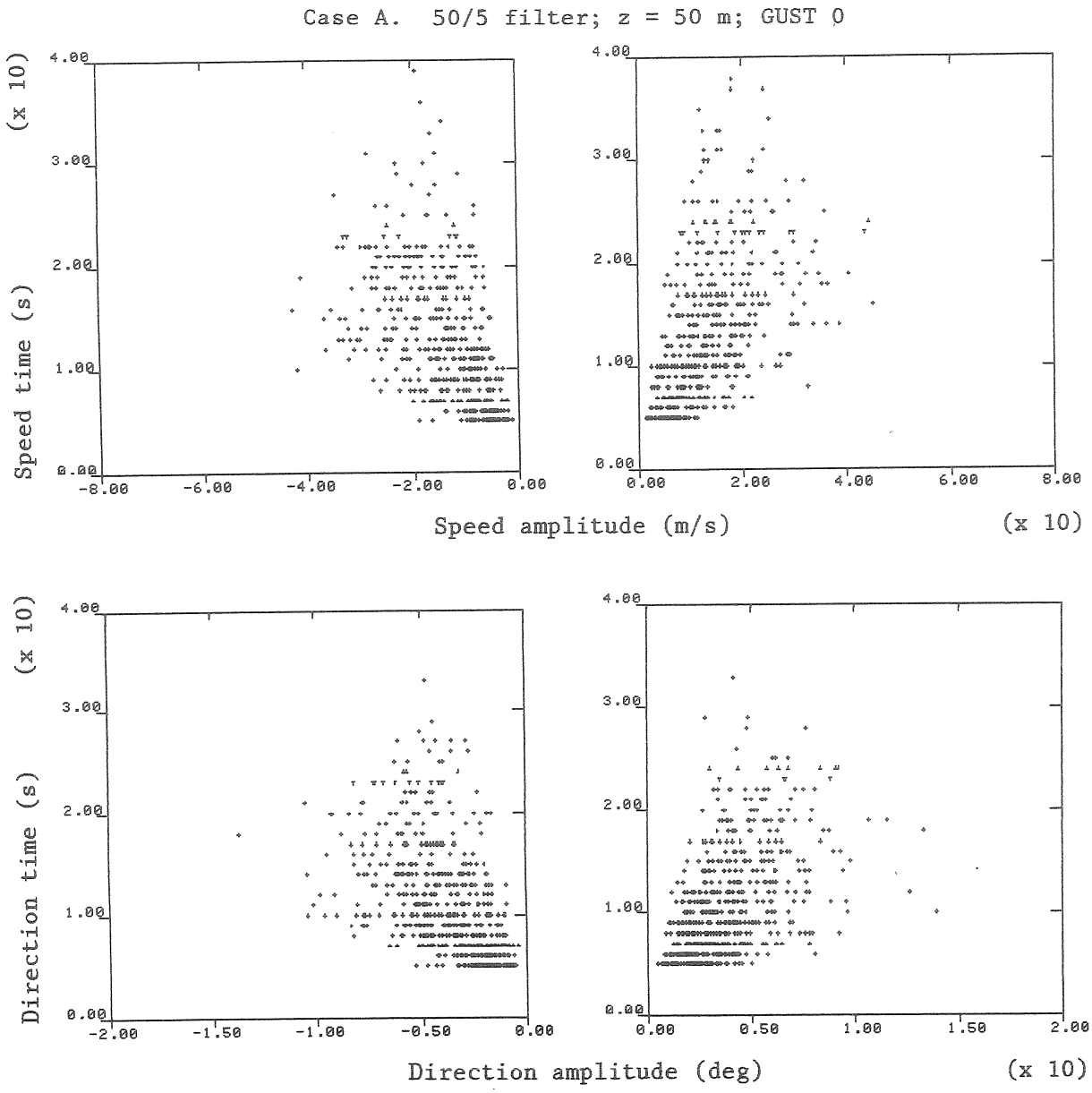

Figure 7.12--Plots of GUST 0 amplitudes vs. times for Case A at 50 m (50/5 filter).

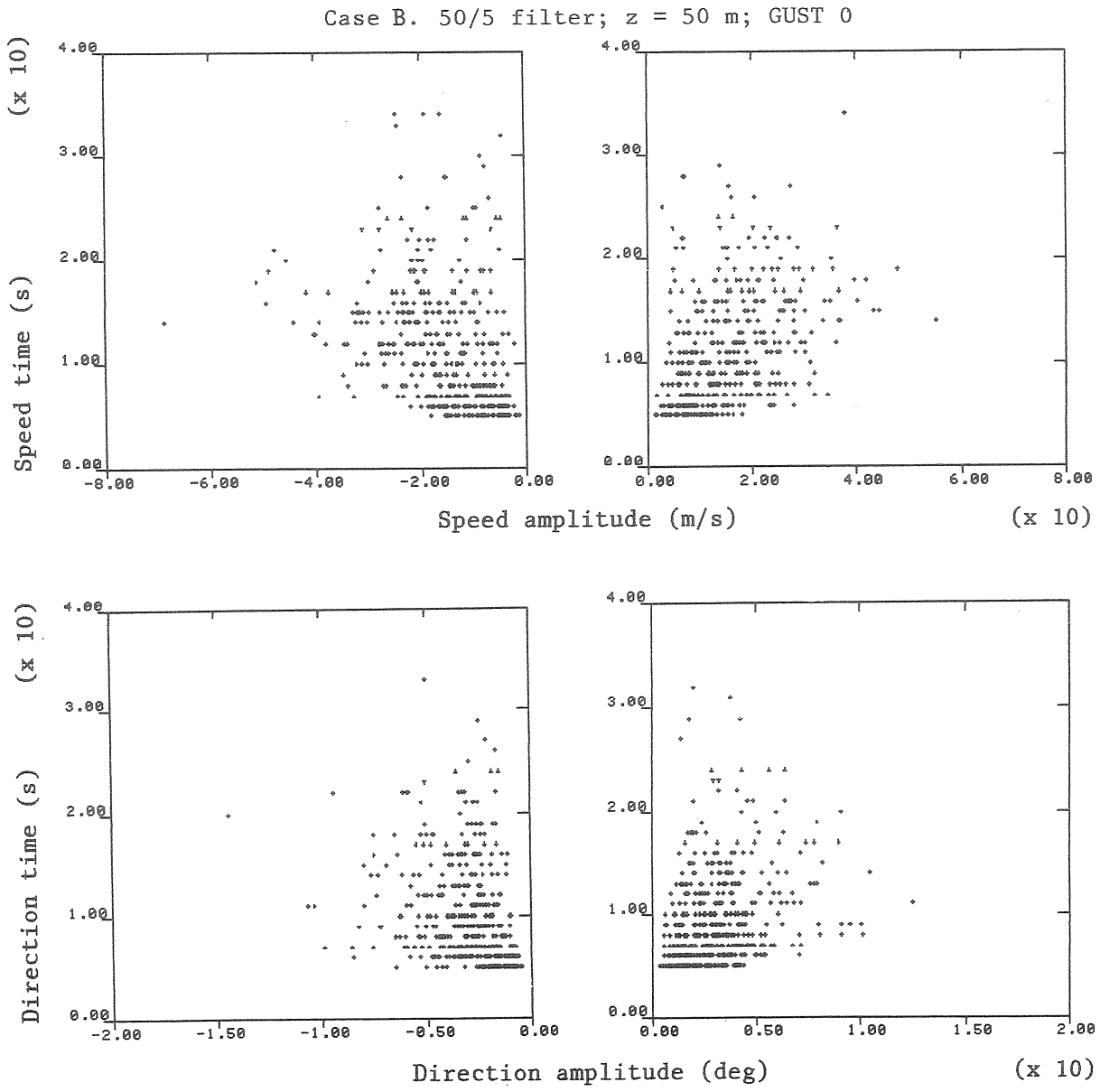

Figure 7.13--Plots of GUST 0 amplitude vs. time for Case B at 50 m (50/5 filter).

8.0 ANALYSIS OF GUST 1 PARAMETERS

In the GUST 1 model, the definitions of gust amplitude and gust time (designated A_1 and T_1) differ from those of GUST 0 in that the gust amplitude is the peak-to-peak amplitude and the gust time is the time interval between the two peaks (see Fig. 4.2). A positive sign indicates positive rate of change in the variable and a negative sign a negative rate of change. An advantage of this model is its insensitivity to the low-frequency trends in the data. The disparity between the filtered and unfiltered data in the statistical results is therefore not so great as in the GUST 0 results. The main disadvantage of the model is the need for an arbitrary specification of a minimum speed or time change that will qualify as a GUST 1 event. Otherwise, the smallest scale fluctuations will be the only ones recognized. For our definition of a GUST 1 event we impose the condition that T_1 be equal to or larger than the lowpass filter time used in the bandpass filter. The sensitivity of the model to the tolerance interval is a factor that has to be considered when interpreting the statistical results in Figs. 8.1-8.3. Distribution plots showing positive and negative events, similar to those presented for GUST 0, are shown in Figs. 8.4-8.9; the scatter plots for the same events are in Figs. 8.10-8.13.

Comparing the GUST 1 statistics of Figs. 8.1 and 8.2 with those in Figs. 7.1 and 7.2, we find in the former set a greater sensitivity to height change. It is also apparent that the standard deviation of A_1 is roughly twice as large as the standard deviation of A_0, while the reverse is true with the standard deviations of T_1 and T_0. Despite these differences, the A_1 T_1 cross correlations behave much like the A_0 T_0 cross correlations in Fig. 7.3.

Here, as in the GUST 0 model, the relevant parameters for WECS design are the rms values of the gust amplitudes and the gust times. The time averages used for converting the standard deviations into rms values are presented in Table 8.1. The calculated rms values are given in Table 8.2.

Table 8.1--Average GUST 1 amplitudes and times (SI units)

Parameter	Height	Filter	Case A				Case B			
			$+\bar{A}_1$	$+\bar{T}_1$	$-\bar{A}_1$	$-\bar{T}_1$	$+\bar{A}_1$	$+\bar{T}_1$	$-\bar{A}_1$	$-\bar{T}_1$
Speed	10	30/3	2.23	4.29	-2.08	-4.66	2.65	3.94	-2.62	-4.29
		50/5	2.51	6.55	-2.32	-7.21	2.84	6.05	-2.72	-6.45
		100/10	2.88	10.99	-2.59	-11.98	3.09	10.37	-3.12	-11.21
	50	30/3	1.72	4.54	-1.61	-4.71	2.16	4.02	-2.10	-4.34
		50/5	2.06	7.04	-1.94	-7.60	2.57	6.05	-2.26	-6.61
		100/10	2.44	11.75	-2.24	-12.64	2.90	10.56	-2.52	-11.53
	150	30/3	1.50	4.63	-1.45	4.95	1.49	4.26	-1.45	-4.51
		50/5	1.76	7.11	-1.74	-7.63	1.71	6.61	-1.66	-6.93
		100/10	2.19	12.09	-2.07	-12.66	1.93	11.24	-1.93	-11.53
Direction	10	30/3	7.45	4.00	-7.35	-4.02	8.08	3.70	-8.01	-3.68
		50/5	8.02	6.24	-7.84	-6.22	8.41	5.81	-8.10	-5.64
		100/10	9.06	10.74	-8.73	-10.82	8.72	10.26	-9.06	-10.02
	50	30/3	5.64	4.32	-5.49	-4.30	4.97	3.78	-4.97	-3.74
		50/5	6.00	6.53	-6.06	-6.61	5.21	5.83	-5.15	-5.85
		100/10	6.57	10.77	-6.48	-11.02	5.76	10.23	-6.06	-10.34
	150	30/3	4.60	4.52	-4.55	-4.43	3.39	4.10	-3.40	-4.09
		50/5	5.18	6.91	-5.07	-6.77	3.75	6.46	-3.75	-6.55
		100/10	5.62	10.97	-5.66	-11.11	3.98	11.23	-4.08	-11.34

Table 8.2--Root-mean-square GUST 1 amplitudes and times (SI units)

Parameter	Height	Filter	Case A				Case B			
			$\sigma_{rms}(+A_1)$	$\sigma_{rms}(+T_1)$	$\sigma_{rms}(-A_1)$	$\sigma_{rms}(-T_1)$	$\sigma_{rms}(+A_1)$	$\sigma_{rms}(+T_1)$	$\sigma_{rms}(-A_1)$	$\sigma_{rms}(-T_1)$
Speed	10	30/3	2.67	4.59	2.44	5.06	3.05	4.15	2.98	4.59
		50/5	2.90	6.87	2.63	7.63	3.18	6.22	3.01	6.72
		100/10	3.23	11.31	2.86	12.53	3.34	10.60	3.34	11.45
	50	30/3	2.09	4.92	1.94	5.12	2.62	4.26	2.51	4.65
		50/5	2.41	7.44	2.25	8.13	2.94	6.28	2.60	6.92
		100/10	2.75	12.18	2.54	13.25	3.22	10.79	2.84	11.14
	150	30/3	1.85	4.97	1.77	5.42	1.90	4.56	1.85	4.88
		50/5	2.10	7.52	2.06	8.18	2.09	6.90	2.03	7.29
		100/10	2.50	12.66	2.37	13.26	2.27	11.60	2.31	11.94
Direction	10	30/3	7.57	4.22	7.48	4.26	8.15	3.86	8.08	3.83
		50/5	8.20	6.46	8.05	6.48	8.48	5.92	8.16	5.73
		100/10	9.36	11.00	9.22	11.22	8.85	10.37	9.33	10.26
	50	30/3	5.87	4.62	5.74	4.61	5.11	3.96	5.09	3.90
		50/5	6.29	6.80	6.37	6.89	5.36	5.96	5.31	5.99
		100/10	6.94	11.00	6.92	11.28	6.19	10.48	6.49	10.60
	150	30/3	4.95	4.88	4.85	4.74	3.71	4.37	3.74	4.37
		50/5	5.66	7.27	5.51	7.10	4.21	6.74	4.29	6.88
		100/10	6.11	11.23	6.29	11.44	4.82	11.55	4.98	11.70

The rms values and averages in the tables confirm what the scatter plots of Figs. 8.10-8.13 show: that gust amplitudes tend to be larger and the corresponding gust times smaller in GUST 1 than in GUST 0. The effect of our gust time limit, $|T_1| > \tau_\ell$, in the analysis is therefore particularly severe in the distribution plots of Figs. 8.1-8.9. Although the $+T_0$'s and $-T_0$'s cover the range between τ_ℓ and τ_h, the $+T_1$'s and $-T_1$'s are confined to a narrow range between τ_ℓ and 2.5 τ_ℓ. Tests for Gaussian distribution will have little meaning under those conditions.

It appears from the full set of distribution plots (only a few are shown here) that the highpass filter has no direct effect on the upper range of T_1's observed. Only the unfiltered data show a distribution that is nearly Gaussian, but T_1's are limited to ±10 s. An appropriate combination of lowpass filtering and amplitude tolerance specification could, conceivably, yield more realistic distribution curves.

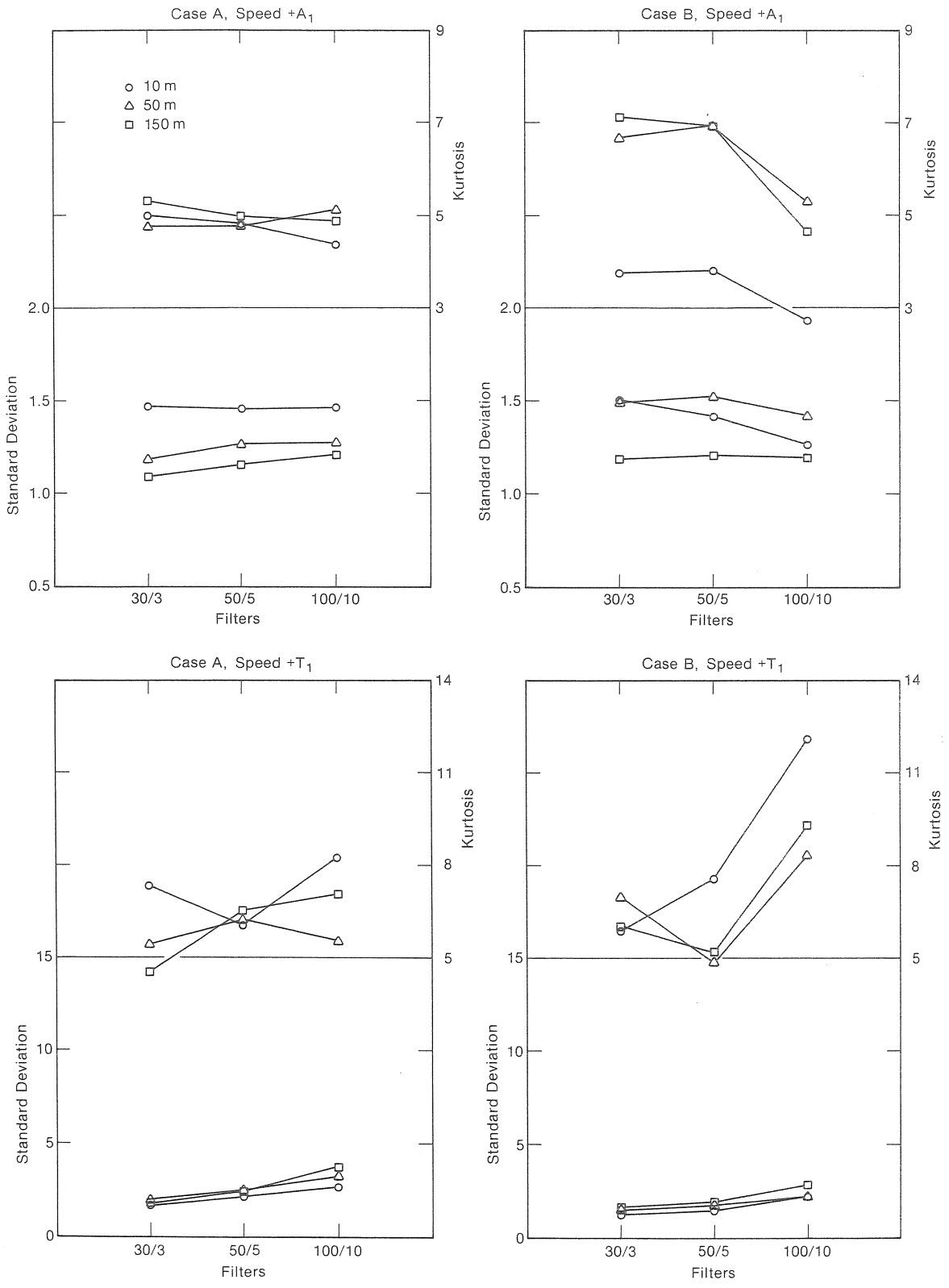

Figure 8.1--GUST 1 speed $+A_1$ and speed $+T_1$ statistics as a function of bandpass filtering. Standard deviations are in m/s and degrees.

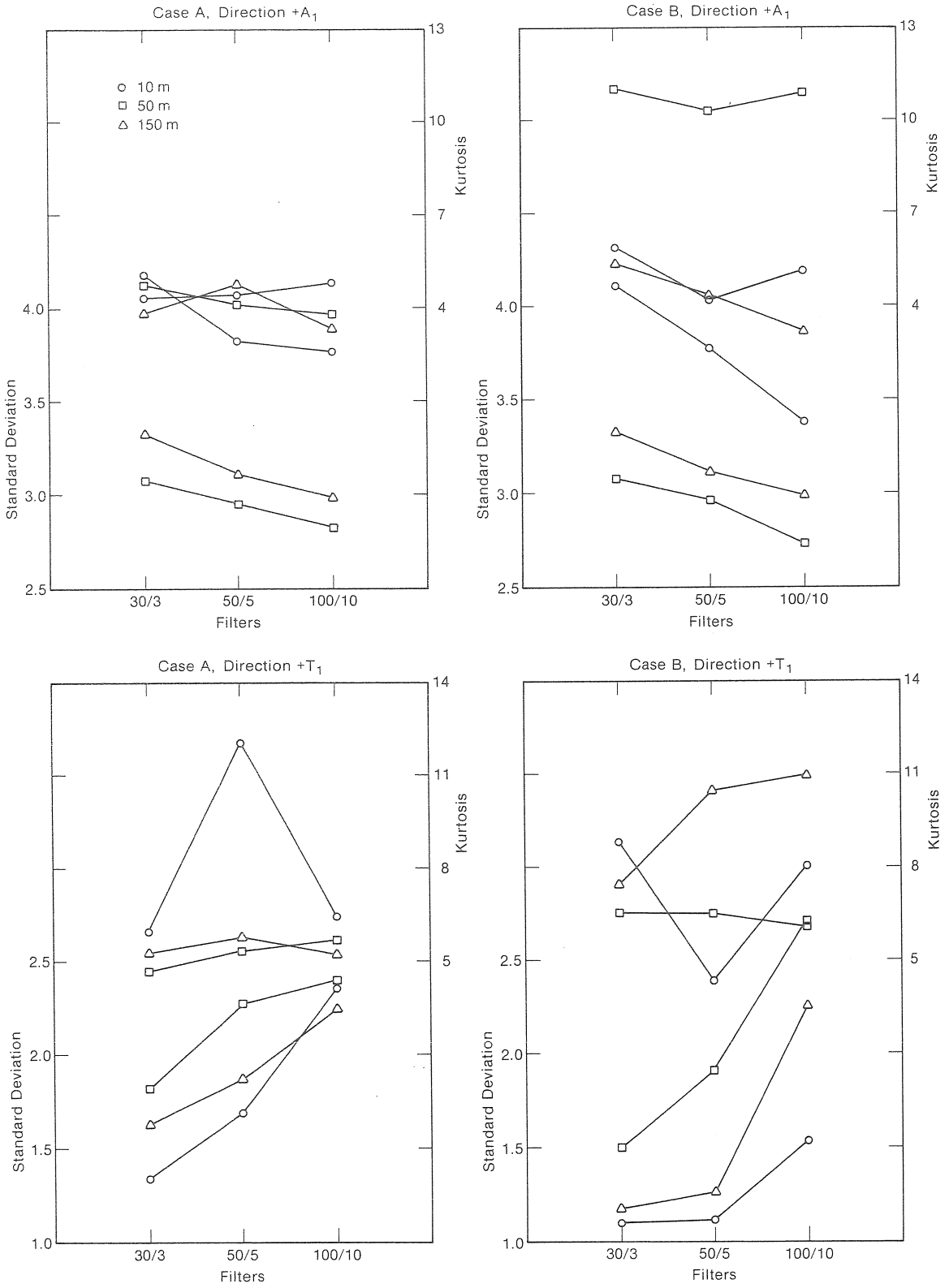

Figure 8.2--GUST 1 direction $+A_1$ and direction $+T_1$ statistics as a function of bandpass filtering. Standard deviations are in m/s and degrees.

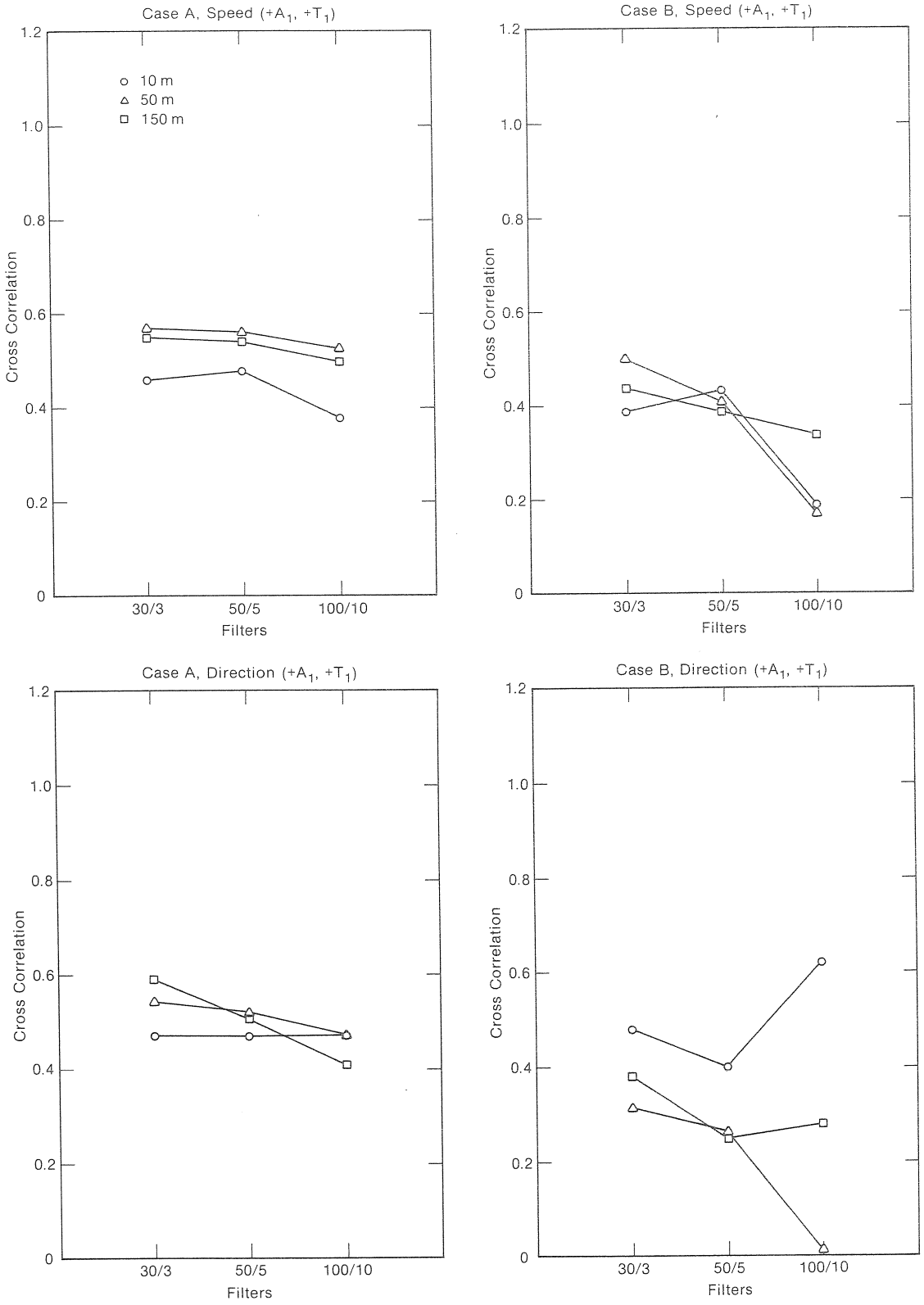

Figure 8.3--GUST 1 amplitude-time cross correlation coefficients as a function of bandpass filtering.

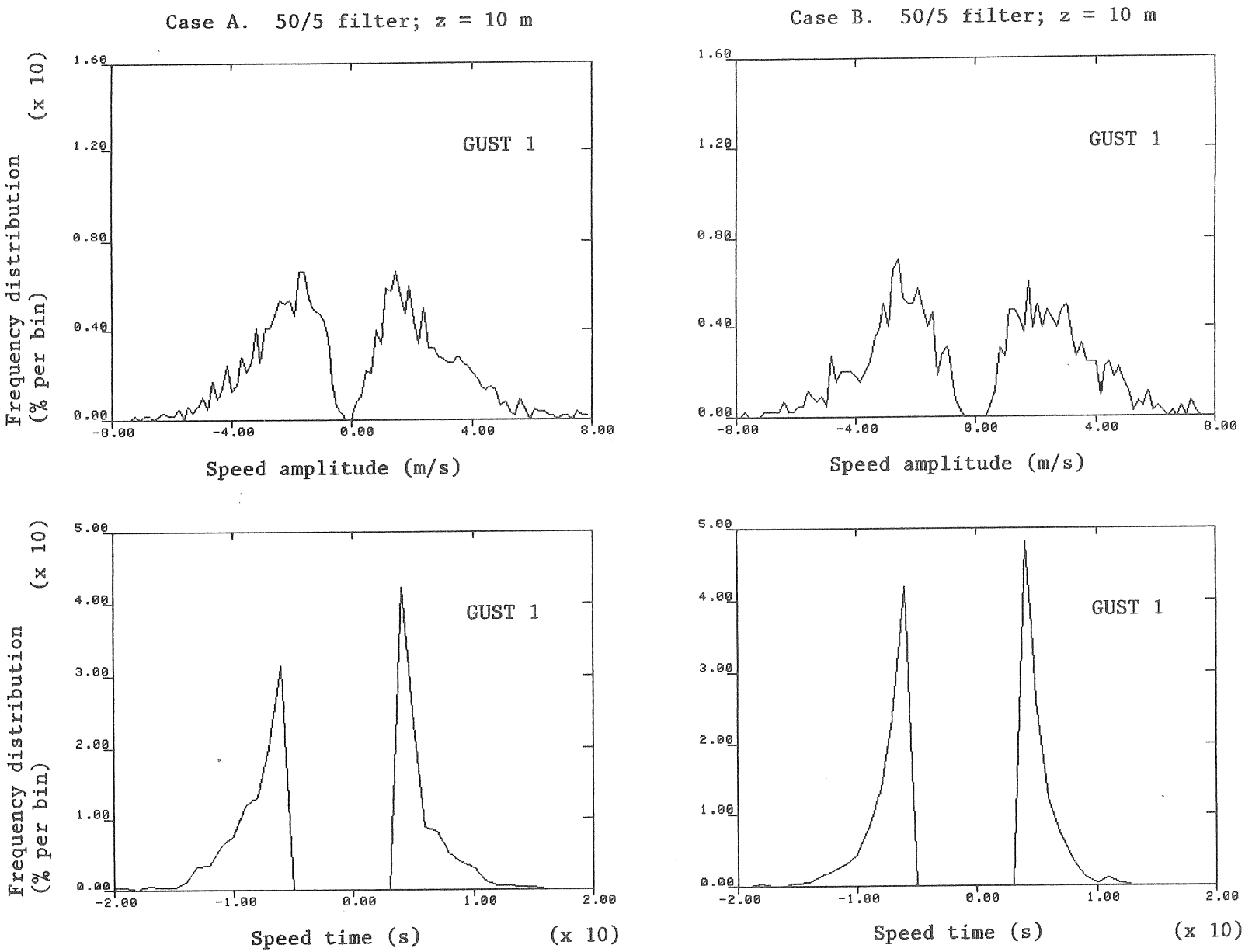

Figure 8.4--GUST 1 speed A_1 and speed T_1 distributions for 50/5 filter at 10 m. ΔA_1 = 0.16 m/s; ΔT_1 = 0.4 s.

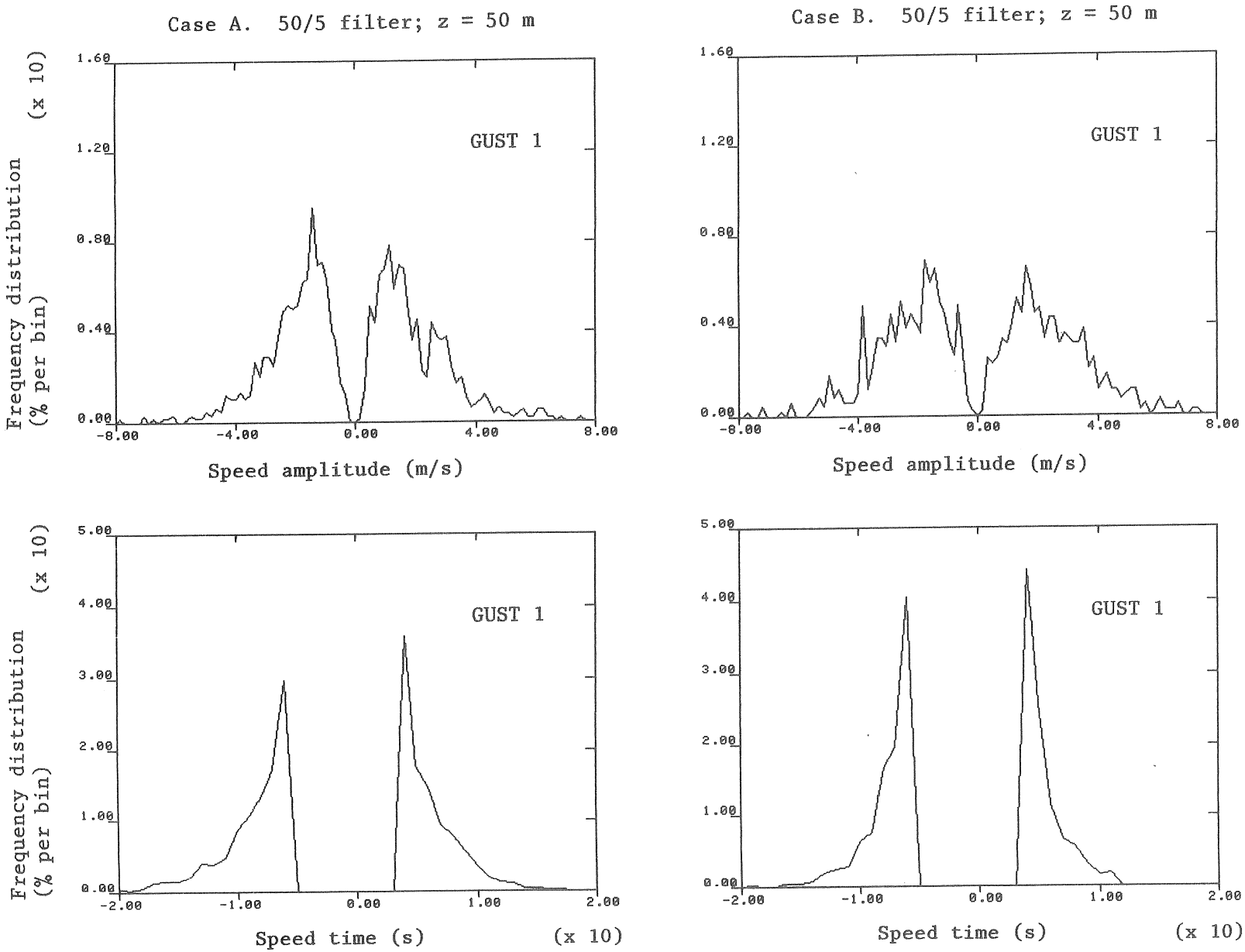

Figure 8.5--GUST 1 speed A_1 and speed T_1 distributions for 50/5 filter at 50 m. ΔA_1 = 0.16 m/s; ΔT_1 = 0.4 s.

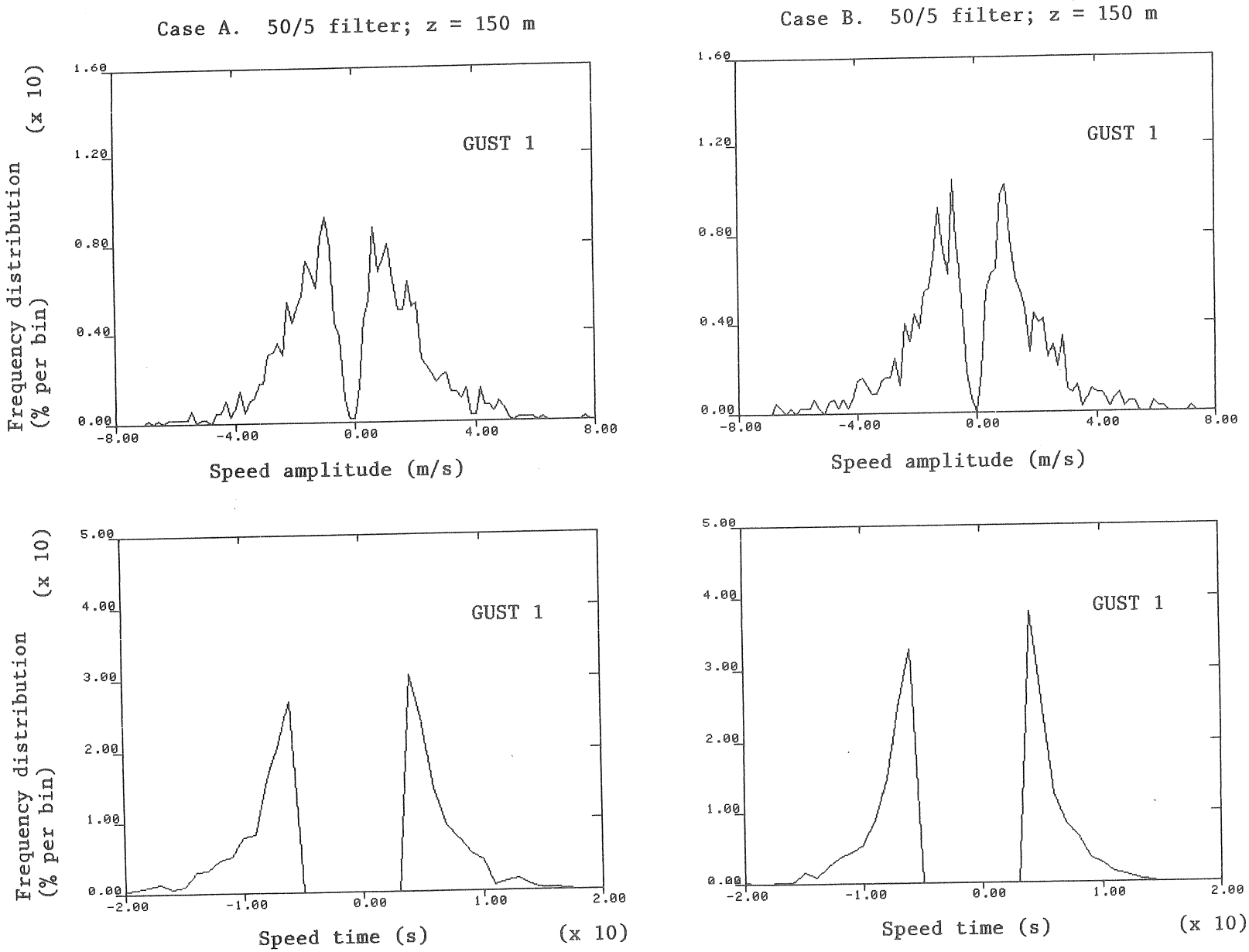

Figure 8.6--GUST 1 speed A_1 and speed T_1 distributions for 50/5 filter at 150 m. ΔA_1 = 0.16 m/s; ΔT_1 = 0.4 s.

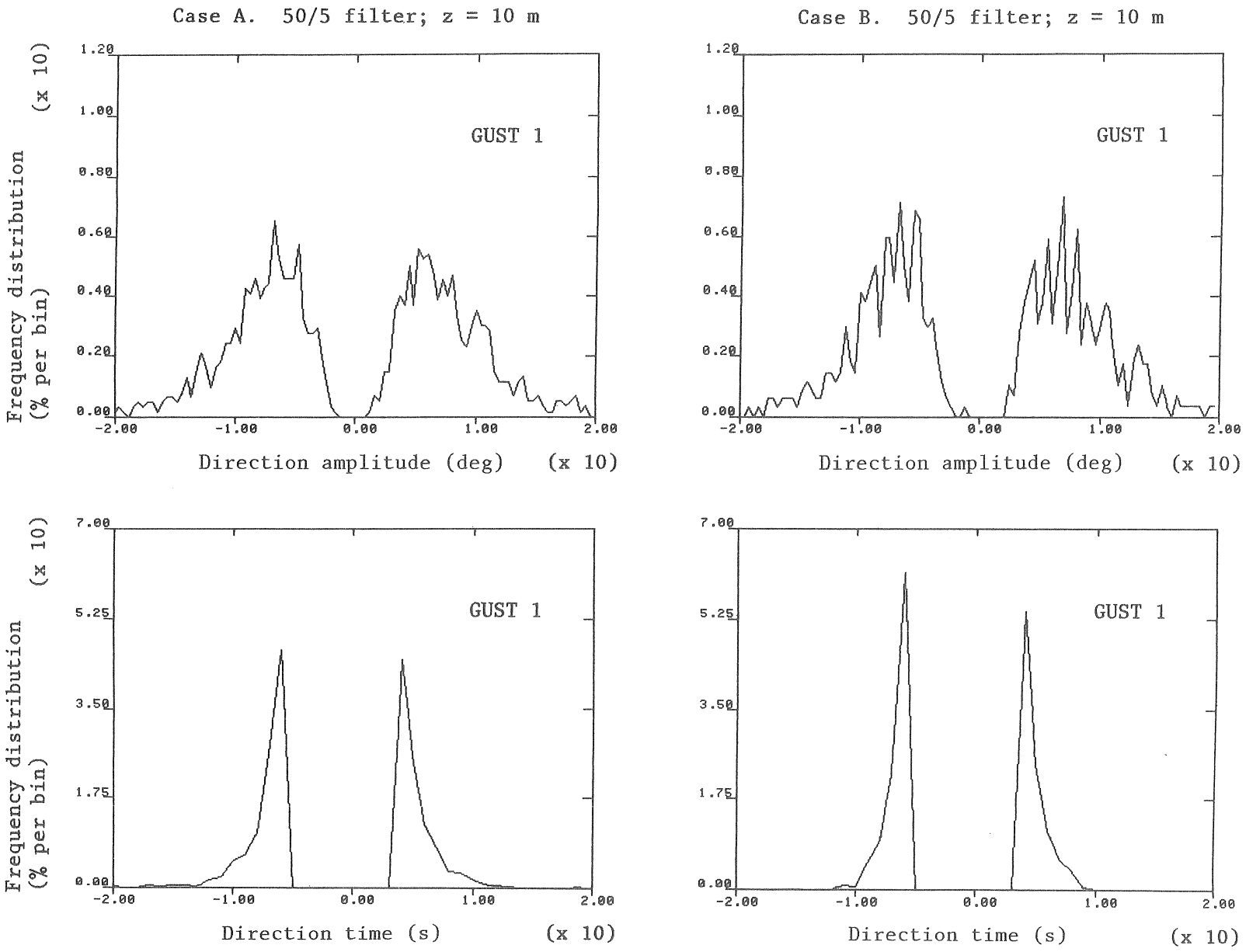

Figure 8.7--GUST 1 direction A_1 and direction T_1 distributions for 50/5 filter at 10 m. ΔA_1 = 0.4 deg; ΔT_1 = 0.4 s.

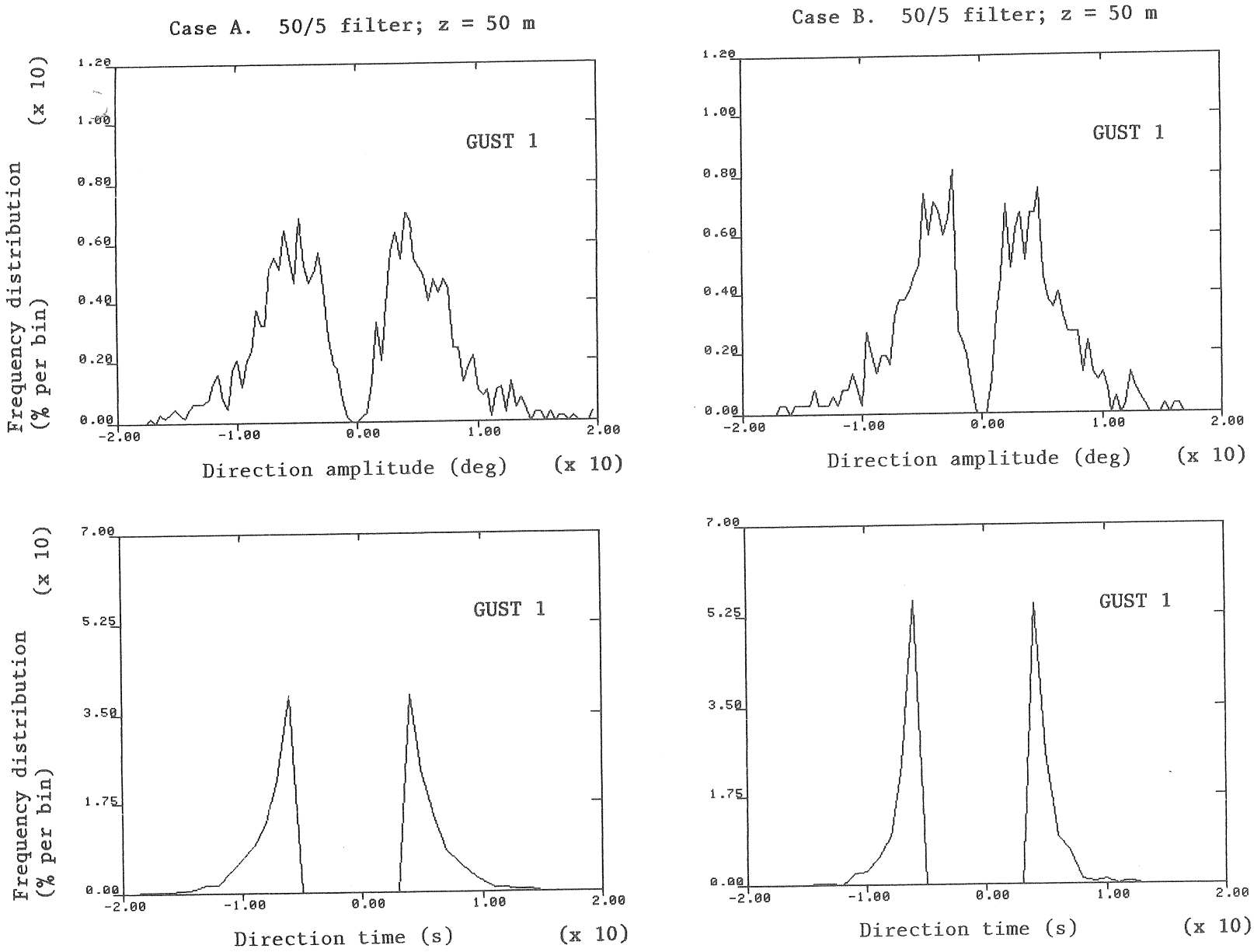

Figure 8.8--GUST 1 direction A_1 and direction T_1 distributions for 50/5 filter at 50 m. ΔA_1 = 0.4 deg; ΔT_1 = 0.4 s.

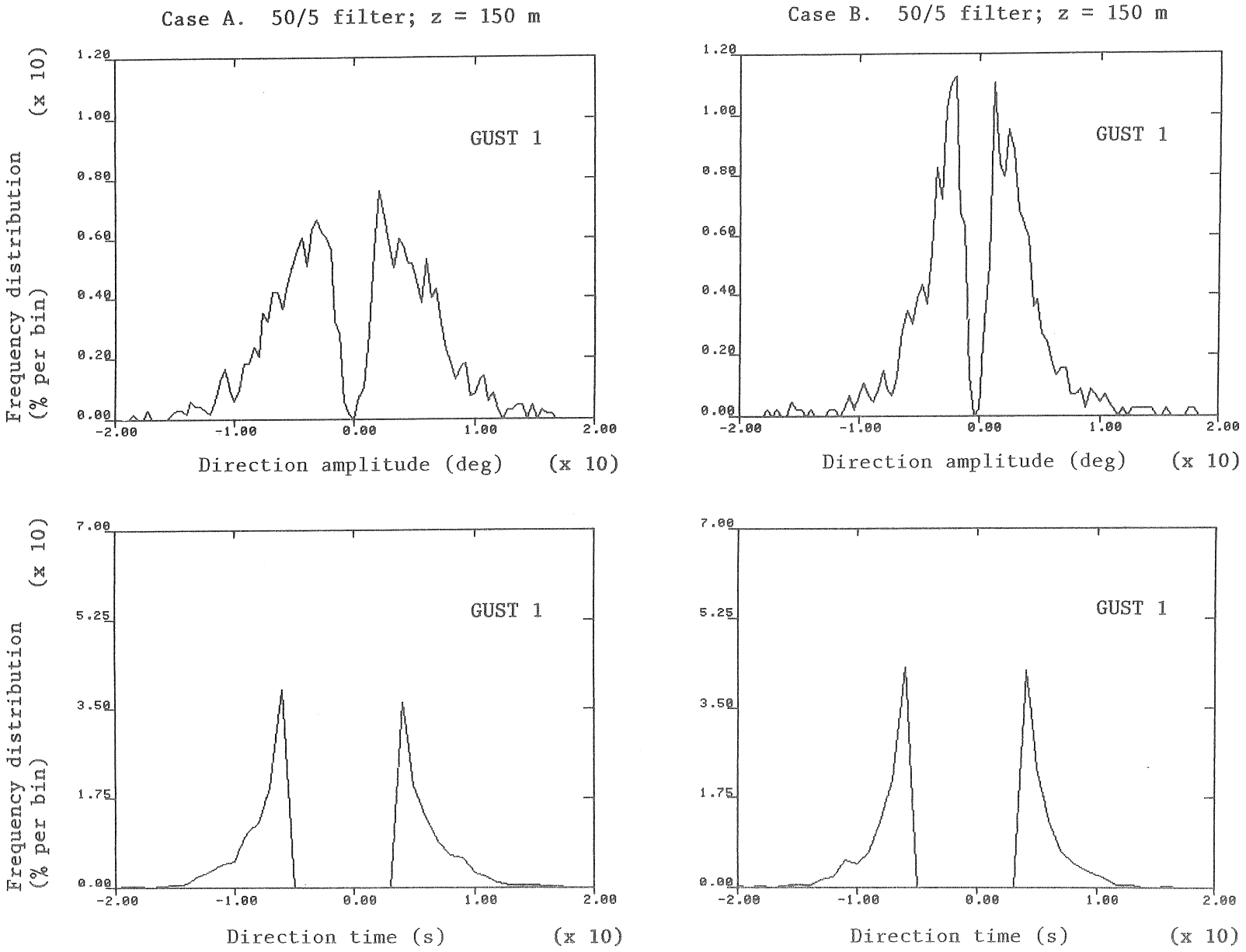

Figure 8.9--GUST 1 direction A_1 and direction T_1 distribution for 50/5 filter at 150 m. ΔA_1 = 0.4 deg; ΔT_1 = 0.4 s.

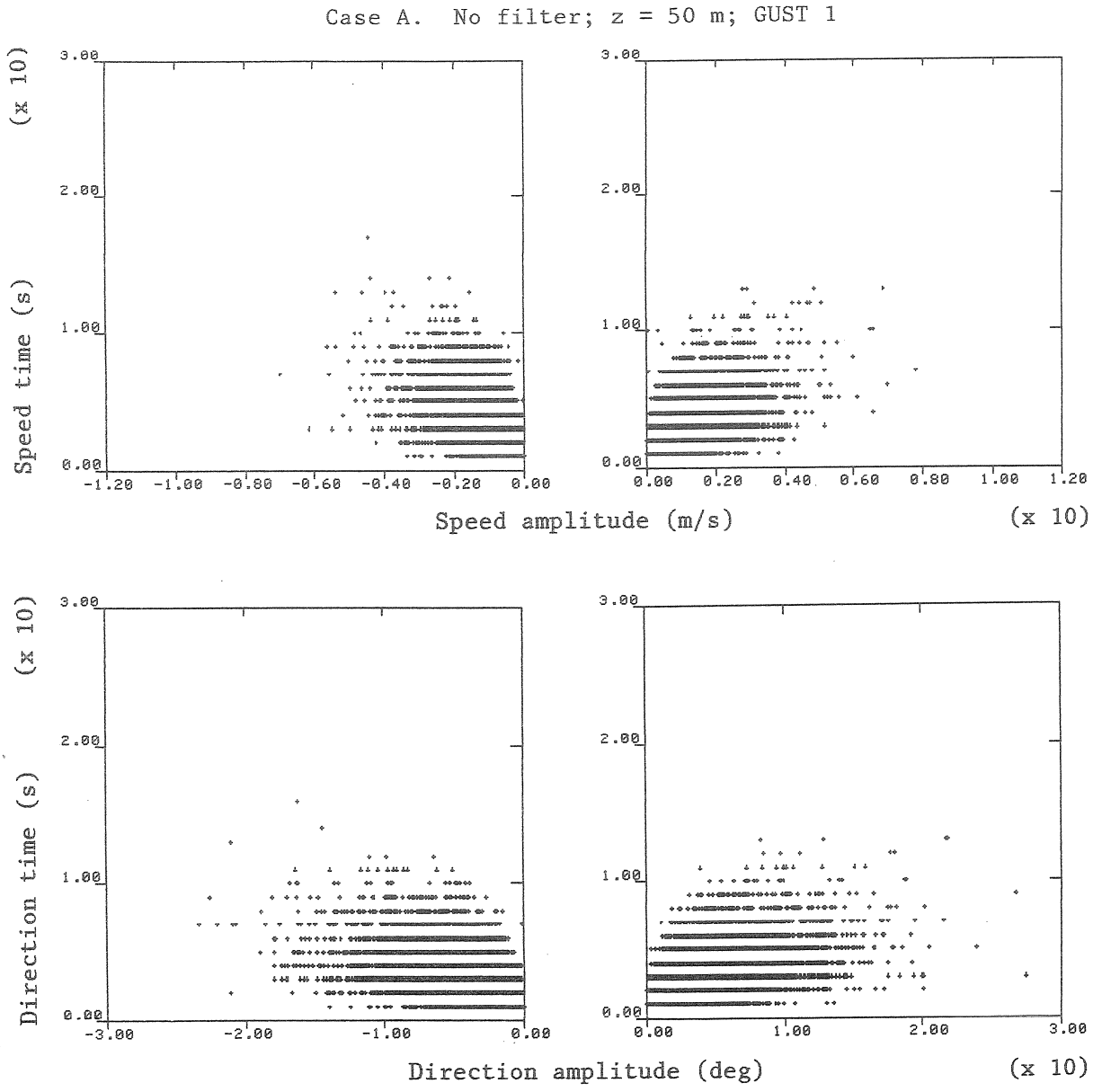

Figure 8.10--Plots of GUST 1 amplitudes vs. times for Case A at 50 m (no filter).

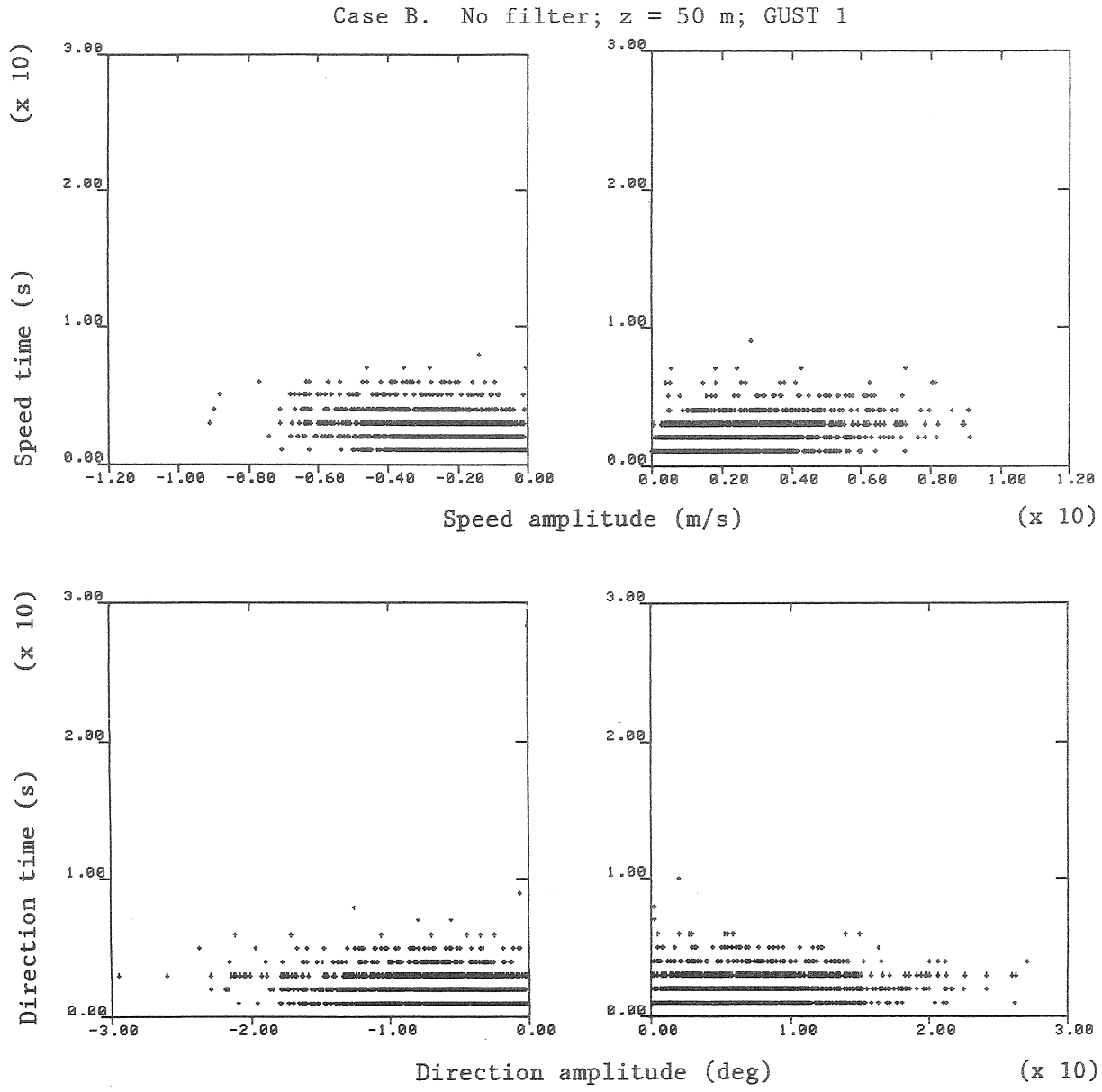

Figure 8.11--Plots of GUST 1 amplitudes vs. times for Case B at 50 m (no filter).

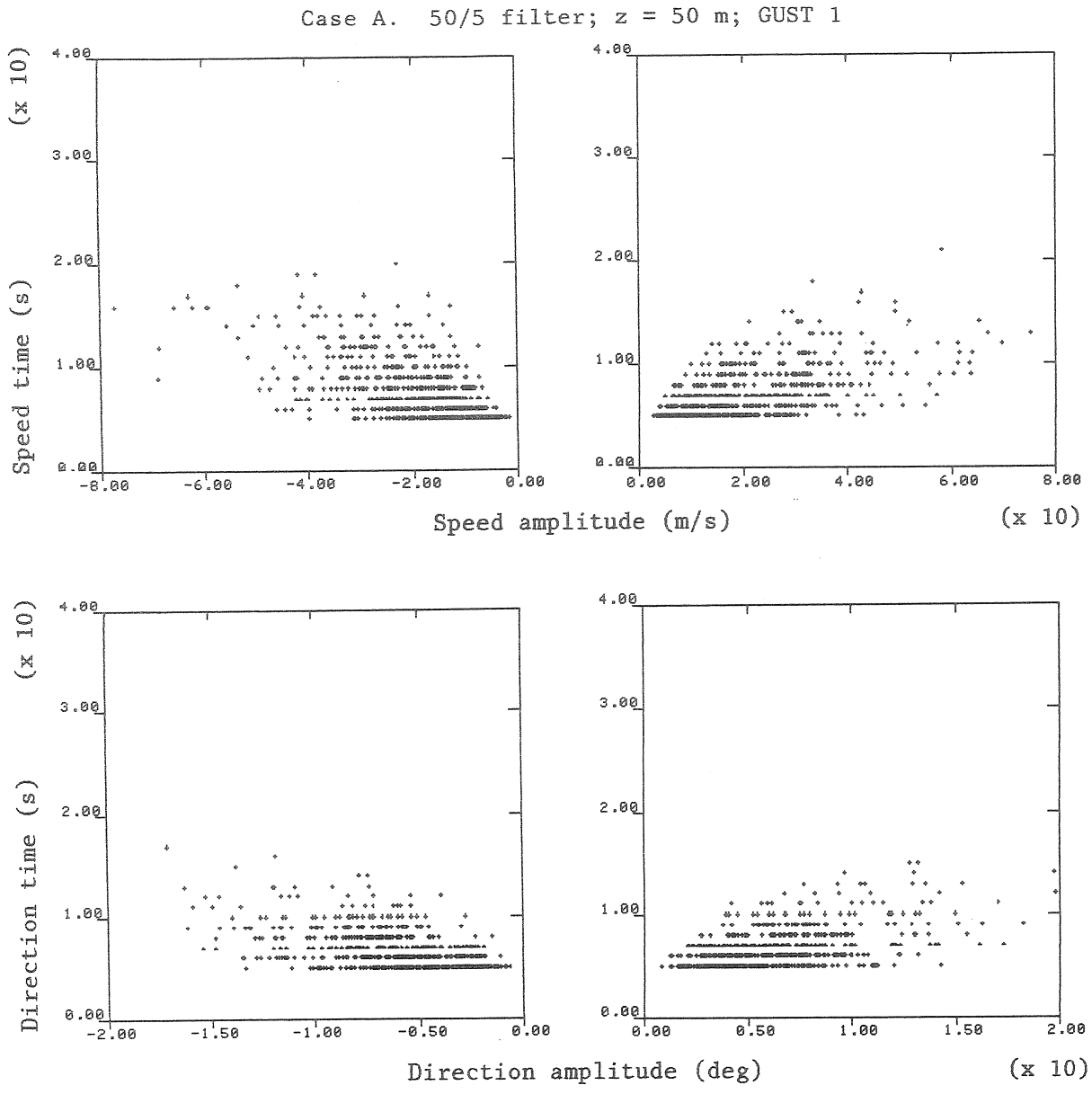

Figure 8.12--Plots of GUST 1 amplitudes vs. times for Case A at 50 m (50/5 filter).

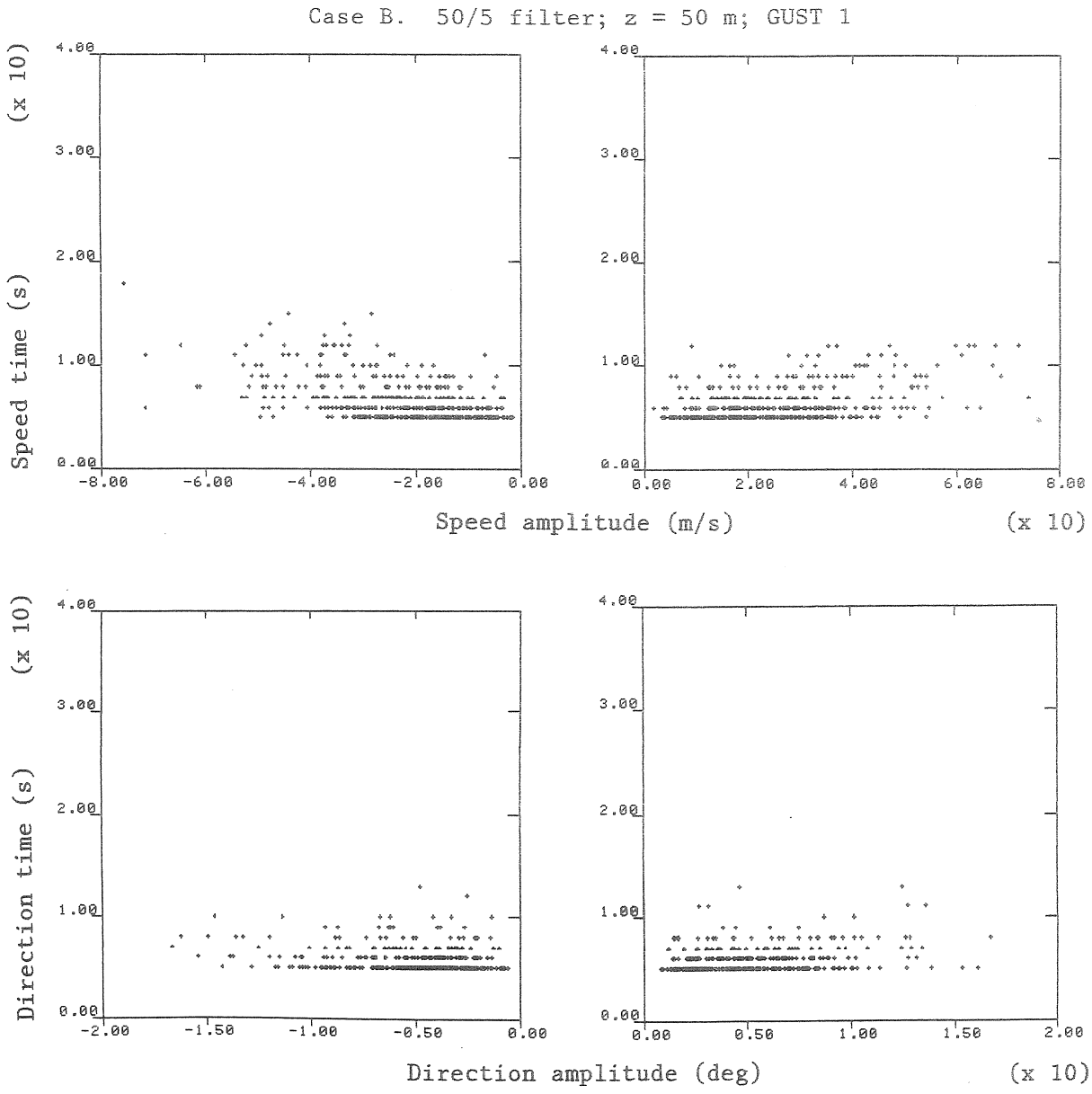

Figure 8.13--Plots of GUST 1 amplitudes vs. times for Case B at 50 m (50/5 filter).

9.0 CHARACTERISTIC MAGNITUDE ANALYSIS

For model applications it is often necessary to characterize the gust parameters with appropriate turbulent (or mean) properties of the flow. Here we follow the approach of Powell and Connell (1980) and normalize the rms gust amplitudes by the standard deviation of the original filtered time series. (For bandpass filtered data the definitions of the standard deviation and the rms value become equivalent.) The rms gust times are normalized by the appropriate gust time average.

The normalized values in Tables 9.1-9.4 show remarkable consistency. The following approximations can be made on the basis of these results:

$$\left[\frac{\sigma_{rms}(+A_0)}{\sigma(X)}\right]_F \approx \left[\frac{\sigma_{rms}(-A_0)}{\sigma(X)}\right]_F \approx 1.5 \; ; \qquad (9.1)$$

$$\left[\frac{\sigma_{rms}(+A_1)}{\sigma(X)}\right]_F \approx \left[\frac{\sigma_{rms}(-A_1)}{\sigma(X)}\right]_F \approx 2.3 \; ; \qquad (9.2)$$

$$\left[\frac{\sigma_{rms}(+T_0)}{+\bar{T}_0}\right]_F \approx \left[\frac{\sigma_{rms}(-T_0)}{-\bar{T}_0}\right]_F \approx 1.1 \; ; \qquad (9.3)$$

$$\left[\frac{\sigma_{rms}(+T_1)}{+\bar{T}_1}\right]_F \approx \left[\frac{\sigma_{rms}(-T_1)}{-\bar{T}_1}\right]_F \approx 1.1 \; ; \qquad (9.4)$$

The approximations are valid for both speed and direction.

As pointed out by Powell and Connell,

$$\left[\frac{\sigma_{rms}(+A_0)}{\sigma(X)}\right]_F = 1.3 \qquad (9.5)$$

and

$$\left[\frac{\sigma_{rms}(+T_0)}{+\bar{T}_0}\right]_F = 1.25 \qquad (9.6)$$

for a Gaussian distribution. Our larger ratio in (9.1) can be attributed to the gap centered around zero in the A_0 distribution (Figs. 7.4-7.9). Removal of values close to zero has the effect of raising the rms value. Presumably, with the gap filled in, the ratio will drop to 1.3. We have no comparable theoretical expectation for the ratio in (9.2), but can assume from the same reasoning that the ratio would be slightly lower for a Gaussian distribution. In any case we can deduce from our results a relationship between GUST 0 and GUST 1 amplitudes:

$$[\sigma_{rms}(+A_1)]_F \tilde{\sim} 1.5[\sigma_{rms}(+A_0)]_F \ . \qquad (9.8)$$

For the gust times we have a smaller ratio in (9.2) than the 1.25 required for a Gaussian distribution. Here we have two factors working in tandem. The increase in the rms value (in the numerator) due to the gap in the frequency distribution is offset by a larger increase in the average gust time (in the denominator), causing a net reduction in the ratio. A relationship similar to (9.7) can be offered for the gust times

$$[\sigma_{rms}(+T_1)]_F \tilde{\sim} 0.5[\sigma_{rms}(+T_0)]_F \ . \qquad (9.8)$$

Table 9.1--Normalized rms GUST 0 amplitudes $[\sigma_{rms}(A_0)/\sigma(X)]_F$

Parameter	Height	Filter	Case A		Case B	
			$+A_0$	$-A_0$	$+A_0$	$-A_0$
Speed amplitude	10	30/3	1.45	1.5	1.54	1.46
		50/5	1.53	1.54	1.60	1.48
		100/10	1.56	1.50	1.71	1.58
	50	30/3	1.45	1.51	1.44	1.54
		50/5	1.45	1.51	1.51	1.58
		100/10	1.55	1.53	1.54	1.64
	150	30/3	1.43	1.48	1.45	1.53
		50/5	1.47	1.50	1.49	1.58
		100/10	1.46	1.57	1.52	1.61
Direction amplitude	10	30/3	1.49	1.52	1.53	1.51
		50/5	1.57	1.56	1.68	1.63
		100/10	1.58	1.61	1.73	1.71
	50	30/3	1.49	1.47	1.57	1.50
		50/5	1.51	1.50	1.64	1.62
		100/10	1.59	1.55	1.72	1.72
	150	30/3	1.45	1.48	1.51	1.52
		50/5	1.49	1.53	1.60	1.59
		100/10	1.53	1.65	1.64	1.66

Table 9.2--Normalized rms GUST 0 amplitudes $[\sigma_{rms}(T_0)/\bar{T}_0]_F$

Parameter	Height	Filter	Case A		Case B	
			$+T_0$	$-T_0$	$+T_0$	$-T_0$
Speed time	10	30/3	1.12	1.12	1.11	1.13
		50/5	1.12	1.13	1.11	1.13
		100/10	1.11	1.10	1.10	1.11
	50	30/3	1.12	1.12	1.13	1.12
		50/5	1.13	1.11	1.11	1.13
		100/10	1.11	1.11	1.14	1.13
	150	30/3	1.13	1.12	1.13	1.12
		50/5	1.12	1.11	1.13	1.11
		100/10	1.13	1.13	1.13	1.14
Direction time	10	30/3	1.13	1.12	1.12	1.11
		50/5	1.11	1.12	1.09	1.10
		100/10	1.14	1.11	1.11	1.11
	50	30/3	1.12	1.11	1.12	1.12
		50/5	1.12	1.12	1.12	1.12
		100/10	1.13	1.13	1.13	1.13
	150	30/3	1.11	1.12	1.13	1.13
		50/5	1.12	1.11	1.14	1.14
		100/10	1.13	1.09	1.13	1.14

Table 9.3--Normalized rms GUST 1 amplitudes $[\sigma_{rms}(A_0)/\sigma(X)]_F$

Parameter	Height	Filter	Case A		Case B	
			$+A_1$	$-A_1$	$+A_1$	$-A_1$
Speed amplitude	10	30/3	2.26	2.07	2.29	2.24
		50/5	2.36	2.14	2.47	2.33
		100/10	2.50	2.22	2.74	2.74
	50	30/3	2.15	2.00	2.24	2.15
		50/5	2.23	2.08	2.56	2.22
		100/10	2.25	2.08	2.82	2.49
	150	30/3	2.10	2.01	2.16	2.10
		50/5	2.14	2.10	2.30	2.23
		100/10	2.29	2.17	2.32	2.36
Direction amplitude	10	30/3	2.01	1.99	2.23	2.21
		50/5	2.27	2.22	2.71	2.61
		100/10	2.65	2.61	3.29	3.47
	50	30/3	1.98	1.93	2.08	2.07
		50/5	2.15	2.18	2.43	2.40
		100/10	2.46	2.45	3.19	3.35
	150	30/3	1.91	1.87	1.90	1.92
		50/5	2.20	2.14	2.22	2.26
		100/10	2.49	2.57	2.62	2.71

Table 9.4--Normalized rms GUST 1 amplitudes $[\sigma_{rms}(T_0)/\bar{T}_0]_F$

Parameter	Height	Filter	Case A		Case B	
			$+T_1$	$-T_1$	$+T_1$	$-T_1$
Speed time	10	30/3	1.07	1.09	1.05	1.07
		50/5	1.05	1.06	1.03	1.04
		100/10	1.03	1.05	1.02	1.02
	50	30/3	1.08	1.09	1.06	1.07
		50/5	1.06	1.07	1.04	1.05
		100/10	1.04	1.05	1.02	1.04
	150	30/3	1.07	1.09	1.07	1.08
		50/5	1.06	1.07	1.04	1.05
		100/10	1.05	1.05	1.03	1.04
Direction time	10	30/3	1.06	1.06	1.04	1.04
		50/5	1.04	1.04	1.02	1.02
		100/10	1.02	1.04	1.01	1.02
	50	30/3	1.07	1.07	1.05	1.04
		50/5	1.04	1.04	1.02	1.02
		100/10	1.02	1.02	1.02	1.03
	150	30/3	1.08	1.07	1.07	1.07
		50/5	1.05	1.05	1.04	1.05
		100/10	1.02	1.03	1.03	1.03

10.0 CONCLUSIONS

1) The statistics computed for the two wind storms represented by Case A and Case B exhibit a high degree of internal consistency. When normalized, the gust parameters become insensitive to differences in static stability, height, and choice of bandpass filter.

2) Bandpass filtering is essential for approximating Gaussian distribution in the original speed and direction time series, more so for the speed than for the direction. The basic 50/5 bandpass filter of Powell and Connell appears to be a proper choice for the types of analyses performed here.

3) A consistent relationship exists between the standard deviation of the speed (and direction) differences and the standard deviation of the original filtered speed (and direction) time series. For the 50/5 filtered data, at the optimum differencing interval of 10 s, the ratio of the two standard deviations is 1.5.

4) Normalized gust statistics for GUST 0 and GUST 1 models show consistent and constant relationships that are directly applicable to WECS design.

5) Further work is needed to determine the best approach for eliminating the gaps in the GUST 0 and GUST 1 distributions.

6) Because of the internal consistency in their statistical properties, the two cases studied here constitute an ideal data set for validation of other gust models.

REFERENCES

Cliff, W.C. and G.H. Fichtl, 1978. Wind Velocity-Change (Gust Rise) Criteria for Wind Turbine Design. PNL-2526, Pacific Northwest Laboratory, Richland, Wash.

Connell, J.R., 1979. Overview of wind characteristics for design and performance. Proceedings: Conference and Workshop on Wind Energy Siting 1979, Portland, Oregon (June 19-21). American Meteorological Society Boston, Mass., pp. 5-12.

Connell, J.R., 1980. Turbulence spectrum observed by a fast rotating wind turbine blade. PNL-3426, Pacific Northwest Laboratory, Richland, Wash.

Doran, J.C. and D.C. Powell, 1980. Gust Characteristics for WECS Design and Performance Analysis. PNL-3421, Pacific Northwest Laboratory, Richland, Wash.

Huang, C.H. and G.H. Fichtl, 1979. Gust-Rise Exceedance Statistics for Wind Turbine Design. PNL-2530, Pacific Northwest Laboratory, Richland, Wash.

Kaimal, J.C., J.C. Wyngaard, Y. Izumi and O.R. Coté, 1972. Spectral characteristics of surface layer turbulence. Quart. J. Roy. Meteorol. Soc., 98, 563-589.

Kaimal, J.C., 1973. Turbulence spectra, length scales and structure parameters in the stable surface layer. Bound.-Layer Meteorol., 4, 289-309.

Kaimal, J.C., 1978a. NOAA instrumentation at the Boulder Atmospheric Observatory. Preprints: 4th Symposium on Meteorological Observations and Instrumentation, 1978, Denver, Colorado, American Meteorological Society, Boston, Mass., pp. 35-40.

Kaimal, J.C., 1978b. Horizontal velocity spectra in an unstable surface layer. J. Atmos. Sci., 35, 18-24.

Kaimal, J.C., 1980. BAO sensors for wind, temperature and humidity profiling. Chapter 1 in The Boulder Low-Level Intercomparison Experiment - Preprint of WMO Report, J.C. Kaimal et al., Eds., NOAA/NCAR Boulder Atmospheric Observatory Report No. 2, pp. 1-6.

Lawrence, R.S. and M.H. Ackley, 1979. Interactive access to the BAO data. Chapter 17 in Project PHOENIX: The September 1978 Field Operation, W.H. Hooke, Ed., NOAA/NCAR Boulder Atmospheric Observatory Report No. 1., pp. 267-281.

Powell, D.C., 1979. Wind fluctuations described as discrete events. Proceedings: Conference and Workshop on Wind Energy Characteristics and Wind Energy Siting 1979, Portland, Oregon (June 19-21). American Meteorological Society, Boston, Mass., pp. 71-79.

Powell, D.C. and J.R. Connell, 1980. Definition of Gust Model Concepts and Review of Gust Models. PNL-3138, Pacific Northwest Laboratory, Richland, Wash.

Ramsdell, J.V., 1975. Wind and Turbulence Information for Vertical and Short Take-off and Landing (V/STOL) Operations - Results of Meteorological Survey. Report No. FAA-RO-75-94, Dept. of Transportation, Federal Aviation Administration Systems Research and Development Service, Washington, D.C.

☆ U.S. GOVERNMENT PRINTING OFFICE: 1981 — 777-002/1263 Region No. 8